DISSERTATION

AN ASSESSMENT OF DISCRETIZATION METHODS FOR COMPUTATION OF THE RADIATION HEAT TRANSFER IN BUILDING ENCLOSURES

Submitted by
Ricardo Ganem
Department of Mechanical Engineering

In partial fulfillment of the requirements
For the Degree of Doctor of Philosophy
Colorado State University
Fort Collins, Colorado
Fall 1999

UMI Number: 9950888

UMI®

UMI Microform 9950888

Bell & Howell Information and Learning Company
300 North Zeeb Road
P.O. Box 1346
Ann Arbor, MI 48106-1346

COLORADO STATE UNIVERSITY

July 30, 1999

WE HEREBY RECOMMEND THAT THE DISSERTATION PREPARED UNDER OUR SUPERVISION BY RICARDO GANEM, ENTITLED "AN ASSESSMENT OF DISCRETIZATION METHODS FOR COMPUTATION OF THE RADIANT HEAT TRANSFER IN BUILDING ENCLOSURES," BE ACCEPTED AS FULFILLING IN PART REQUIREMENTS FOR THE DEGREE OF DOCTOR OF PHILOSOPHY.

Committee on Graduate work

Richard Loehrke

Patrick J. Burns

Douglas C. Hittle

Robert N. Meroney

Allan Kirkpatrick

Adviser

Department Head/ Director

ABSTRACT OF DISSERTATION

AN ASSESSMENT OF DISCRETIZATION METHODS FOR COMPUTATION OF THE RADIATION HEAT TRANSFER IN BUILDING ENCLOSURES.

Two different methods to compute local radiative heat flux and mean radiant temperatures inside transparent enclosures are discussed. Both of these methods: the Discrete Ordinates Method (DOM) and the Discrete Transfer Method (DTM) solve the equation of radiative transfer for a discrete number of angular directions. In the DOM a Cartesian grid is used to solve numerically the above equation. It is discovered that sharp intensity gradients rapidly degrade the perfomance of the DOM in such a way that its accuracy is poor in a room with more than one window or with more than one heat source. Furthermore, it is also discovered that the most common quadrature sets produce large errors in local heat flux calculations. This is due in part to the small number of angular directions available in these sets, and in part to the poor distribution of angular directions and weights that these quadratures present. The Thurgood quadrature family can have as many angular directions as desired and it also has a better distribution of weights and directions. It is recommended and used throughout this thesis.

In contrast to the DOM, the DTM solves the equation of radiative transfer along the direction of the beams. A DTM, modified by the author to deal with transparent enclosures, is proposed as an alternative to the DOM. The method developed in this thesis works with short as well as with long wave radiation. Since the DTM does not have the problems of false scattering and false oscillations present in the DOM, it outperforms the DOM in heat flux as well as in mean radiant temperature calculations.

In conclusion, it is shown that this novel version of the DTM is a valuable tool to calculate short and long wave radiant heat flux in an enclosure as well as mean radiant temperature in its interior. Therefore this version of the DTM, can be used to design radiant heat panels, to help in the evaluation of comfort conditions inside a building, or together with other models to compute the airflow inside a room.

Ricardo Ganem
Department of Mechanical Engineering
Colorado State University
Fort Collins, CO 80523
Fall 1999

With love:

To my children Ana Paula and Andres

To my wife Maria Esther

To my parents Amin and Ana Luz

ACKNOWLEDGMENTS

This thesis would not have been possible without the support of many people. It is really the product of a community working together. It would be impossible for me to mention all the people that contributed, in one way or another, to the development of this work.

However I wish to express gratitude to all the committee members that helped to improve this work with their suggestions and commentaries, specially to Dr. Allan Kirkpatrick whose enthusiastic support and dedication were beyond the ordinary. His guidance was essential throughout this work.

I also appreciate the unconditional support of my wife, without her help this thesis would not have been possible. Last but not least I wish to thank CONACYT (Consejo Nacional de Ciencia y Tecnologia) they provided the material support for our family throughout these years.

NOMENCLATURE

A	Area
E	Emissive power (W/m^2)
E_b	Blackbody emissive power (W/m^2)
F_{ij}	View factor
G	Irradiation (W/m^2)
$G_{surf\,i}$	Irradiation on surface i due to the rest of the surfaces of the enclosure. It does not include direct solar radiation (W/m^2)
I	Intensity ($W/sr\,m^2$)
I_p	Intensity at the center of an interior cell
J	Radiosity (W/m^2)
N_{octant}	Number of angular directions per octant
Q_{rad}	Radiant heat (W)
T	Temperature (Kelvin)
T_{mrt}	Mean radiant temperature (Kelvin)
a	Absorption coefficient
$d\Omega$	Infinitesimal solid angle around direction Ω (sr)
$\mathbf{n}$	Unit normal vector
n^2	Number of area elements on a surface
q_{rad}	Radiant heat flux (W/m^2)
q_{cond}	Conduction heat flux (W/m^2)
q_{conv}	Convection heat flux (W/m^2)
r	Position on a surface, arbitrary integer
t_{vf}	CPU time required to calculate view factors in the Radiosity Intensity Method
t_{se}	CPU time required to solve the system of equations in the Radiosity Intensity Method
x, y, z	Distances along x, y or z axes of Cartesian coordinate system
α	Interpolation constant
$\Gamma(\ )$	Gamma function
ε	emissivity
Φ	Phase function for scattering
μ, η, ξ	Direction cosines of Ω
ρ	Reflectivity
σ	Stefan-Boltzmann constant ($5.6693.\ 10^{-8}$ $W/m^2 K^4$)
σ_s	Scattering coefficient
τ	Transmittance
Ω	Unit vector pointing towards the beam direction
ω	Weight of a direction in a quadrature set

Subscripts

b	Blackbody
beam	Direct solar radiation
boundary	Radiation leaving a surface
diff	Diffuse solar radiation
DOM	Discrete ordinates method
E	East
N	North
S	South
W	West
λ	Wavelength

Superscripts

l	Long wave
s	Short wave

LIST OF FIGURES

Chapter 1

Figure 1.1	Radiation exchange methods used in this work	3
Figure 1.2	Case 1	10
Figure 1.3	Case 2	10
Figure 1.4	Case 3	11
Figure 1.5	Case 4	11
Figure 1.6	Case 5	12
Figure 1.7	Case 6	12
Figure 1.8	Case 7	13

Chapter 2

Figure 2.1	Short wave radiant fluxes in a window	19
Figure 2.2	Short wave energy analysis for opaque and sunlit surfaces	21
Figure 2.3	Complete heat flux calculation procedure	25
Figure 2.4	RIM convergence for case 1	28
Figure 2.5	RIM convergence for case 2	29
Figure 2.6	CPU time utilized by RIM	30

Chapter 3

Figure 3.1	The equation of radiative transfer	31
Figure 3.2	Specification of direction in the radiative transfer equation	32
Figure 3.3	Beams striking a surface	34
Figure 3.4	Mean radiant temperature calculation using the DOM	35
Figure 3.5	Short wave energy analysis for opaque and sunlit surfaces	37
Figure 3.6	Short wave radiant heat fluxes in a window	39
Figure 3.7	DOM double discretization process	41
Figure 3.8	A 2-D slice of a grid for the DOM	43
Figure 3.9	DOM treatment of irregular domains	47
Figure 3.10	The ray effect	50
Figure 3.11	The ray effect in transparent media	51
Figure 3.12	Ray effect wavelength	51
Figure 3.13	Scattering of a collimated beam	52
Figure 3.14	Numerical experiment of Chai et al.	54
Figure 3.15	False scattering and false oscillation examples	55
Figure 3.16	Rms error calculation for false scattering	56
Figure 3.17	Rms error as a function of theta	57
Figure 3.18	Chai et al. experiment with a smooth intensity distribution	58
Figure 3.19	False oscillations in sharp and smooth intensity gradients	59
Figure 3.20	Alpha optimal as a function of theta	61
Figure 3.21	Rms error calculation 3 – D	62
Figure 3.22	Effect of alpha on heat flux (Case 1)	64
Figure 3.23	Effect of alpha on heat flux (Case 2)	65

Chapter 4

Figure 4.1	A 2-D example of a 90 degrees symmetric angular quadrature set	67
Figure 4.2	Ninety degree symmetry: the heat flux in any wall should have the same value whether frame 1 or frame 2 is used	69
Figure 4.3	Reflection symmetry on a typical case: If P is a direction in the quadrature set so is P" and both have the same weight	70
Figure 4.4	Interchange symmetry: Equivalent to rotations plus reflections	70
Figure 4.5	Nomenclature for moment integrals	71
Figure 4.6	Some quadrature sets	73
Figure 4.7	The directions of the S6 quadrature scheme as seen on a unit sphere	74
Figure 4.8	Equal weight points for some Sn quadrature sets	75
Figure 4.9	Basal triangle for the construction of the Tn quadrature set	78
Figure 4.10	Tesselation of the basal triangle to generate the T4 quadrature set	78
Figure 4.11	Distribution of angular directions for the T6 and S16 quadrature sets	80
Figure 4.12	Angular distribution of weights in quadrature S16 and T6	81
Figure 4.13	Ray effect in two different quadrature sets	82
Figure 4.14	Heat flux comparison of angular schemes	84
Figure 4.15	Heat flux comparison of angular schemes	85
Figure 4.16	Heat flux. RIM and Chapman DOM calculation	86
Figure 4.17	Local heat flux. Tn convergence (Case 1)	87
Figure 4.18	Local heat flux. Tn convergence (Case 2)	88

Chapter 5

Figure 5.1	Rms error vs. CPU time for a beam	93
Figure 5.2	Rms error experiment for three beams	94
Figure 5.3	Optimal alpha with multiple beams	95
Figure 5.4	Average intensities inside a cell	96
Figure 5.5	Best possible extrapolation for I_N	97
Figure 5.6	No oscillation value for alpha	99
Figure 5.7	No oscillation alpha rms error	100

Chapter 6

Figure 6.1	The original Discrete Transfer Method idea	103
Figure 6.2	Block diagram for the Discrete Transfer Method for transparent enclosures	105
Figure 6.3	Step 2: Irradiation calculation for the Discrete Transport Method	106
Figure 6.4	A 2-D example of the DTM in transparent enclosures	107
Figure 6.5	Step 2: Calculating the intensity of the impinging ray	109
Figure 6.6	Equation of the beam in three dimensions	109
Figure 6.7	DTM convergence test	117
Figure 6.8	Floor midline local heat flux	118
Figure 6.9	Comparison of DTM and DOM	120
Figure 6.10	Comparison between DTM and RIM	121
Figure 6.11	Case 2 Tmrt: Chapman and DTM	123
Figure 6.12	Case 7 Tmrt for 2 heat panels: DTM and DOM	124
Figure 6.13	Tmrt in a non-rectangular enclosure	125

Chapter 7

Figure 7.1	Energy balance in passive and active surfaces	130
Figure 7.2	Complete simulation: temperature boundary conditions	132
Figure 7.3	Comparison of floor short wave heat fluxes	134
Figure 7.4	Comparison of wall 3 short wave heat fluxes	135
Figure 7.5	Comparison of ceiling short wave heat fluxes	136
Figure 7.6	Short wave ray effect	137
Figure 7.7	Sloped vs. non-sloped short wave floor heat flux	138
Figure 7.8	Sloped vs. non-sloped wall 3 short wave heat flux	139

CONTENTS

Abstract iii

Dedication v

Acknowledgments vi

Nomenclature vii

Table of Figures ix

1 Radiant heat exchange in transparent enclosures 1

1.1 Introduction 1
1.2 Radiation exchange solution methods 2
1.3 Previous work 4
1.4 Research needs 7
1.5 Contribution of thesis 8
1.6 Description of test cases 8

2 The radiosity intensity method 14

2.1 The long-wave model 14
2.2 Radiosity two band model 17
2.3 Disadvantages of the radiosity method 26
2.4 Convergence tests 27

3 Discretization of radiative transfer: the discrete ordinates method 31

3.1 The equation of radiative transfer 31
Radiation boundary conditions 32
The mean radiant temperature 34
3.2 Two band model 35
Short wave boundary conditions 36
3.3 The discrete ordinates method 40
DOM angular discretization 41
DOM spatial discretization 42
DOM long wave solution procedure 45
DOM short wave solution procedure 46
DOM treatment of irregular geometries 47
3.4 The shortcomings of the discrete ordinates method 49
Ray effect 49
False scattering 52
False oscillations 58
3.5 Test Cases 62
3.6 Summary 63

4 Angular discretization schemes 67

4.1 Introduction 67
4.2 Quadrature construction criteria 68
Symmetry 68
Moment matching criteria 71
4.3 Different families of quadrature sets 73

The angular segmentation quadrature (Sn) 73
Equal weights quadratures 76
Thurgood quadrature 77
4.4 Comparison between quadrature sets 79
4.5 Test cases 83
4.6 Summary 89

5. Minimization of discrete ordinates method errors **90**

5.1 Introduction 90
5.2 The rms experiment 91
5.3 False scattering & false oscillations 91
5.4 Model to explain false oscillations 95
5.5 Summary 100

6. The discrete transfer method applied to transparent enclosures **102**

6.1 Introduction 102
6.2 The discrete transfer method for nonparticipating media 103
6.3 Solution scheme for the DTM 104
A two dimensional example 111
6.4 Discussion of characteristics of the DTM algorithm 115
6.5 Test cases and results 116
Mean radiant temperature calculations and comparisons with the DOM 121
6.6 Summary 126

7. The discrete transfer method as applied to practical cases **128**

7.1 Introduction 128
7.2 Short-wave solution procedure 128
7.3 Non-rectangular enclosures 129
7.4 Boundary conditions for a complete simulation 130
7.5 Test cases 133
7.6 Summary 140

8. Summary and conclusions **141**

8.1 Summary and conclusions 141
8.2 Recommendations for future work 142
Specular reflection 141
Non-rectangular surfaces 143
Embedded objects 144
Comparison between monte carlo and the discrete transfer method 144
Complete simulations 144

References **146**

Chapter 1

RADIANT HEAT EXCHANGE IN TRANSPARENT ENCLOSURES

1.1 INTRODUCTION

There are many situations where it is of practical interest to calculate radiative exchange within enclosures. These include buildings, solar collectors, electronic circuits, furnaces and combustion chambers. In the case of buildings there are three areas where the need to compute radiant heat transfer arises:

1. -Heat Load Calculations: According to Stefanizzi et al. (1990), long wave radiation heat transfer accounts for up to 10 % of the total heat loss of a conventional building. Its influence may be even larger in non-conventional buildings, since in atria or glazed enclosures radiation has a large impact on heat losses. Therefore, to obtain an accurate estimate of the annual energy consumption of a building it is necessary to have a fast and reliable method to compute radiative exchange in non-participating media. In this type of calculation, the parameter of interest is the surface average heat flux, so there is no need to make calculations of the local heat flux. In the usual procedure utilized in programs such as BLAST and NBSLD, the radiative exchange between the surfaces of the enclosure is linearized. According to Walton (1980), however, unless the surfaces involved are similar in size, a violation of the law of energy conservation is produced. Since radiation is not the main heat transfer mechanism in buildings, this estimation might be sufficient for many cases. However, in atriums or in passive buildings for instance, a more accurate estimation of radiative heat transfer is needed.

2. - The Design of Radiant Heat Panels and the Estimation of Comfort Conditions It is here where a detailed analysis of radiation heat transfer is of paramount importance. Specifically, in order to determine the mean radiant temperature (T_{mrt}) inside a room, an important component for the comfort of the occupant, the radiant intensities inside the enclosure need to be calculated. According to Fanger (1972) the mean radiant temperature for a particular location inside a room

can be calculated using the view factors between the location in question and the surfaces of the room. However it is generally difficult to calculate these view factors and therefore this method is difficult to automate. In many practical situations a single mean radiant temperature is assumed to be valid for the whole enclosure. As Fanger remarks, this procedure is highly questionable.

3. - Simulation of Flow and Heat Transfer in Enclosures. The calculation of air movement inside an enclosure is a hybrid problem involving convection and radiation heat transfer. Airflow is an important factor affecting the comfort conditions at the interior of a room. To predict the airflow pattern, information about the surface temperature distribution of the enclosure is required (Yuguo, Li and Laszlo Fuchs, 1992). In atriums, large spaces with glass roofs, the thermal environment is greatly affected by solar radiation. Moreover, because the scale of atriums is large, the three-dimensional distribution of temperature and air velocity must be considered for the control of the environment. The importance of radiative heat transfer in these kinds of enclosures has been shown by Shild (1997) and by Ozeki et al. (1993). It is also an important problem in solar collectors, double-pane windows and double–wall insulation. In the case of solar collectors, it has been observed that even at moderate temperatures the radiative mode of heat transfer is important. In particular an increase in incident radiation produces a rise in the internal circulation of the air(Behnia, Reizes and De Vahl, 1990).

1.2 RADIATION EXCHANGE SOLUTION METHODS

There are several methods available to solve the problem of radiant interchange within an enclosure. The methods used in this thesis are listed in Figure 1.1. In almost all the methods the first step is to divide the enclosure into n small surface segments in such a way that constant temperature, irradiation and radiosity can be assumed within each segment. The radiosity intensity method (RIM) (Incropera and DeWitt, 1996) computes the heat fluxes on each segment by performing an energy balance on all the n segments of the enclosure, generating in this way a system of n linear equations. In principle, this method is as accurate as desired provided that n is large enough and the surfaces are gray and opaque. For this reason it is used as a benchmark throughout this work. The RIM, however, works only for geometrically simple rooms. Furthermore, in its traditional surface to surface form, the RIM does not perform any calculation of the intensity fields inside the enclosure and is, therefore, unable to calculate mean radiant temperatures at the interior of a room. A more detailed description of the method is given in Chapter 2. Other methods use stochastic processes such as the Markov chain (Naraghi and Chung 1984) or the Monte Carlo method (Burns & Pryor 1989). The Monte Carlo method has had considerable development. It is capable of making accurate calculations of heat fluxes in complex geometry. It can be used to simulate internal objects and non-gray walls. However it normally does not calculate intensities inside enclosures.

Another method to approach the problem is to use a basic radiation heat transfer differential equation, the equation of radiative transfer. The Discrete Ordinates Method (DOM) as well as the Discrete Transfer Method (DTM) calculates the radiative exchange within an enclosure using a discrete form of the equation of radiative transfer.

Radiation Exchange Solution Methods

- **Radiosity Intensity Method (RIM): Chapter 2**
- **Discrete Ordinates Method (DOM): Chapters 3, 4 and 5**
- **Discrete Transfer Method (DTM): Chapters 6 and 7**

Figure 1.1 Radiation exchange methods used in this work

1.3 PREVIOUS WORK

The first exposition of the Discrete Ordinates Method (DOM) was made in 1950 by the astrophysicist S. Chandrasekhar, who was interested in radiation transport inside stars. He thought that the integrals that appear in the energy transport equation and the boundary conditions could be solved by modeling the intensity field as a series of discrete streams. His idea was to use Gauss quadrature formulae to calculate the integrals. In 1965 Lathrop and Carlson used a very similar method for solving problems in neutron energy transport. They proposed a series of angular discretization schemes that are still used by many researchers. Fiveland in 1984 developed the first version of the DOM by applying it to 2-D rectangular enclosures. Later Fiveland (1988) applied it to three-dimensional enclosures. He also showed, in 1989, how to apply the method to enclosures filled with a non-gray medium.

The DOM has been a popular method to compute radiative heat transfer in furnaces and combustion chambers. Among its capabilities, the DOM can be used in a participating medium; it can easily be coupled with other kinds of heat transfer modes (Behnia, Reizes & Davis 1990) and is also capable of handling the spectral characteristics of gases and boundaries. Usually, researchers in this field have reported that the DOM has given satisfactory accuracy in a reasonable amount of time.

Another aspect of the DOM is its capability to deal with non-rectangular enclosures and embedded objects. Smith and Sanchez (1992) examined what happens at the border of two different adjacent control volumes (solid-solid, solid-transparent, transparent-solid and transparent-transparent) and obtained a formula that gives the intensity entering the downstream cell. They tried their method with straight-edged protrusions and obstructions in a 2-D geometry. Later, Ehlert & Smith (1994) used the same procedure in a 3-D rectangle with a centered obstruction. In 1993, Chai, Lee and Patankar introduced a general procedure similar to the one used in computational fluid dynamics (Patankar 1980). Beckner and Howell (1997) proposed a modification to improve the procedure of Chai et al.

From the building energy calculation viewpoint, besides helping to estimate the annual heat loss (Chapman 1997), the DOM has also been used to design radiant heat panels (Chapman 1995). In the Building Comfort Analysis Program (BCAP) designed by Chapman in 1997, the DOM is used to obtain the power consumption used by radiant heat panels and the mean radiant temperature (T_{mrt}) that these heat panels would produce in the interior of the room. The mean radiant temperatures are very important in the assessment of the comfort of the occupants inside the room (Fanger 1972). However, the procedure used to design radiant heat panels before Chapman (Howell, R. and Suryanarayana 1990) did not calculate the T_{mrt}. In his 1995 paper, Chapman tested the DOM for simple enclosures with constant temperatures and emisivitty for each wall. In general he found good agreement between the average heat flux at each wall as calculated by the DOM and the Radiosity method, but he did not show detailed heat flux calculations for those walls.

The DOM has been used with relatively simple boundary conditions. Almost always constant temperature or constant heat flux surfaces have been used (Fiveland, Smith & Sanchez, Truelove, Smith and Ehlert, Chapman). However, as Chai, Lee and Patankar (1993a) demonstrated, two of the three main problems of the method, the ray effect and false oscillations, arise when sharp intensity gradients, resulting from more complex boundary conditions, are present within a surface. In addition, in previous work, the DOM has primarily been used with participating medium enclosures that mitigate both of the above problems.

Therefore, a question arises about the accuracy of the DOM with respect to non-participating enclosures with non-uniform boundary conditions. The question is important because a building, besides having transparent media, may contain heating panels and windows that may produce sharp intensity gradients. Smith and Sanchez (1992) found spurious oscillations, calculated by the DOM, superimposed on the local heat flux on the wall of a 2-D rectangle. Using a standard quadrature set and working with a rectangular duct and a gray medium, Thurgood (1992) observed oscillations and poor accuracy results with the DOM. In 1990, Fiveland and Pollard reported that by using the so called High Resolution (HR) spatial schemes they had been able to eliminate false oscillations for a 2-D case. Liu, Becker and Pollard (1996) suggested the use of

SMART, one of these HR schemes, to eliminate the oscillations in a 3-D geometry. However, as the author will in section 5.4, when the SMART differential scheme was used, a considerable amount of CPU time and a very fine grid were required for satisfactory computations. Thus the price of eliminating the oscillations is to increase enormously the CPU time required to perform the task. Fiveland & Jessee (1996) recognized this new problem and proposed some acceleration techniques, but these new techniques work only for enclosures with a participating medium. More recently, Ramankutty and Crosbie (1998) proposed a new formulation of the DOM that significantly reduces the oscillations produced by the ray effect. However their method also requires the existence of a participating medium.

Thurgood (1992) proposed a new family of quadrature sets capable of handling as many angular directions as necessary. This new family significantly reduce the ray effect oscillations. Thurgood applied it to a two-dimensional rectangular cylinder. He also proposed a new spatial differential scheme to deal with false scattering and false oscillations. Although this last one is difficult to adapt to three dimensions, the quadrature family he proposed can easily be used in this situation.

The Discrete Transfer Method (DTM) was developed by Saha in 1979. As Saha mentioned, the DTM does not use arbitrary constants such as the interpolation factor of the DOM. It is geometrically flexible and, as in the case of the DOM, it is easily coupled with a computational fluid dynamic solver. Cumber & Beeri (1998) showed how the DTM could take advantage of parallel architecture computers. The angular quadrature sets for the DTM had been developed independently of the angular quadrature sets developed for the DOM. Cumber in 1994 proposed a new angular quadrature scheme for the DTM. However, since the same restrictions apply for both methods with regards to angular discretization, there is no reason why the quadrature sets developed for the DOM cannot be used by the DTM, as will be done in this work.

The DTM has been applied exclusively to furnaces and combustion chambers (Meng et al. 1992). Cumber mentions, as examples of the applications of the DTM, the analysis of fire hazards in enclosures, the prediction of flashover and flame spread. As another example, the method has been used in the design of burners and furnaces where a primary objective is the minimization of emission of oxides of nitrogen as these oxides are highly sensitive to changes in the temperature field. However as far as this author knows, the DTM has not been previously applied to transparent enclosures.

Finally, the DOM and the DTM can easily be coupled with other forms of heat transfer. It is this characteristic that has made these methods increasingly popular in furnaces and combustion chambers. Abraham & Magi (1997), for instance, used the DOM to include radiant heat losses in a diesel engine. They found that this inclusion reduced the predicted peak temperature inside the engine by ten percent, reducing the predicted levels of frozen NO. Hyde & Truelove (1977) presented a detailed description of the application of the DOM in furnaces and Selcuk and Kayakol (1996) evaluated the DOM and the DTM as applied to them. They concluded that the DOM required a CPU time three orders of magnitude less than that required by the DTM. In this work both of these methods will be discussed with application to transparent enclosures.

1.4 RESEARCH NEEDS

From the above discussion, the following research needs are deduced:

a) The ability of the Discrete Ordinates Method (DOM) to calculate the distribution of local heat fluxes has not been tested in the case of transparent enclosures. In particular, the performance of the method has not been tested in the presence of sharp intensity gradients. In the case of buildings, these sharp intensity gradients are due to windows and heat panels.

b) In the case of the DOM, new methods of spatial and angular discretization are needed in order to minimize false scattering, false oscillations and the ray effect.

c) Since the DOM and the DTM methods were first applied to furnaces and heat chambers, they have not been used with non-gray surfaces. In the case of buildings it is important to test both methods in the short wave part of the spectrum.

d) The applicability of both methods to compute the radiative exchange in non-rectangular, non-cylindrical, three-dimensional enclosures needs to be investigated.

e) The DTM needs to be evaluated for transparent media. Like the DOM, it can be used to obtain the distribution of heat flux on the surfaces of an enclosure as well as the mean radiant temperature at the interior of the enclosure.

f) The performance of both methods applied to three-dimensional enclosures with inner obstacles needs to be further evaluated.

g) The capability of the DOM or the DTM method to deal with specular reflection has not been explored.

1.5 CONTRIBUTION OF THESIS

In general, this thesis make addresses the problem of quantifying and minimizing errors due to the discretization of the equation of transfer. In particular the points a and b above applied to the DOM are addressed. Points c, d, e are also addressed for the case of the DTM.

1.6 DESCRIPTION OF TEST CASES

The cases used throughout this work are described in Table 1.1 and are shown in Figures 1.2 to 1.8. Case one represents a classic example of the type of enclosure where the DOM method has been used with constant temperature walls. Case two is intended to show a more realistic case. As will be shown in the following chapters, with case two, the three numerical problems of the Discrete Ordinates Method: the ray effect, false diffusion and false oscillations become evident. Case three is designed to illustrate the ray effect for two different quadrature schemes. Case four is similar to case number 2 except for the sloped surface. It is intended to test the performance of the DTM with non-rectangular geometries. Cases five and six are designed to test the short-wave capabilities of the DTM method. Finally case seven will illustrate the performance of the DOM and the DTM methods when more than one heat panel is present. In cases 1, 2, 3 and 5, the Radiosity Intensity Method is used as a benchmark.

Table 1.1 Summary of Test Cases

Case	Figure	Description
1	1.2	Cube with constant temperature on surfaces. ε =1.0 on all the walls. $T_{ceiling}$ = 300 K, T_{walls} = 200 K, T_{floor} = 100 K
2	1.3	Cube with heat panel on ceiling and one window
3	1.4	Cube at uniform temperature T = 298 K. Except for hot spot at T =330 K on the ceiling
4	1.5	Case 2 with a surface tilted 45 degrees
5	1.6	Case 2 with sunlit surface. G_{beam} = 300 W/m^2, G_{diff} = 50 W/m^2
6	1.7	Case 4 with sunlit surface. G_{beam} = 300 W/m^2, G_{diff} = 50 W/m^2
7	1.8	Case 2 substituting the 200 W/m^2 heat panel with two 100 W/m^2 heat panels

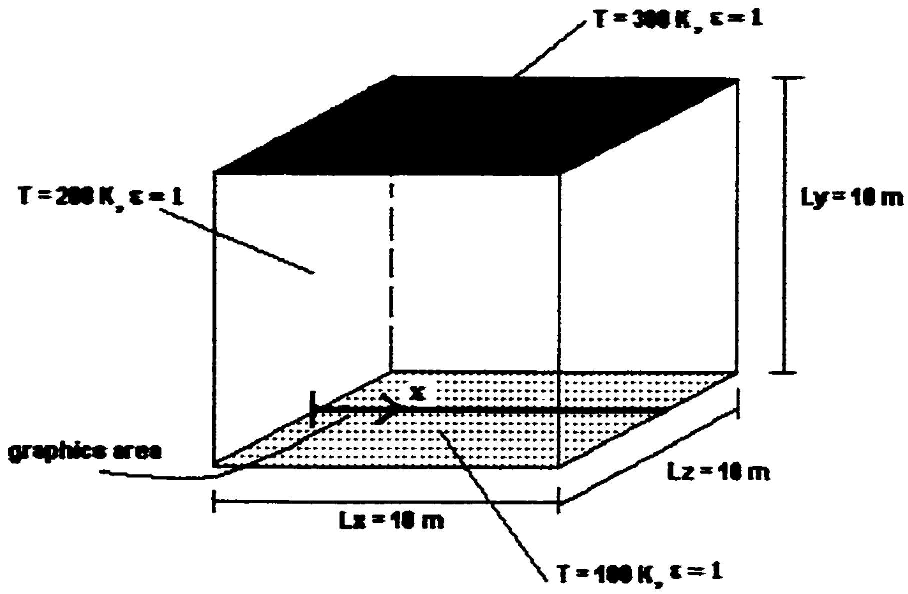

Figure 1.2 Case 1

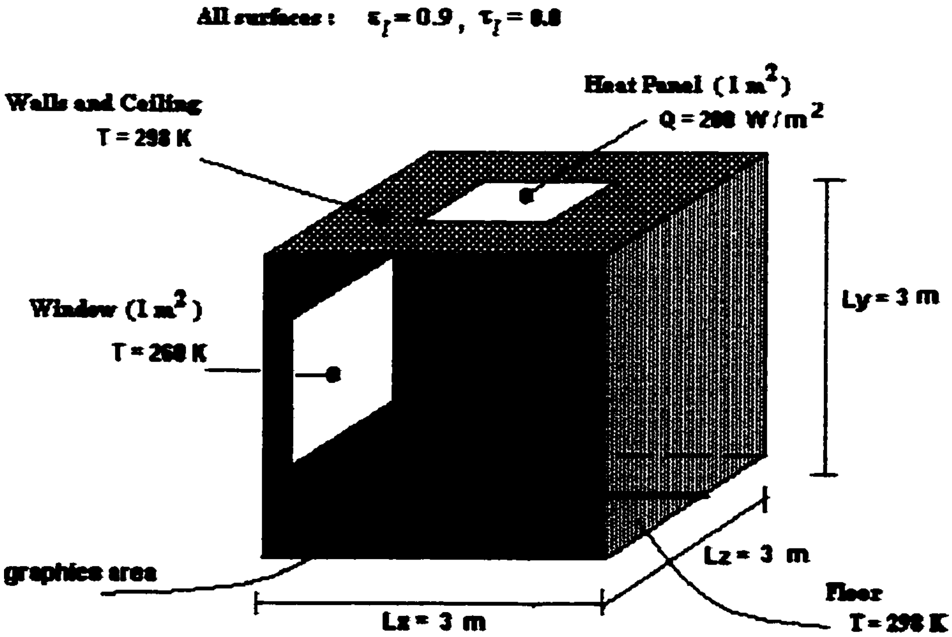

Figure 1.3 Case 2

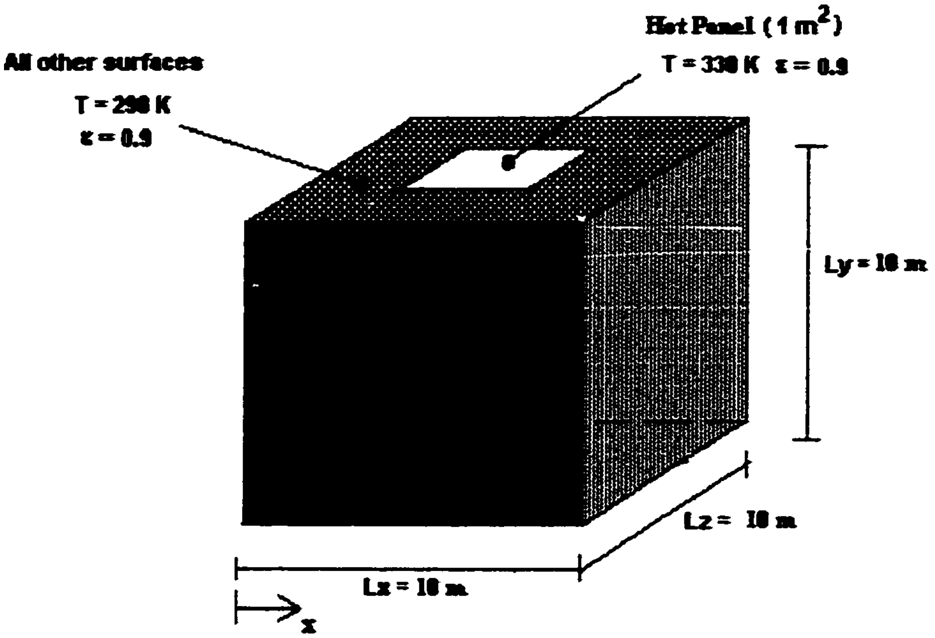

Figure 1.4 Case 3

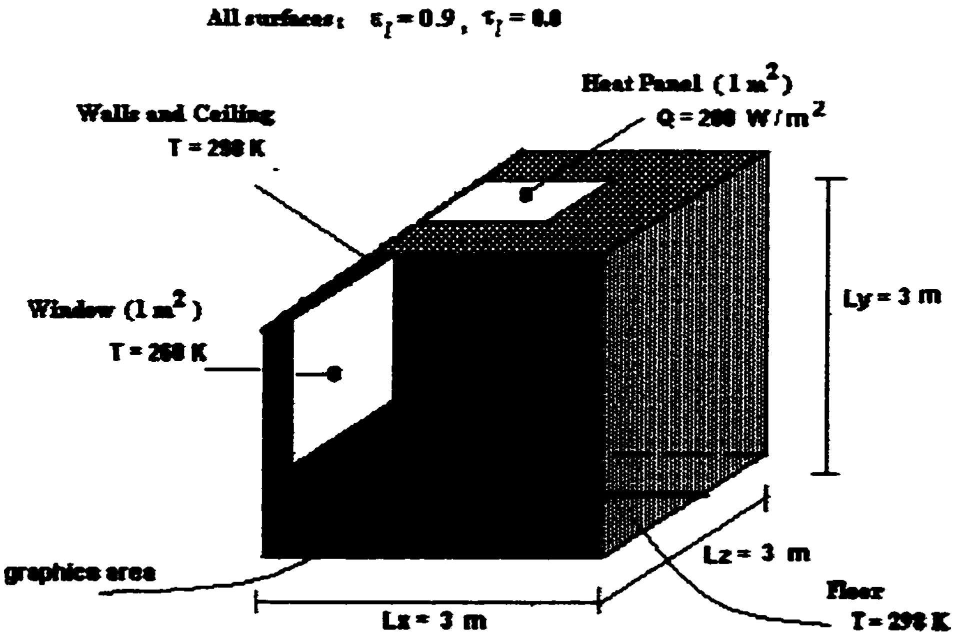

Figure 1.5 Case 4

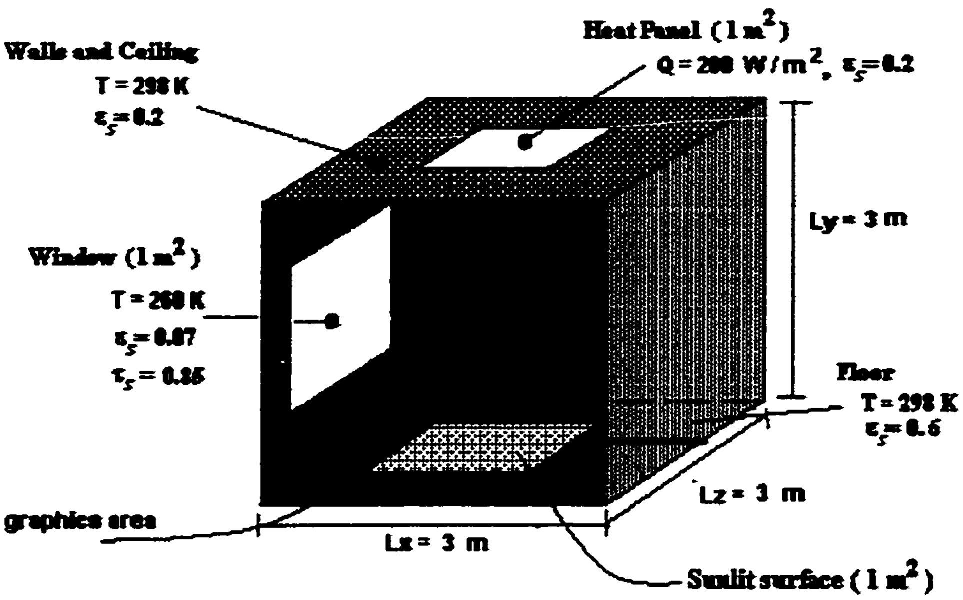

Figure 1.6 Case 5

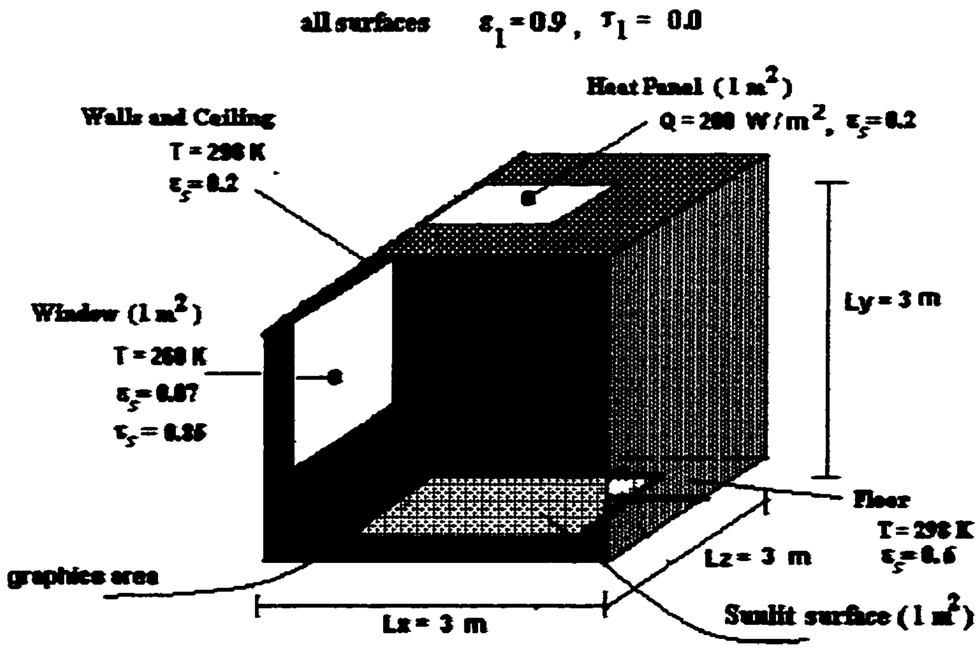

Figure 1.7 Case 6

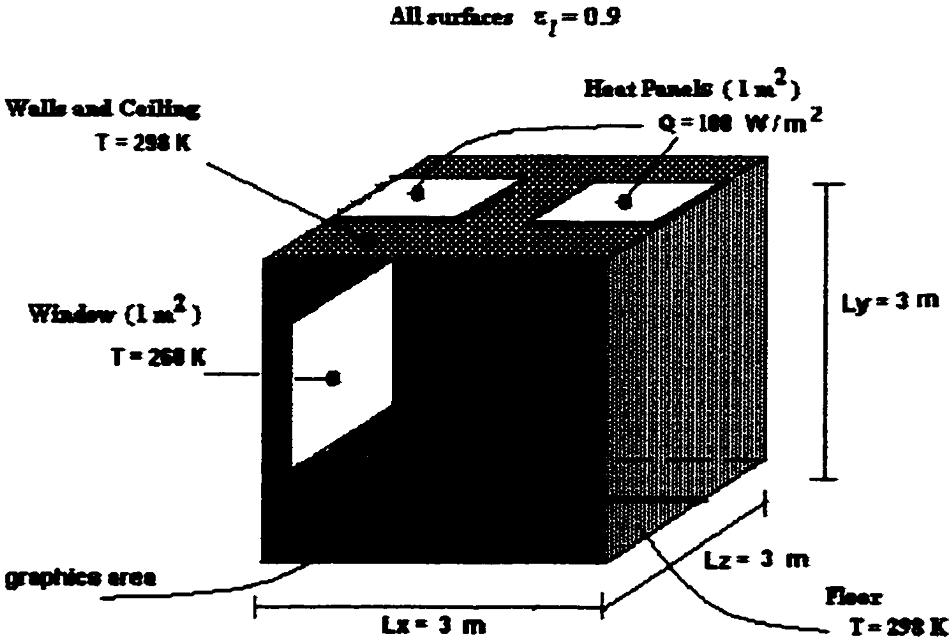

Figure 1.8 Case 7

Chapter 2

THE RADIOSITY INTENSITY METHOD

2.1 LONG WAVE RADIOSITY METHOD

The Radiosity Intensity Method (RIM) is extensively used throughout this work as a benchmark method. It has been described in a number of textbooks, for example, see Incropera & DeWitt (1996), and Siegel & Howell (1992). The RIM assumes that the enclosure is divided into n segments with the following characteristics:

a) Each segment is a gray and opaque body

b) Each segment is at a constant temperature

c) The radiosity over the element is constant

d) The media within the enclosure is assumed to be transparent.

Let us define the radiant heat, $Q_{rad\,i}$, as the net rate at which radiation leaves surface i and the radiant heat flux, $q_{rad\,i}$, as the radiant heat per unit area. $Q_{rad\,i}$ is equal to the difference between the total radiation leaving surface i (radiosity, J_i) and the total radiation impinging upon the same surface (irradiation, G_i):

$$Q_{radi} = A_i\left(J_i - G_i\right) \tag{2.1}$$

If $Q_{rad\,i} > 0$ the radiation leaving surface i is greater than the radiation that this surface is receiving. Therefore, some energy would need to be added, by means other than radiation, to keep the temperature of surface i from changing. If $Q_{rad\,i} < 0$ heat would need to be removed from the surface to maintain it at a constant temperature.

The radiosity of a surface, J_i, is equal to the energy emitted by this surface plus the total energy reflected by it. That is:

$$J_i = E_i + \rho_i G_i \tag{2.2}$$

or, in terms of black body emission:

$$J_i = \varepsilon_i E_{bi} + \left(1 - \varepsilon_i\right) G_i \tag{2.3}$$

The irradiation, G_i, represents the total radiative energy falling upon surface i. It can be determined from the radiosities of all the other surfaces on the enclosure:

$$A_i G_i = \sum_{j=1}^{n} F_{ji} A_j J_j \tag{2.4}$$

The term G_i can be eliminated from equations 2.1 and 2.3. If this is done an equation can be found that relates $Q_{rad\,i}$ to the emission of a black body at the same temperature, E_{bi}, and the radiosity, J_i:

$$Q_{radi} = \frac{\left(E_{bi} - J_i\right)}{\left[\left(1-\varepsilon_i\right) / \varepsilon_i A_i\right]} \tag{2.5}$$

In addition with the use of the reciprocity relation, equation 2.4 is substituted into equation 2.1 (and after some algebraic manipulation):

$$Q_{radi} = \frac{\sum_{j=1}^{n} \left(J_i - J_j\right)}{\left(A_i F_{ij}\right)^{-1}} \tag{2.6}$$

and by using 2.6 and 2.5:

$$\frac{(E_{bi} - J_i)}{\left\{\frac{(1-\varepsilon_i)}{\varepsilon_i A_i}\right\}} = \sum_{j=1}^{n} \frac{(J_i - J_j)}{(A_i F_{ij})^{-1}} \qquad (2.7)$$

Equations 2.6 and 2.7 can be used to construct a linear system of n by n equations where the unknowns are the radiosities J_i. There are three types of boundary conditions:

1) The radiant heat fluxes, $Q_{rad\,i}$, are known in all the segments. In that case equation 2.6 applied to every segment can be written as:

$$\begin{bmatrix} 1 & -F_{12} & -F_{13} \cdots & -F_{1n} \\ -F_{21} & 1 & -F_{23} \cdots & -F_{2n} \\ \vdots & & & \vdots \\ -F_{n1} & -F_{n2} & -F_{n3} \cdots & 1 \end{bmatrix} \begin{bmatrix} J_1 \\ J_2 \\ \vdots \\ J_n \end{bmatrix} = \begin{bmatrix} q_{rad1} \\ q_{rad2} \\ \vdots \\ q_{radn} \end{bmatrix} \qquad (2.8)$$

2) The temperatures, or equivalently, the black body radiant emission E_{bi}, are known in all the segments. In that case equation 2.7 can be written as:

$$\begin{bmatrix} 1/(1-\varepsilon_1) & -F_{12} & -F_{13} \cdots & -F_{1n} \\ -F_{21} & 1/(1-\varepsilon_2) & -F_{23} \cdots & -F_{2n} \\ \vdots & & & \vdots \\ -F_{n1} & -F_{n2} & -F_{n3} & 1/(1-\varepsilon_n) \end{bmatrix} \begin{bmatrix} J_1 \\ J_2 \\ \vdots \\ \vdots \\ J_n \end{bmatrix} = \begin{bmatrix} \varepsilon_1 E_{b1}/(1-\varepsilon_1) \\ \varepsilon_2 E_{b2}/(1-\varepsilon_2) \\ \vdots \\ \varepsilon_n E_{bn}/(1-\varepsilon_n) \end{bmatrix} \qquad (2.9)$$

3) The radiant heat flux is known in some segments and the temperature is known in the rest of them. In that case, a combination of 2.6 and 2.7 can be used to obtain the system of equations. For instance, if the radiant heat flux were specified in the first segment and the temperatures in the rest, the system of equations would look like:

$$\begin{bmatrix} \frac{1}{(1-\varepsilon_1)} & -F_{12} & -F_{13}\cdots- & F_{1n} \\ -F_{21} & 1 & -F_{23}\cdots- & F_{2n} \\ \vdots & & & \vdots \\ -F_{n1} & -F_{n2} & -F_{n3} & 1 \end{bmatrix} \begin{bmatrix} J_1 \\ J_2 \\ \vdots \\ \vdots \\ J_n \end{bmatrix} = \begin{bmatrix} \varepsilon_1 E_{b1} / (1-\varepsilon_1) \\ q_{rad2} \\ \vdots \\ q_{radn} \end{bmatrix} \tag{2.10}$$

In any case the final result will be a system of linear equations of the form:

$$\{Geo\}^{l}[J]^{l} = [BC]^{l} \tag{2.11}$$

The matrix $\{Geo\}^l$, depends only on the geometry of the enclosure and on its material properties, whereas the matrix $[BC]^l$ depends on the boundary conditions applied to the enclosure. With $\{Geo\}^l$ and $[BC]^l$ known, $[J]^l$, the matrix of radiosities, can be calculated. After that, the heat flux or the temperatures at each segment of the enclosure can be obtained using equations 2.6 and 2.7.

2.2) RADIOSITY TWO BAND MODEL

Siegel (1973) published a radiation method for enclosures involving partially transparent walls. Although the following short wave radiosity method was developed independently, it can be regarded as a simplified form of Siegel's model. In the following pages, the properties of windows are treated as given.

The majority of materials used in buildings have different radiative properties in different parts of the spectrum. In particular, they have different properties at the long-wave band resulting from the ambient temperature, around T = 300 K, and at the short-wave band resulting from solar radiation. Therefore it is convenient to use a two band model to be able to separate the effects of short and long wave radiation.

Although strictly speaking the model developed above works for gray bodies over the whole spectrum, it can also be used to obtain the long wave radiative heat transfer since almost all the radiation emitted by objects at room temperature has a wavelength $\lambda > 3\ \mu m$. Therefore, in the following paragraphs a RIM for short wave radiative heat transfer will be developed. The steps to be followed are analogous to the steps used to derive the RIM for the whole spectrum.

Let us assume that the radiant heat, $Q_{rad\,i}$ can be divided into long and short wavelength portions in the following way:

$$Q_{radi} = Q^{l}_{radi} \quad + \quad Q^{s}_{radi} \tag{2.12}$$

In order to calculate the short wave heat flux three kind of surfaces inside the enclosure have to be considered: windows, sunlit surfaces and "opaque" surfaces. By " opaque surfaces " we mean opaque surfaces with no direct sunlight falling upon them.

Before proceeding with the derivation some terms need to be defined. Referring to Figure 2.1 for the radiation heat transfer on a window:

.- I_{beam} is the direct solar radiation outside of the enclosure

.- I_{diff} is the diffuse solar radiation outside the enclosure

.- I_{sun} is total solar radiation impinging upon the outer part of the window. It is the summation of I_{beam} and I_{diff}

.- $G_{surf\,i}$ is the irradiation falling upon surface i, coming from the rest of the surfaces of the enclosure. That is:

$$G_{surf\,i} \quad = \quad \sum F_{ij}\, J_j \tag{2.13}$$

.- J_i is the radiosity coming from surface i to the interior of the enclosure. In the case of a window, J_i does include the diffusive solar radiation passing through the window, $\tau^{s}_{diff} I_{diff}$ but it does not include the solar beam radiation I_{beam}. Therefore, for a window:

$$J_i^s = \tau_{diff}^s I_{diff} + \rho^s G_{surf\,i} \tag{2.14}$$

All of the above quantities are short wave quantities. The short wave subscript s is dropped in order to make the presentation easier.

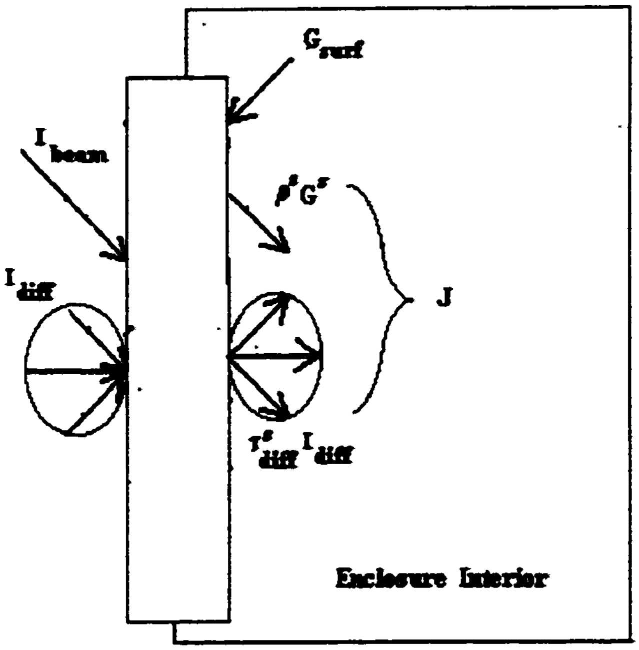

Figure 2.1 Short wave radiant fluxes in a window

The procedure to obtain the radiosity equations is similar to the procedure used in the long wave case: An energy balance is performed on each surface. In the short wave case there are three different cases:

CASE 1: WINDOWS

The short wave radiation balance of a window is (Figure 2.1):

$$q^{s}_{rad\,w} = J^{s}_{i} - G^{s}_{surf\,i} \qquad (2.15)$$

Using equation 2.13, $G_{surf\,i}$ can be eliminated from 2.15 and this equation can be put of the radiosities of all the surfaces in the enclosure:

$$q^{s}_{rad\,w} = \sum_{j=1}^{n} F_{ij}\left[J_i - J_j\right] \qquad (2.16)$$

On the other hand equations 2.14 and 2.13 can be directly substituted into equation 2.15:

$$q^{s}_{rad\,w} = \tau^{s}_{diff}\, I_{diff} - \left(1-\rho^{s}\right) G_{surf\,i} \qquad (2.17)$$

By matching equations 2.17 and 2.16, a relation between the radiosities, J_i and the boundary condition, I_{diff}, is finally obtained. Assuming for the moment that the window is surface number one the equation would read:

$$\tau^{s}_{diff}\, I_{diff} = J_1 - \rho_1 F_{12} J_2 - \rho_1 F_{13} J_3 \quad \cdots \quad -\rho_1 F_{1n} J_n \qquad (2.18)$$

CASE 2: SUNLIT SURFACE

For the other two kinds of surfaces, sunlit and opaque surfaces, the energy balance is an equation similar to 2.1:

$$Q_{rad\,i} = A_i\left(J_i - G_i\right) \qquad (2.19)$$

The radiosity in both cases is due just to reflected radiation:

$$J_i^s = \rho_i G_i \tag{2.20}$$

The total irradiation G $_i$ for sunlit surfaces is:

$$G_i = G_{surf\,i} + \tau_{beam}^s I_{beam} \cos(\theta_i) \tag{2.21}$$

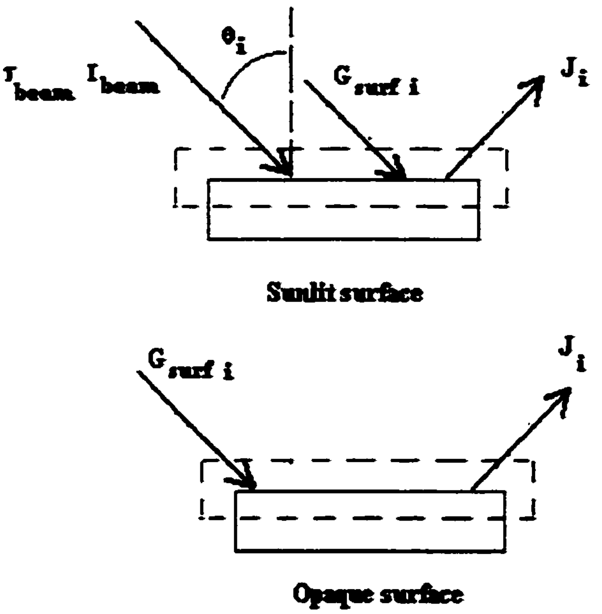

Figure 2.2 Short wave energy analysis for opaque and sunlit surfaces

Or using the definition of $G_{surf\,i}$:

$$G_i^s = \sum_{j=1}^{n} F_{ji} J_i + \tau_{beam}^s I_{beam}^s \cos(\theta_i) \tag{2.22}$$

The term, τ_{beam} represents the transmissivity of the window where the beam radiation passes through. Eliminating G_i from equations 2.19 and 2.20 :

$$q^s_{rad\,i} = -\frac{J^s_i\left(1-\rho^s_i\right)}{\rho^s_i} \qquad (2.23)$$

On the other hand, if equation 2.22 is used in equation 2.19 the following expression is found.

$$q^s_{rad\,i} = \sum_{j=1}^{n} F_{ij}\left(J^s_i - J^s_j\right) - \tau^s_{beam} I_{beam} \cos\left(\theta_i\right) \qquad (2.24)$$

If equation 2.23 is substitutes into the left-hand side of this equation, we arrive at the following equation:

$$\frac{-J^s_i\left(1-\rho^s_i\right)}{\rho^s_i} = \sum_{j=1}^{n} F_{ij}\left(J^s_i - J^s_j\right) - \tau^s_{beam} I_{beam} \cos\left(\theta_i\right) \qquad (2.25)$$

Rearranging this equation:

$$\tau^s_{beam} I_{beam} \cos\left(\theta_i\right) = J_1 - F_{12} J_2 - F_{13} J_3 \quad \cdots \quad - F_{1n} J_n \qquad (2.26)$$

Therefore, we have again a set of equations. If, for example, surface number one is a window and the rest of the surfaces are opaque or sunlit surfaces, the system of equations would be:

$$\begin{bmatrix} 1 & -\rho_1 F_{12} & -\rho_1 F_{13} \cdots - & \rho_1 F_{1n} \\ -F_{21} & & -F_{23} \cdots - & F_{2n} \\ \vdots & & & \vdots \\ -F_{n1} & -F_{n2} & -F_{n3} & 1 \end{bmatrix} \begin{bmatrix} J_{s1} \\ J_{s2} \\ \vdots \\ \vdots \\ J_{sn} \end{bmatrix} = \begin{bmatrix} G_{net} \\ G_{net} \\ \vdots \\ \vdots \\ G_{net} \end{bmatrix} \tag{2.27}$$

In these matrix equation G_{net} is the solar irradiation impinging onto point I without taking into consideration G_{surf}. The situation is summarized in Table 2.1

Table 2.1: Surface Characteristics in the Short Wave Band

Surface Type:	Window	Sunlit	Opaque
ρ_s :	$1-\varepsilon^s-\tau^s$	$1-\varepsilon^s$	$1-\varepsilon^s$
J :	$\tau_{diff} I_{diff} + \rho^s G_{surf}$	$\rho[G_{surf} + \tau_{beam} I_{beam} \cos(\theta)]$	$\rho^s G_{surf}$
G :	G_{surf}	$G_{surf} + \tau_{beam} I_{beam} \cos(\theta)$	G_{surf}
G_{net}:	$\tau_{diff} I_{diff}$	$\tau_{beam} I_{beam} \cos(\theta)$	0

As in the long wave case, this equation can be written as:

$$\{Geo\}^s[J]^s = [BC]^s \tag{2.28}$$

Notice that, in this case, the boundary conditions are not defined by temperatures or heat fluxes but, rather, by the incident solar radiation. After solving the system represented by equation 2.27 the short wave heat flux at each surface can be found by using equation 2.23.

To calculate the total heat flux the procedure outlined in Figure 2.3 can be followed. In this figure it is evident that the view factors need to be calculated just once. However the short and long wave systems of equations need to be computed separately since the matrices $\{Geo\}^s$ and $\{Geo\}^l$ are not equal. Therefore, if t_{vf} is the CPU time required to find the view factors and t_{se} is the time needed to solve the system of equations, the total time required to perform the calculation is:

$$total\_time \approx t_{vf} + 2t_{se} \tag{2.29}$$

With a parallel processor, the short and long wave systems of equations can be solved at the same time and therefore, the total time needed to perform the calculation would be equal to t_{vf} plus t_{se}.

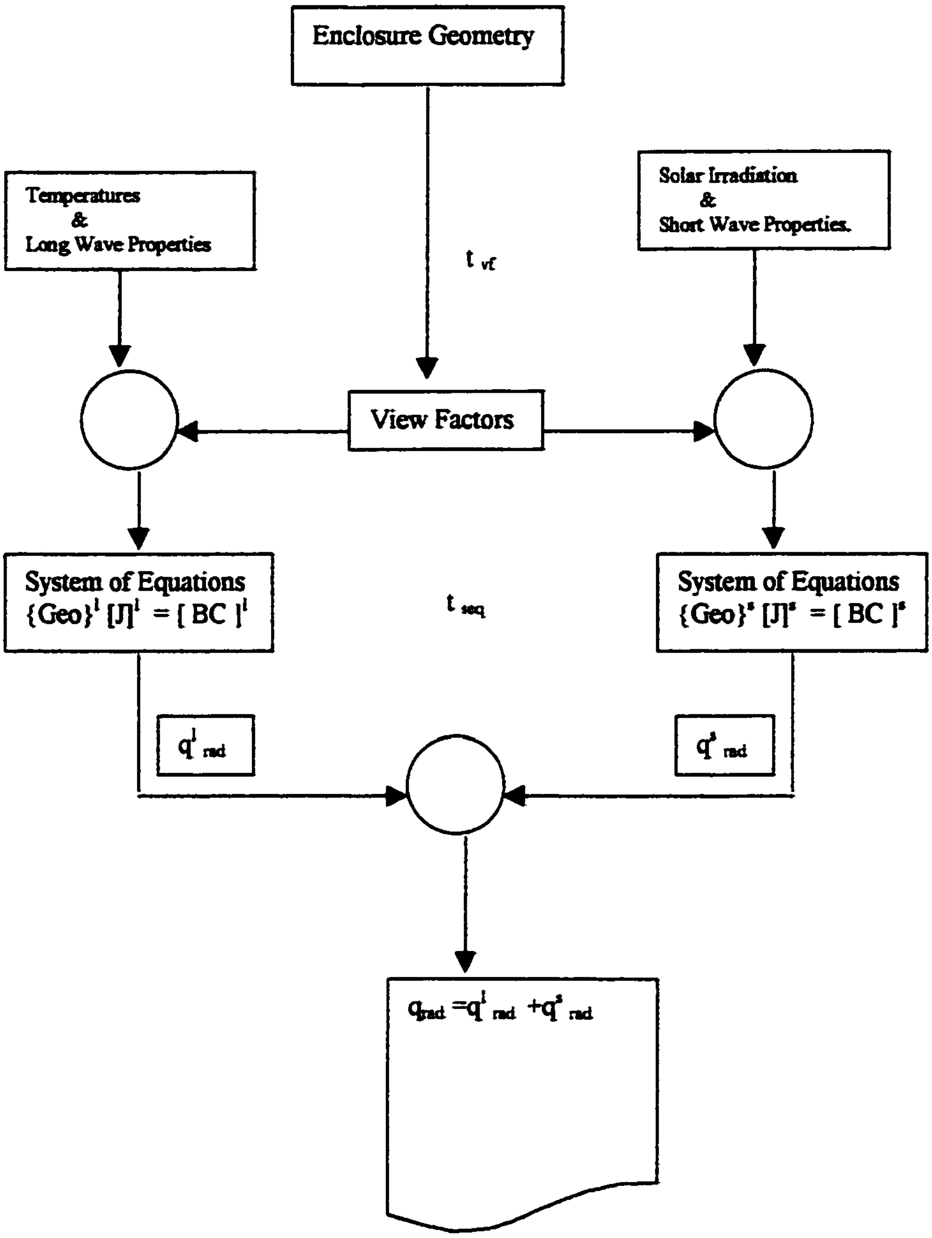

FIGURE 2.3. Complete heat flux calculation procedure

2.3) DISADVANTAGES OF THE RADIOSITY METHOD

The RIM is considered an accurate procedure to determine radiant heat fluxes in an enclosure. However the method has several disadvantages:

a) It is difficult to obtain view factors for complex configurations. A table of view factors is found in Howell (1982), and different methods to approximate this calculation are found in Shapiro (1985). In particular Ehlert & Smith (1994) published a set of equations to calculate F_{ij} between parallel and perpendicular parallelepipeds. This set of equations was used to calculate F_{ij} in this Thesis.

b) The RIM requires the solution of a large system of equations. In particular if the enclosure is a cube and if each side of the cube is divided in " n " segments, a system of size $6\ n^2 * 6\ n^2$ would have to be solved. This means that the size of the system of equations grows very rapidly. As an example if n = 6 the system would be 216 by 216. Thus the memory requirements grow as $36\ n^4$.

c) Note that even when every F_{ij} decreases as n increases, the matrix is not a sparse one and therefore the methods used to deal with sparse matrices cannot be applied. Furthermore, for large values of n (around n = 20) every F_{ij} is so small that the matrix needs to be renormalized (Curtis 1978) and double precision needs to be used. This requirement further increases the memory requirements of the method.

d) The CPU time needed to solve the system of equations grows exponentially as n increases (Figure 2.6).

2.4) CONVERGENCE TESTS

The RIM was used as a benchmark in cases 1 and 2. In order to do this a convergence test was performed for both cases. In Figure 2.4 the results of this test can be seen. Since in this case, the walls are assumed to be black bodies ($\varepsilon = 1$), their reflectivity equals zero and therefore their radiosity is equal to the emitted energy and does not depend on the irradiation. This is obvious in Figure 2.4 where the number of segments does not have any apparent significance in the results. On the other hand, for case number 2 shown in Figure 2.5, the radiosity of the surfaces does change over a wall at constant temperature and, therefore, it is important to divide the enclosure into a sufficient number of segments to obtain an accurate answer.

The CPU times required to run cases 1 and 2 for the long wave case are shown in Figure 2.6. This time is divided in two parts, the time needed to calculate the view factors and the time needed to solve the corresponding system of equations. This seems a convenient way to divide the CPU time because for an annual simulation the view factors would need to be calculated just once. The results shown in Figure 2.6 were produced in a PC computer at 333 MHz.

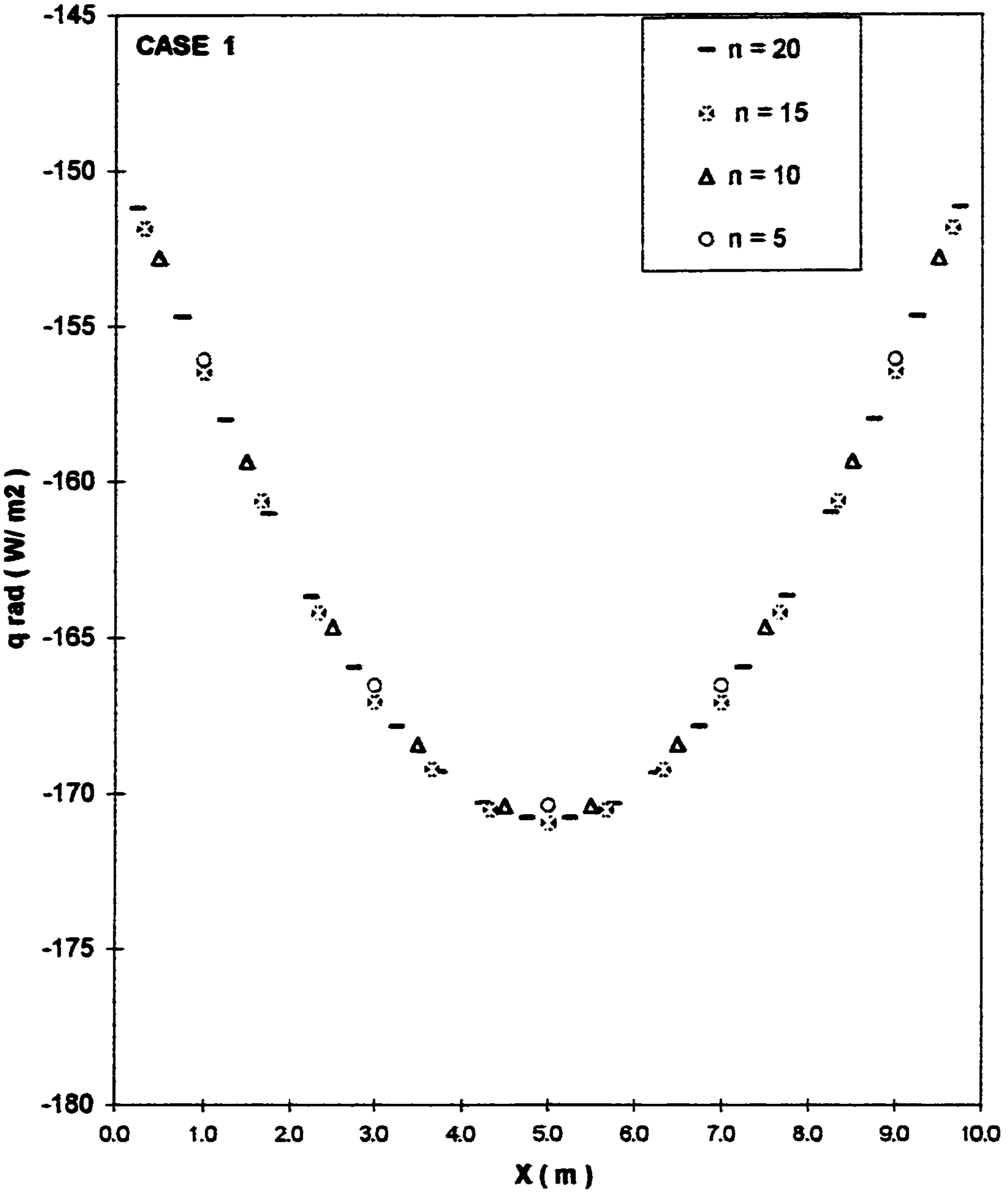

Figure 2.4 RIM convergence for case 1

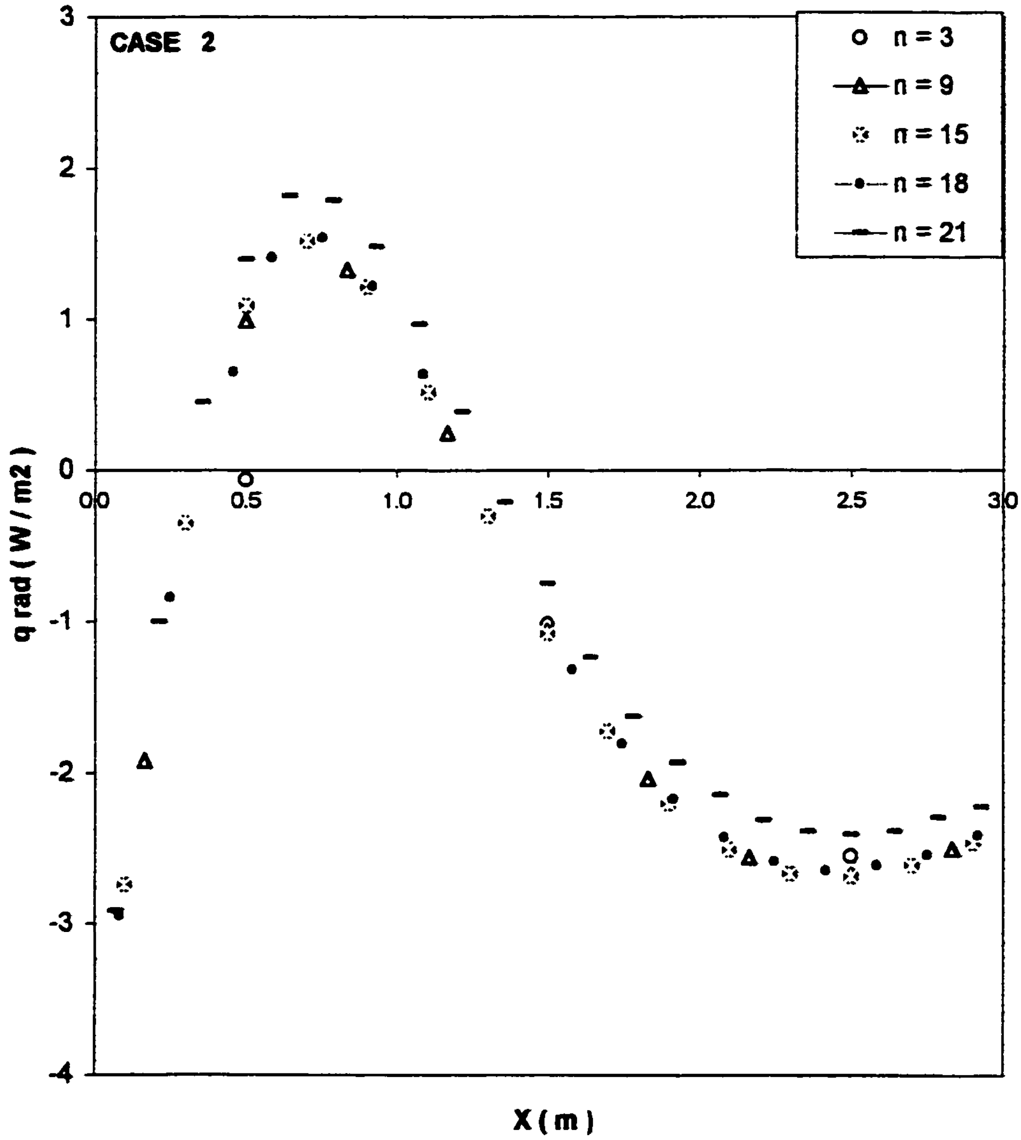

Figure 2.5 RIM convergence for case 2

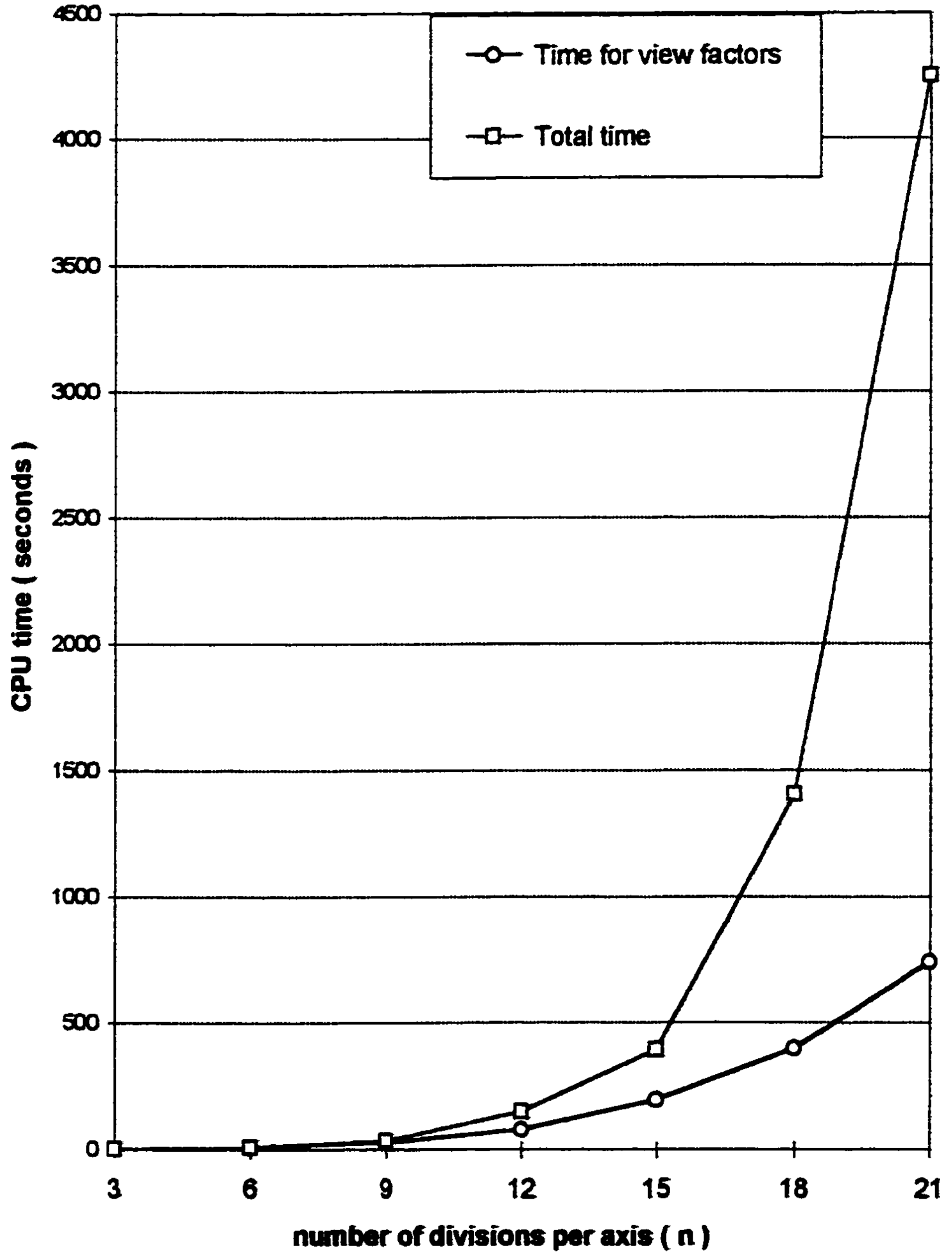

Figure 2.6 CPU time utilized by RIM

Chapter 3

DISCRETIZATION OF RADIATIVE TRANSFER: THE DISCRETE ORDINATES METHOD

3.1 THE EQUATION OF RADIATIVE TRANSFER

The change in intensity (I_λ) of a beam of wavelength λ, traveling inside a medium in a certain direction " S " is modeled by the equation of radiative transfer, as shown in Figure 3.1.

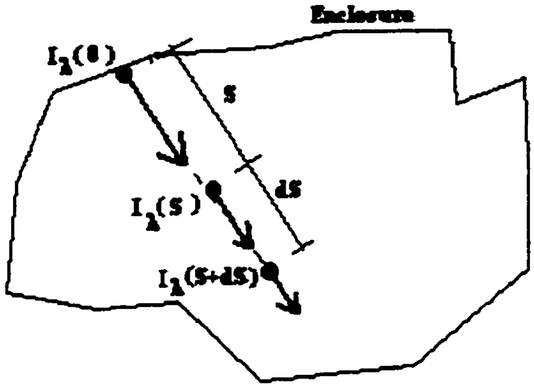

Figure 3.1 The equation of radiative transfer

According to Siegel & Howell (1992), a general form of the equation of transfer is:

$$\frac{\partial I_\lambda}{\partial S} = -\left(a_\lambda + \sigma_{s\lambda}\right) I_\lambda(S) + a_\lambda I_{b\lambda}(S) + \frac{\sigma_{s\lambda}}{4\pi}\int_{\Omega_i=0}^{4\pi} I_\lambda\left(S,\omega_i\right)\Phi\left(\lambda,\omega,\omega_i\right) d\Omega_i \qquad (3.1)$$

The left-hand side term is the change of intensity I_λ along the " S " direction within the solid angle $d\Omega$. The right-hand side represents the gain or loss of the intensity of the beam by scattering and/or absorption of radiation. a_λ is the absorption coefficient, $\sigma_{s\lambda}$ is the scattering coefficient and Φ is the phase function for scattering. In the special case of a non-participating medium all the terms on the RHS are zero. Therefore:

$$\frac{\partial I_\lambda^j}{\partial S} = 0 \tag{3.2}$$

Or, in Cartesian coordinates:

$$\mu\frac{\partial I_\lambda^j}{\partial x} + \eta\frac{\partial I_\lambda^j}{\partial y} + \xi\frac{\partial I_\lambda^j}{\partial z} = 0 \tag{3.3}$$

The superscript " j " stands for a particular direction. As shown in Figure 3.2, Ω (μ, η, ξ) is a unit vector parallel to the beam and μ, η and ξ are its direction cosines.

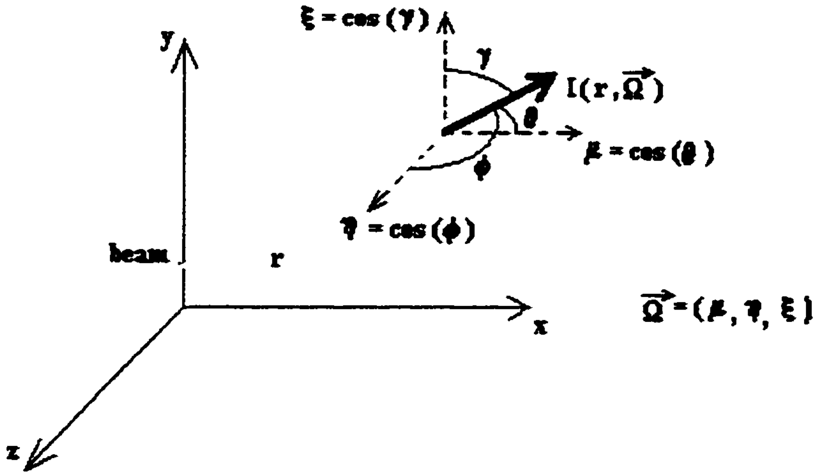

Figure 3.2 Specification of direction in the radiative transfer equation

RADIATION BOUNDARY CONDITIONS

In the infrared region of the spectrum all the surfaces in a building are opaque. The radiation intensity from an opaque surface is equal to the emitted intensity plus the reflected radiation. The radiative boundary condition including both emission and reflection is:

$$I_{\lambda,boundary} = \varepsilon_\lambda I_{b,\lambda} + \frac{\rho_\lambda}{\pi}\int_{n.\Omega\leq 0} \left| n \bullet \Omega \right| I_\lambda(\Omega')d\Omega' \tag{3.4}$$

The term **n.Ω** is the vector dot product . Note that the entire intensity field is needed in order to compute this boundary condition. In practice, this means that equation 3.2 has to be solved iteratively from the known boundary conditions. The known boundary conditions usually are either temperature or heat flux.

The irradiation at point r, $G_\lambda(r)$, defined as the radiation impinging upon a surface with normal unit vector **n** (Figure 3.3), is equal to the integral of the intensity over the surface solid angle.

$$G_\lambda(r) = \int_{n\bullet\Omega<0} \left| n\bullet\Omega \right| I_\lambda(\Omega)\, d\Omega \tag{3.5}$$

Note that the integral is performed only when $n.\Omega < 0$, i.e., when the beam is striking the surface. The heat flux, $q_{rad\,\lambda}(r)$, for a surface is the difference between radiosity and irradiation. For an opaque object, $q_{rad\,\lambda}$ is the net radiation leaving the surface. For a gray body:

$$q_{rad\lambda}(r) = \pi\varepsilon_\lambda I_{b\lambda} - \varepsilon_\lambda \int_{n.\Omega<0} \left| n\bullet\Omega \right| I_\lambda(\Omega)\, d\Omega \tag{3.6}$$

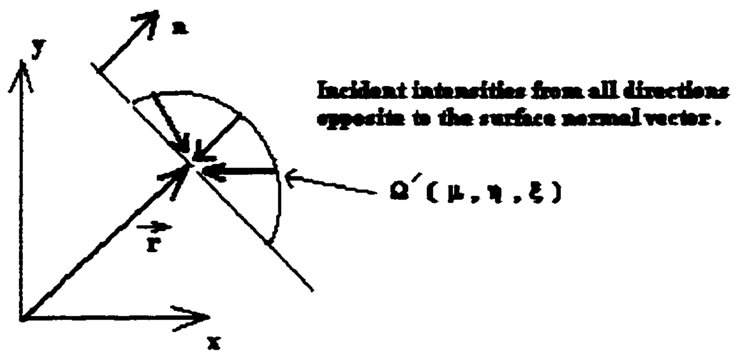

Figure 3.3 Beams striking a surface

THE MEAN RADIANT TEMPERATURE

The mean radiant temperature (T_{mrt}) can be defined in relation to any body or surface. Since we are interested in the pointwise calculation of the mean radiant temperature, we choose as our object an infinitesimal sphere anywhere inside a room. In this case, the mean radiant temperature would be defined as (Fanger,1972) : " that uniform temperature of black surroundings which will give the same radiant heat loss from an infinitesimal sphere as the actual case under study ".

Thus, as shown in Figure 3.4, the real distribution of intensity radiation around the sphere in question has to be replaced by a uniform mean. This mean intensity is calculated as an angular average :

$$\overline{I}(r) = \frac{1}{4\pi}\int_0^{\infty}\int_0^{4\pi} I_\lambda(\lambda,\Omega)\,d\Omega\,d\lambda \tag{3.7}$$

If, as the above definition demands, it is assumed that this intensity comes from a black enclosure, the mean angular intensity would be equal to:

$$\overline{I}(r) = \frac{\sigma T_{mrt}^4}{\pi} \tag{3.8}$$

Combining equations 3.7 and 3.8. We can now compute Tmrt as shown in equation 3.9.

$$T_{mrt}^4 = \frac{1}{4\sigma}\int_0^\infty \int_0^{4\pi} I_\lambda(\lambda,\Omega)\, d\Omega\, d\lambda \tag{3.9}$$

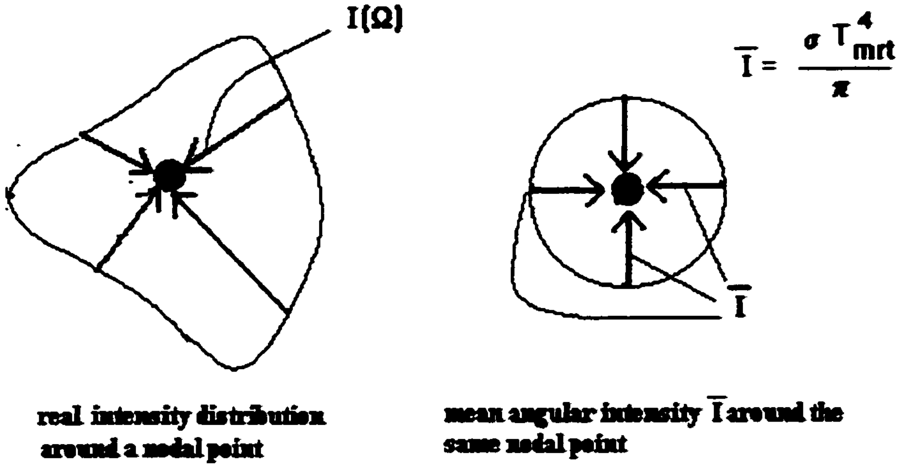

Figure 3.4 Mean radiant temperature calculation using the DOM

3.2 TWO-BAND MODEL

The equations shown above are valid, strictly speaking, for a particular wavelength, λ. If as in the case of a grey body, the radiative properties of the materials involved are kept constant, equations 3.4, 3.5 and 3.6 could be integrated over the whole spectrum to obtain analogous equations valid for the whole range of wavelengths.

As was noted by Li and Fuchs in 1992, it is often convenient when dealing with buildings to divide the radiation in a short wave band with $\lambda < 3$ μm and a long wave band with $\lambda > 3$ μm. The reason for this resides in the fact that normally, the short wave and the long wave properties of building materials are very different.

Therefore equation 3.4 can be integrated in two parts as follows:

$$I_{boundary} = \int_0^{3\mu m} I_\lambda d\lambda + \int_{3\mu m}^{\infty} I_\lambda d\lambda \tag{3.10}$$

The wavelength $\lambda = 3$ μm is used as a division line between long and short wavelengths because objects at room temperature emit no appreciable radiation at $\lambda < 3$ μm. At the same time almost all solar radiation is emitted at $\lambda < 3$ μm. Therefore there is no significant overlap between the two bands. Thus the first integral on the above equation can be called short- wave intensity, I^s, whereas the second one is called the long wave intensity, I^l.

SHORT WAVE BOUNDARY CONDITIONS

There are three different kind of surfaces to be considered: opaque surfaces, windows and sunlit surfaces. By " Opaque surfaces " it is meant opaque surfaces with no sunlight falling upon them.

CASE 1 SUNLIT AND OPAQUE SURFACES

Sunlit and opaque surfaces do not emit significant radiation in the short wave part of the spectrum, therefore the intensity leaving from their surfaces is just the reflected irradiation falling upon them:

$$I^s_{boundary} = \frac{\rho^s}{\pi} G^s \tag{3.11}$$

As shown in Figure 3.5 two kinds of irradiation need to be considered for this type of surfaces. First there is the radiation falling upon surface i coming from the rest of the surfaces in the enclosure, $G_{surf\,i}$. This radiation is falling upon the three kinds of surfaces considered and it is equal to:

$$G_{surf\,i} \;=\; \int\limits_{n.\Omega<0} \left| n \bullet \Omega \right| I^s(\Omega)\, d\Omega \qquad (3.12)$$

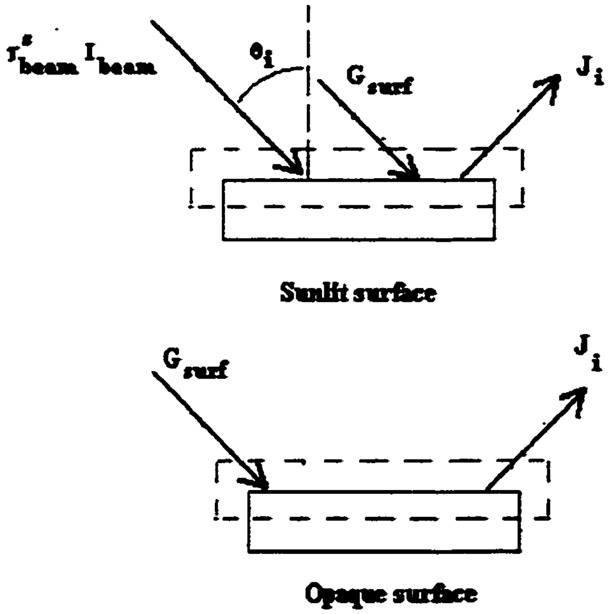

Figure 3.5 Shortwave energy analysis for opaque and sunlit surfaces

The second type of irradiation that needs to be considered, is solar beam radiation , $\tau_{beam} I_{beam}$. This radiation defines a sunlit surface. In summary for opaque surfaces:

$$G_i^s \;=\; G_{surf\,i} \qquad (3.13)$$

And for sunlit surfaces:

$$G_i^s = \tau_{beam}^s I_{beam} \cos(\theta_i) + G_{surf\,i} \tag{3.14}$$

In both cases the surface i heat flux, $q_{rad\,i}$, is equal to the radiation leaving the surface, $\pi I(r)$ in equation 3.11 , minus the irradiation, G^s falling upon that surface. Therefore:

$$q_{rad}^s(r) = -\varepsilon^s G^s \tag{3.15}$$

CASE 2: WINDOWS

Although windows do not emit significant radiation in the short wave part of the spectrum, they may be considered sources of the diffuse radiation passing through them, therefore in this case:

$$I_{boundary}^s = \frac{\tau_{diff}^s I_{diff}}{\pi} + \frac{\rho^s}{\pi} G^s \tag{3.16}$$

It is important to note that in the above equation, $I_{boundary}$ has been redefined as the intensity leaving surface I towards the interior of the enclosure and without considering direct solar radiation. As explained above, direct solar radiation is considered as irradiation for sunlit surfaces. The redefinition just given, as well as all the short wave energy fluxes striking a window, are shown in Figure 3.6.

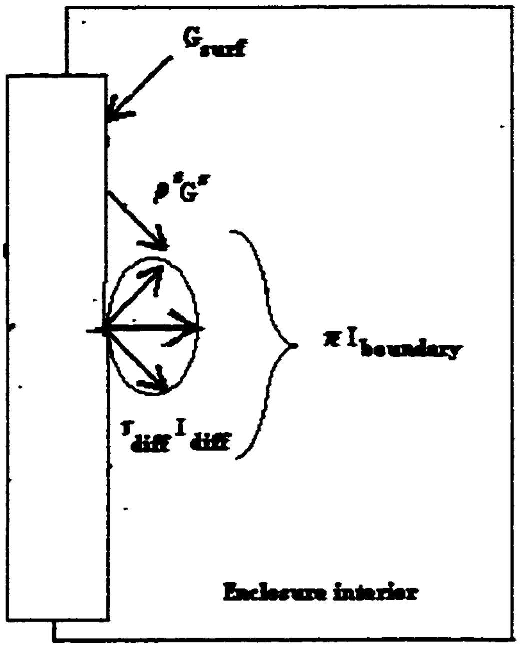

Figure 3.6 Short wave radiant heat fluxes in a window

The irradiation, G^s, in the case of a window is also redefined as the radiation coming from the interior of the enclosure, falling upon the window. Therefore, as in the case of opaque surfaces, G^s is equal to G_{surf} defined in equation 3.10.

As in the other cases, for a window the heat flux is equal to the radiosity minus the irradiation. The use of figure 3.6 to perform an energy balance in the window gives the following result after some algebraic manipulation:

$$q^s_{rad}(r) = -\varepsilon^s \, G^s \tag{3.17}$$

The following table is a summary of properties and boundary conditions for the equation of transfer in the short wave band.

Table 3.1 Short Wave Boundary Conditions

Boundary Conditions	Window	Sunlit	Opaque
ρ^s:	$1-\varepsilon^s-\tau^s$	$1-\varepsilon^s$	$1-\varepsilon^s$
$I_{boundary\ s}$	$(\tau_{diff} I_{diff} + \rho^s G^s)/\pi$	$\rho^s G^s/\pi$	$\rho^s G^s/\pi$
G^s:	G_{surf}	$\tau_{beam} I_{beam}\cos(\theta)+G_{surf}$	G_{surf}
q^s	$-\varepsilon^s G^s$	$-\varepsilon^s G^s$	$-\varepsilon^s G^s$

For simplicity, the description of the Discrete Ordinates Method that follows will be made for the long wave part of the spectrum. The modifications needed to take into account the short wave region will be discussed in section 3.5.

3.3 THE DISCRETE ORDINATES METHOD

The Discrete Ordinates Method (DOM) is a mathematical technique that converts the continous equation of transfer to a discrete form. The main idea of the DOM is to obtain the intensity field by solving the equation of transfer by a double discretization process. (Figure 3.7). The first discretization is an angular one where a finite number of directions are chosen, and equation 3.1 is solved for each of these directions. The second discretization is a spatial discretization over the enclosure volume. Following is a brief description of the DOM method. In Chapter 4 a more comprehensive discussion is offered.

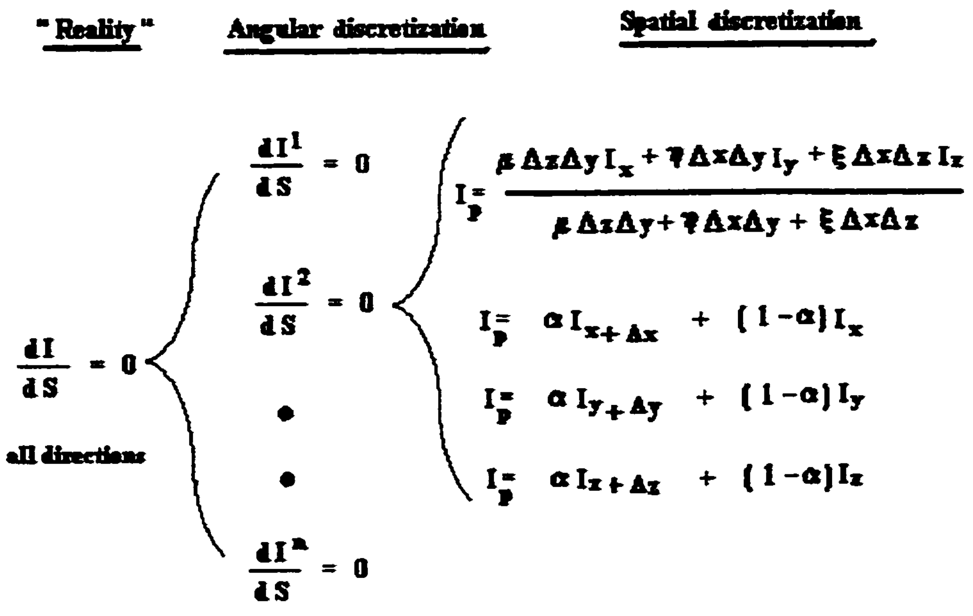

Figure 3.7 DOM double discretization process

DOM ANGULAR DISCRETIZATION

Any function f (x) can be integrated numerically by the following procedure:

$$\int_a^b f(x)dx = \sum_i f(x_i)\omega_i \tag{3.18}$$

The summation is performed over some of the points in the interval (a, b). The accuracy of the approximation depends on how the points and the weights assigned to those points (ω_i) are selected. If the above procedure were applied to the angular integrals on the equation of transfer (3.1) and the boundary conditions we would have:

$$I_{\lambda,boundary} = \varepsilon_\lambda I_{b,\lambda} + \frac{\rho_\lambda}{\pi} \sum_{n.\Omega<0} |n\bullet\Omega| I_j^\lambda \omega_j \tag{3.19}$$

The summation is performed over the specified angular direction (" j "). In the same manner the discretization of equations (3.6) and (3.9) take the following form:

$$q_{rad}^l(r) = \varepsilon^l \sigma T^4 - \varepsilon^l \sum_{n\bullet\Omega<0} |n\bullet\Omega| I_j^l \omega_j \tag{3.20}$$

$$T_{mrt}^4 = \frac{1}{4\sigma} \sum I_j \omega_j \tag{3.21}$$

The particular μ_j and ω_j chosen constitute a quadrature set. It has a substantial effect on the final results. In Chapter Four the criteria used to obtain these sets as well as their relative merits will be discussed.

DOM SPATIAL DISCRETIZATION

The DOM uses finite difference techniques. The space inside the enclosure is divided into elemental volumes of sides: Δx, Δy and Δz. The aim is to calculate the intensity at every point P, the center of the differential volume (Figure 3.8). Equation 3.3 has to be solved for each direction "j ". In the Cartesian version, this equation for a particular direction is integrated by assuming that the intensity on each of the six faces of an elemental cube, remain constant.

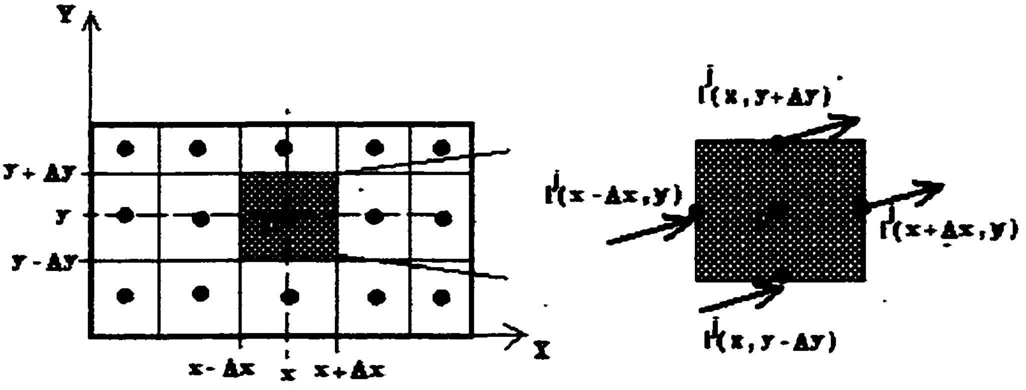

Figure 3.8 A 2-D slice of a grid for the DOM

That is, for each elemental volume, the integral

$$\int_{x-\Delta x}^{x+\Delta x}\int_{y-\Delta y}^{y+\Delta y}\int_{z-\Delta z}^{z+\Delta z}\left[\mu\frac{\partial I_\lambda}{\partial x}+\eta\frac{\partial I_\lambda}{\partial y}+\xi\frac{\partial I_\lambda}{\partial z}\right]dx\,dy\,dz=0 \tag{3.22}$$

is approximated by :

$$\mu^j\Delta z\Delta y\left(I^j_{x+\Delta x}-I^j_{x-\Delta x}\right)+\eta^j\Delta x\Delta y\left(I^j_{z+\Delta z}-I^j_{z-\Delta z}\right)+\xi^j\Delta x\Delta z\left(I^j_{y+\Delta y}-I^j_{y-\Delta y}\right)=0 \tag{3.23}$$

This particular way of discretising the equation of transfer is preferred because it treats the intensity as a conservative quantity (that is, in the absence of sinks or sources), and it allows other modes of heat transfer to be included (Patankar 1984). This equation represents the conservation of energy for a particular direction, and it relates the six different intensities found at the borders of each cell. The equation is not sufficient, however, to find the intensity field since there are still three unknowns : $I_{x+\Delta x}$, $I_{y+\Delta y}$ and $I_{z+\Delta z}$, given the upstream intensities $I_{x-\Delta x}$, I

$I_{y-\Delta y}$ and $I_{z-\Delta z}$. To get around this difficulty, the value of intensity at the center of the cell (I_p) is assumed to be bounded by the intensities at the border. That is

$$I_p^j = \alpha_x I_{x+\Delta x}^j + (1-\alpha_x) I_{x-\Delta x}^j$$

$$I_p^j = \alpha_y I_{y+\Delta y}^j + (1-\alpha_y) I_{y-\Delta y}^j \tag{3.24}$$

$$I_p^j = \alpha_z I_{z+\Delta z}^j + (1-\alpha_z) I_{z-\Delta z}^j$$

The alphas, α_x, α_y and α_z are interpolation constants whose values are chosen to be between 0.5 and 1. The α notation is traditionally used in the DOM literature. If $\alpha_x = \alpha_y = \alpha_z$ the substitution of equation 3.24 into equation 3.23 is:

$$I_p^j = \frac{\mu \Delta y \Delta z\, I_{x-\Delta x}^j + \eta \Delta x \Delta y\, I_{y-\Delta y}^j + \xi \Delta y \Delta z\, I_{z-\Delta z}^j}{\mu \Delta y \Delta z + \eta \Delta x \Delta y + \xi \Delta y \Delta z} \tag{3.25}$$

This is the intensity at point " P " in the " j " direction. If $\alpha = 0.5$ then we are assuming a linear relationship for intensity inside each elemental volume. According to Lathrop (1969) the diamond differencing, as it is called, is of the order of h^2 where h is the grid spacing. On the other hand, if $\alpha = 1$ (step differencing) the scheme is of the order of h. In practice the diamond differencing produces spurious spatial oscillations that, as demostrated by Chai, Lee & Patankar (1994), cannot be removed by any degree of grid refinement. In particular it may produce negative intensities which are physically unrealistic and need to be corrected. The step difference scheme ($\alpha = 1$) is not susceptible to spatial oscillations. However it produces the maximum degree of false scattering which is another numerical problem that diminishes the accuracy of the solution.

In the early years of DOM development, the problem of negative intensities was solved by simply setting negative intensities equal to zero (Fiveland 1984). This procedure, however, violates conservation of energy because equation 3.25 was obtained by assuming the same value of alpha in the three directions. If alpha is changed in a particular direction this is equivalent to changing an intensity at the boundary of a cell arbitrarily. Smith & Sanchez (1992) incremented alpha until a non-zero intensity was found. In this way, energy was conserved but the problem of spatial oscillations was not solved. This problem of spatial oscillations is addressed later in this work.

DOM LONG WAVE SOLUTION PROCEDURE

I. Initially, the boundary surface intensity is assumed to result from only emitted radiation, so the reflectivity in equation 3.19 is set to zero.

$$I^{i}_{boundary} = \varepsilon^{i} I^{i}_{b} + \frac{\rho^{i}}{\pi} \sum_{n.\Omega<0} \left| n \bullet \Omega \right| I^{i}_{j}\, \omega_{j} \tag{3.19}$$

II. Beginning with the first angular direction j, equation 3.25 is used to calculate the intensity I_p throughout the interior of the enclosure and at the surfaces that this particular beam strikes. The next angular direction is chosen and the calculation procedure repeated until all of the discrete directions are computed.

$$I^{j}_{p} = \frac{\mu \Delta y \Delta z\, I^{j}_{x-\Delta x} + \eta \Delta x \Delta y\, I^{j}_{y-\Delta y} + \xi \Delta y \Delta z\, I^{j}_{z-\Delta z}}{\mu \Delta y \Delta z + \eta \Delta x \Delta y + \xi \Delta y \Delta z} \tag{3.25}$$

III. The intensity at the boundaries is recalculated using equation 3.19 incorporating the known boundary conditions plus the intensities calculated in step number II. If the difference between the boundary intensities and the previous values is less than a predetermined limit, the calculation is assured to be converged.

IV. At this point the whole intensity field is known. By applying equations 3.20 & 3.21 local heat fluxes can be calculated at any surface and mean radiant temperatures computed at each nodal point inside the enclosure.

$$q^{l}_{rad}(r) \;=\; \varepsilon^{l}\,\sigma T^{4} \;-\; \varepsilon^{l} \sum_{n\bullet\Omega<0} \left|n\bullet\Omega\right| I^{l}_{j}\,\omega_{j} \tag{3.20}$$

$$T^{4}_{mrt} = \frac{1}{4\sigma}\sum I_{j}\,\omega_{j} \tag{3.21}$$

DOM SHORT WAVE SOLUTION PROCEDURE

In order to take into account short wave radiation, the following modifications would need to be done to the above procedure.

I. The initial short wave intensities leaving a boundary, $I_{boundary}$, can be estimated using Table 3.1 and assuming $G_{surf} = 0$.

II. As with the case of long wave radiation, equation 3.25 is used to obtain the short wave intensities at the interior of the enclosure. Therefore, for a complete calculation, these equations have to be solved twice for each direction, once for the long wave and the second time for the short wave case.

III. Calculate G_{surf} using the discrete form of equation 3.12.

$$G_{surf}(r) = \sum_{n.\Omega'<0} \left| n \bullet \Omega' \right| I_j^s \omega_j \qquad (3.26)$$

IV Recalculate the short wave intensity at the boundaries, $I_{boundary}$. This is done by using table 3.1. If the difference between the boundary intensities and the previous values is less than a predetermined limit, the calculation is assured to be converged.

V At this point the whole intensity field is known. By using the appropiate equations from table 3.1, local heat fluxes can be calculated at any surface.

DOM TREATMENT OF IRREGULAR GEOMETRIES

One of the advantages of the DOM method over zone methods such as the Radiosity Intensity method (RIM) is its capacity to work with irregular geometries both on the boundaries and within the enclosure. Yet not many papers can be found that deal with this issue. In Chai et al. (1993b) procedure, nominal domains are drawn around given physical domains as shown in Figure 3.9.

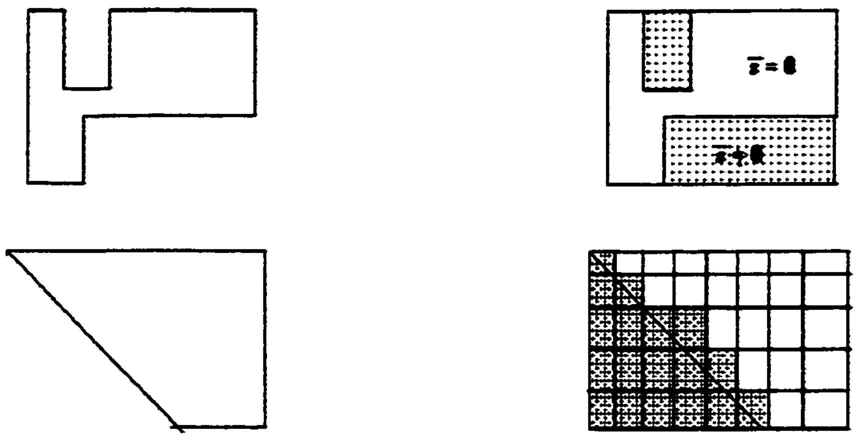

Real domains   Simulated domains

Figure 3.9 DOM treatment of irregular domains

The active regions, where the intensity solution is sought, are unshaded in the figure. The inactive regions, the shaded ones which represent slopes or obstacles, are those where the solution is not meaningful although they are included to obtain a rectangular domain. Chai et al. (1993), incorporate irregular geometry by introducing an artificial source term to the equation of transfer. For transparent media, we have:

$$\mu \frac{\partial I_\lambda}{\partial x} + \eta \frac{\partial I_\lambda}{\partial y} + \xi \frac{\partial I_\lambda}{\partial z} = \bar{S} \tag{3.27}$$

$$\bar{S} = S_C + S_P I_p \tag{3.28}$$

The discrete form of of these equations is:

$$I_p = \frac{\mu \Delta y \Delta z \, I_x^J + \eta \Delta x \Delta y \, I_y^J + \xi \Delta y \Delta z \, I_z^J + S_c \, \alpha \, \Delta x \, \Delta y}{\mu \Delta y \Delta z + \eta \Delta x \Delta y + \xi \Delta y \Delta z - S_p \, \Delta x \, \Delta y} \tag{3.29}$$

S_p and S_C are constants and S_p is negative (Patankar 1980). S_c and S_p are zero in the active regions. In the inactive regions S_c and S_p should be chosen to meet appropriate conditions and α, the interpolation constant, should be made equal to one. If there are inclined or curved boundaries, these boundaries will be approximated by ladder-like lines. Chai, Lee & Patankar implemented the method in 2-D geometries and although the extrapolation to the third dimension should be straight forward, the author does not know of any study in this respect. Beckner and Howell (1997) proposed a modification. Instead of considering every cell as either completely in the active region or completely in the inactive region they represent the geometry information of each cell as volume fractions in such a way that a 1 is assigned to cells completely in the active region and a 0 to the cells completely in the inactive region.

3.4 THE SHORTCOMINGS OF THE DISCRETE ORDINATES METHOD

As Chai, Lee & Patankar (1993) recognized, the Discrete Ordinates Method (DOM) has four main shortcomings:

1) Excessively long computational time in optically thick media
2) Ray effect
3) False Scattering
4) False Oscillations

The first shortcoming applies to enclosures filled with an absorbing and/or scattering media. Since this does not apply to buildings, it will not be mentioned any further. The next three need to be discussed separately.

RAY EFFECT

The ray effect is a false oscillation in the computed flux due to coarse angular divisions failing to detect complex boundary conditions. Even assuming that the equation of transfer (equation 3.1) could be solved exactly for any direction " j ", the radiation, which is really a continuous variable, is represented by a finite number of beams in the DOM. To illustrate the ray effect, consider a two-dimensional black enclosure with a non-participating medium and cold surfaces everywhere except in a small and hot region as shown in Fig 3.10.

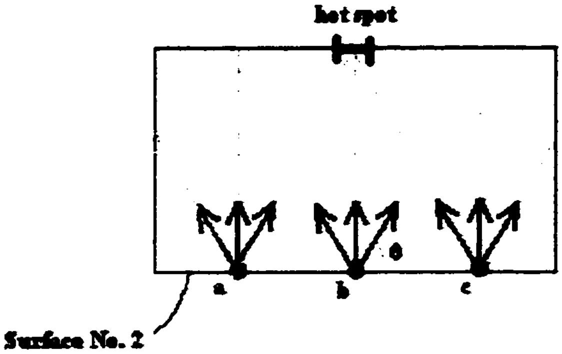

Figure 3.10 The ray effect

Consider the intensity received by surface # 2 coming from the hot spot. If a " DOM " detector were to be used, it could be pointed only to certain directions. As an example, let those directions be θ = 60, 90 and 120 degrees as shown in Figure 3.10. This means that at points a, b and c radiation from the hot spot would be detected, but at all other locations on surface 2, the DOM detector would fail to detect the radiation from the hot spot. More precisely, if the local heat flux is desired at every point on surface # 2, equation 3.20 could be used. Applying it at point a, b and c the result would be:

$$q_a = -\omega_1 I_1 \cos\left(\frac{\pi}{2} - \theta_1\right)$$

$$q_b = -\omega_2 I_2 \cos\left(\frac{\pi}{2} - \theta_2\right) \tag{3.30}$$

$$q_c = -\omega_3 I_3 \cos\left(\frac{\pi}{2} - \theta_3\right)$$

If a graph of the local heat flux were made it would look like:

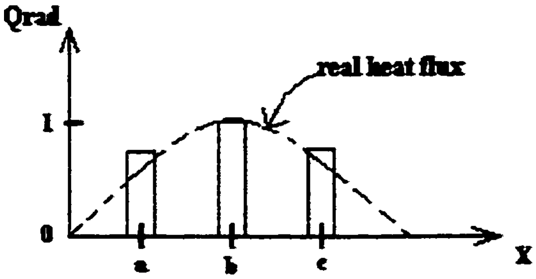

Figure 3.11 The ray effect in transparent media

The ray effect thus produces oscillations in the local heat flux received at a surface. Note, also that if the weighting factors, ω_i, are not equal, this effect could be aggravated.

The wavelength, ΔS, of the oscillations in this 2-D example may be calculated as shown in Figure 3.12. This calculation could be used to separate the ray effect oscillations from the oscillations caused by the spatial discretization scheme.

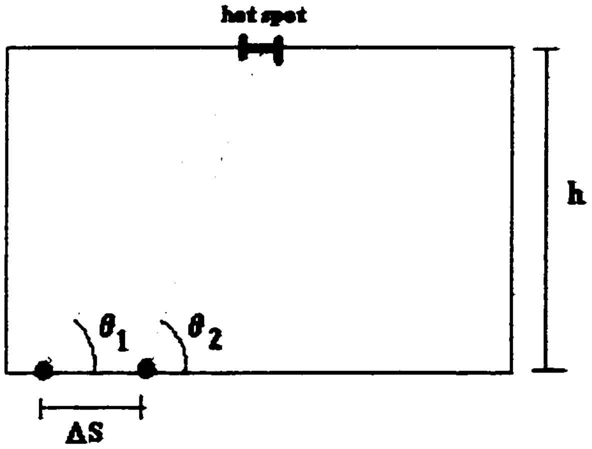

$\Delta S = h\,(\cot(\theta_1) - \cot(\theta_2))$ where θ_1, θ_2 : consecutive directions

Figure 3.12 Ray effect wavelength

Notice that the ray effect is caused by the angular discretization methodology and is independent of the spatial finite difference scheme used. Although several remedies have been proposed (Lathrop 1971, Liou 1997) in most cases the best one according to these authors is, still, to use as many beams as possible. As we will see in Chapter 4, the small number of directions available in the S_n quadrature set seriously limits the ability of the DOM to deal with transparent enclosures with non-uniform boundary conditions.

FALSE SCATTERING

According to Chai et al. (1993a), false scattering is also known in computational fluid dynamics as false diffusion. The term " scattering " refers to the deviation of a beam from its original direction. For example assume a beam of light was launched from the left (Figure 3.13) into the horizontal direction into an enclosure where a vacuum exists. For simplicity, assign to the intensity of this beam a value of I = 1. The beam would cross the room with undiminished intensity in such a way that at the end, it still has an I = 1 and has the same width as at the beginning.

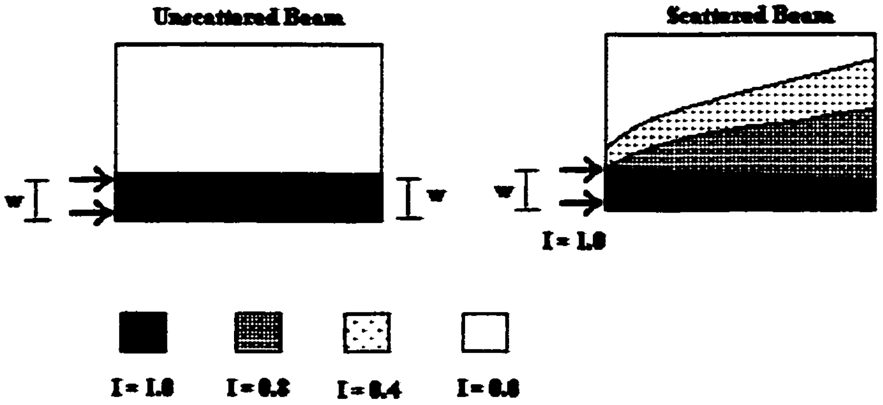

Figure 3.13 Scattering of a collimated beam

If, on the other hand, there are particles inside the room, upon collision with the beam they would redirect the beam . The collisions would cause two effects:

a) The intensity of the beam would be diminished

b) The intensity of the beam would be distributed in the whole room in such a way that sharp gradients would tend to disappear.

All of these represent real phenomena. Returning to the DOM, let us see how it produces some undesirable numerical scattering. Rewriting the DOM equation for 2-D and assuming that $\Delta x = \Delta y$ we would have for the intensity of the beam:

$$I_p = \frac{\mu I_x^j + \eta I_y^j}{\mu + \eta} \tag{3.31}$$

Remember, also, that the intensities at the cell borders and the intensity at the center of the cell are related by:

$$I_p^j = \alpha I_{x+\Delta x}^j + (1-\alpha) I_x^j = \alpha I_{y+\Delta y}^j + (1-\alpha) I_y^j \tag{3.32}$$

Equations 3.31 and 3.32 can be used to predict the intensity field inside in a 2-D enclosure. Chai, Lee and Patankar (1993) proposed a square of unit length. They assume that the intensity at the walls is zero everywhere except on the left wall where a beam with direction θ and intensity $I = 1$ in arbitrary units enters the room.

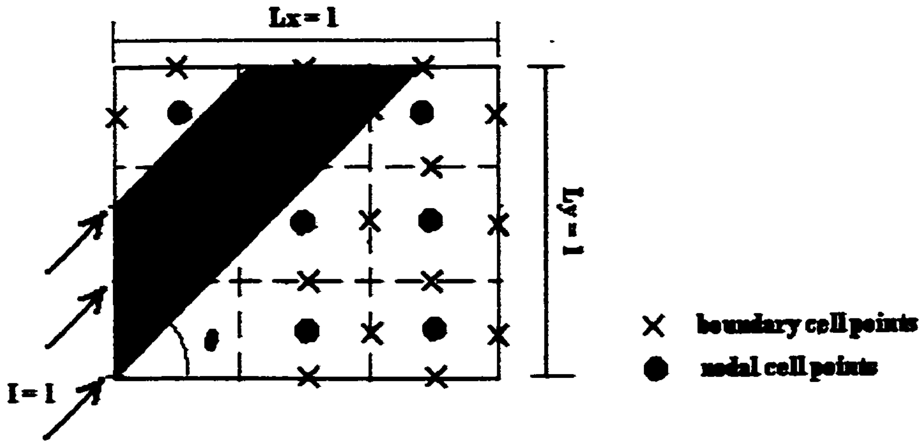

Figure 3.14 Numerical experiment of Chai et al.

Ideally, the intensity field should be as shown in Figure 3.14; The intensity I =1 inside the beam in the gray region in the Figure and I = 0 in any other place. The computed intensity field is shown in Figure 3.15 for alpha = 1 and θ = 60 degrees. In order to quantify the false scattering effect a numerical experiment was performed to calculate, for a number of beam directions θ, the rms error as:

$$rms\ error = \sqrt{\frac{\left(I_{real\ at\ nodal\ point} - I_{DOM\ at\ nodal\ point}\right)^2}{n}} \qquad (3.33)$$

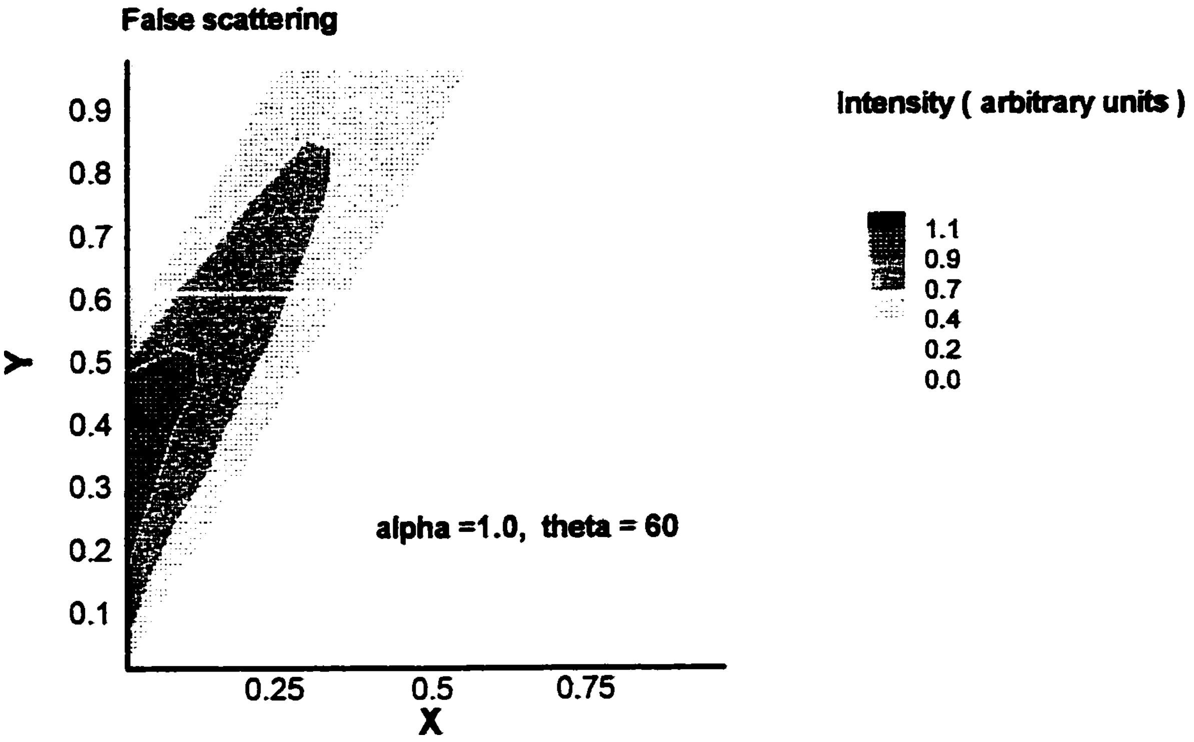

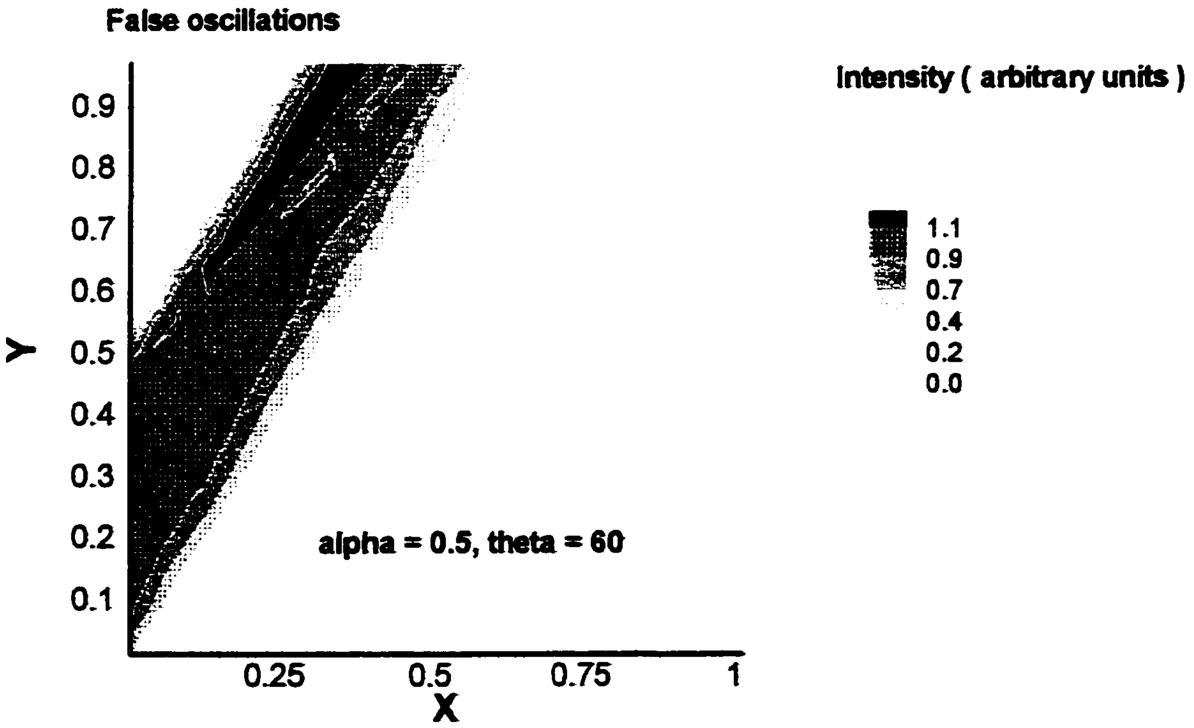

Figure 3.15 False scattering and false oscillation examples

n is the number of interior points (nodal plus boundary in Figure 3.14) inside a circle with radius equal to one. This was done in order to eliminate any corner effects that might affect the rms calculation. Since the width of the beam could also affect the result, it was kept constant by changing y_b in Figure 3.16.

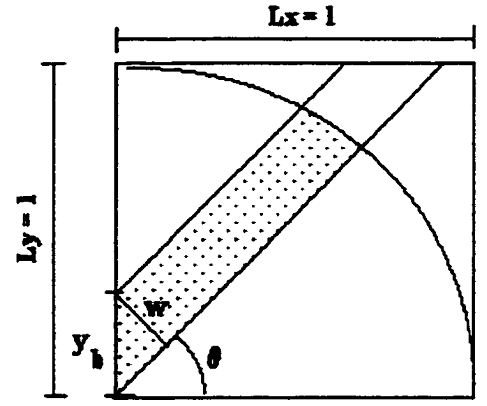

$$y_b = \frac{w}{\cos(\theta)}$$

Figure 3.16 Rms error calculation for false scattering

The result are shown in Figure 3.17. To eliminate other effects such as false oscillations $\alpha = 1$ was used. The experiment shows that there is no false scattering at $\theta = 0$ or $\theta = 90$. The more angular mismatch there is between the beam and any of the coordinate axis, either " x " or " y ", the stronger the false scattering. This means that $\theta = 45$ is the angle where the maximum amount of scattering is present. Figure 3.17 shows that for a specified value of θ, false scattering increases with increasing alpha. Because false oscillations are also present whenever alpha is different from one, Figure 3.17 should be taken with caution.

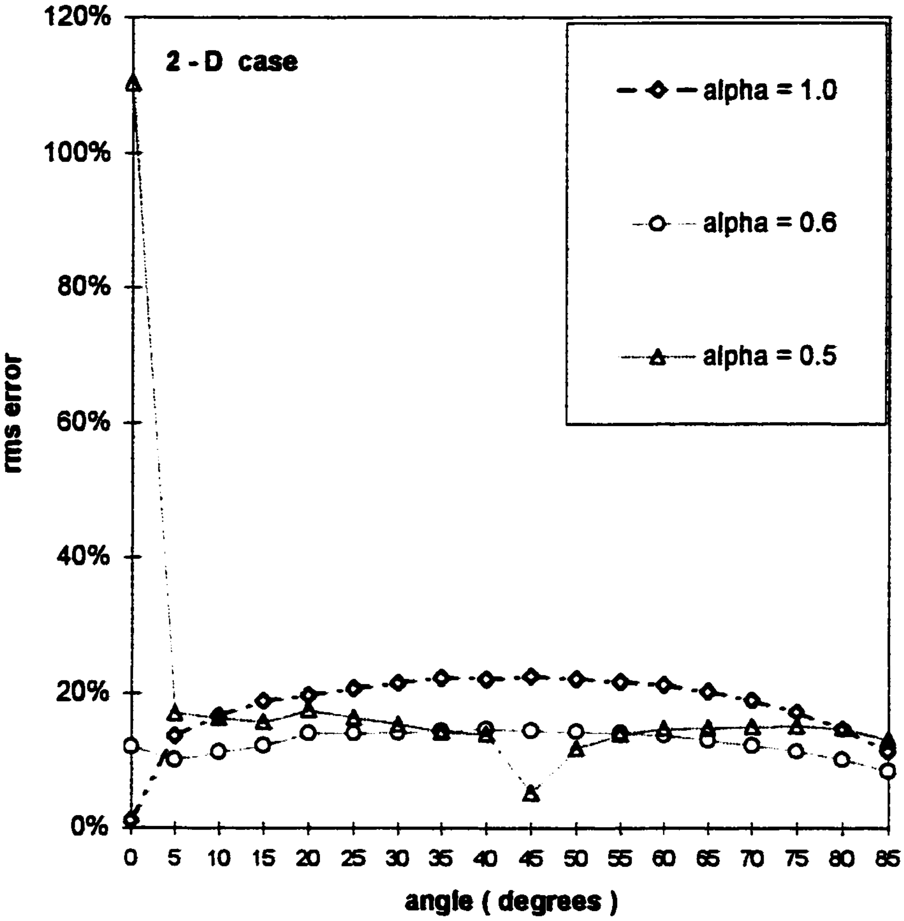

Figure 3.17 Rms error as a function of theta

A relevant note is in order: To calculate the rms error in the above experiment as well as in the following ones, it is important to take into consideration all the interior points and not only the nodal cell points of Figure 3.14. The reason for this is that although the boundary cell points are not used in the interior of the enclosure, they are used to calculate the irradiation at the surfaces of the enclosure, and they should be considered as real intensities and not just as auxiliary quantities to calculate Ip, the intensity at the center of the cell. Further, if embedded objects or protrousions are present inside the enclosure, the intensity at their surface would be represented by boundary cell points.

FALSE OSCILLATIONS

In addition to the ray effect and false scattering there is also another effect, false oscillations, caused by the spatial difference scheme used. False oscillations consist of a series of non-physical oscillations in the intensity of the beam. It is illustrated by the following numerical experiment: in the 2-D enclosure discussed above, instead of sending a constant intensity beam, we choose to send a beam with a distribution of intensity as shown in Figure 3.18.

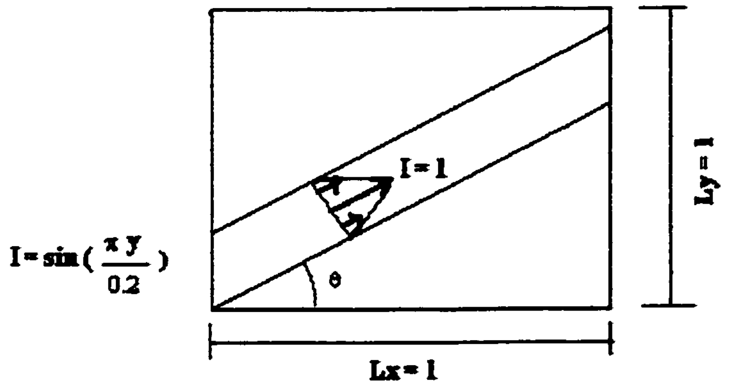

Figure 3.18 Chai et al. experiment with a smooth intensity distribution

Figure 3.19 shows the result for the original experiment and the smooth intensity distribution experiment with a value of θ where large oscillations are expected. In this experiment even when $\alpha = 0.5$, almost no oscillations are seen where the intensity changes smoothly. Only when the slope in the curve intensity vs. distance changes abruptly are these oscillations produced. As in the case of false scattering, however, there exists a dependence between the angle θ and false oscillations.

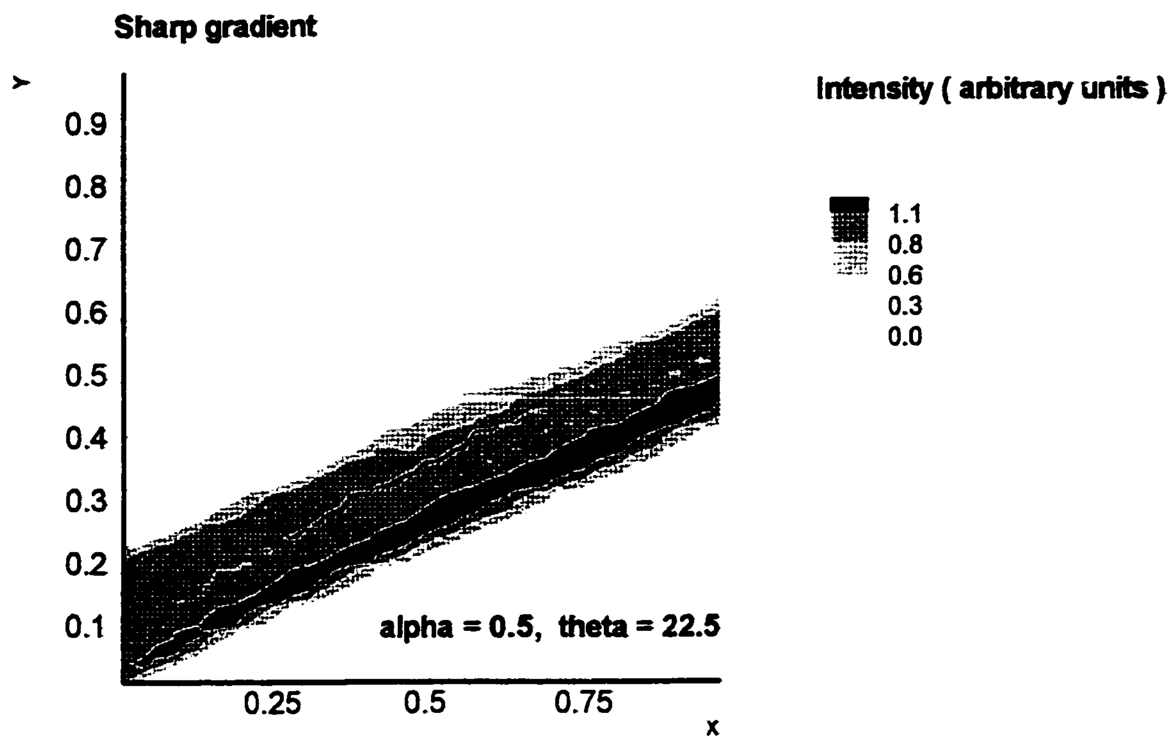

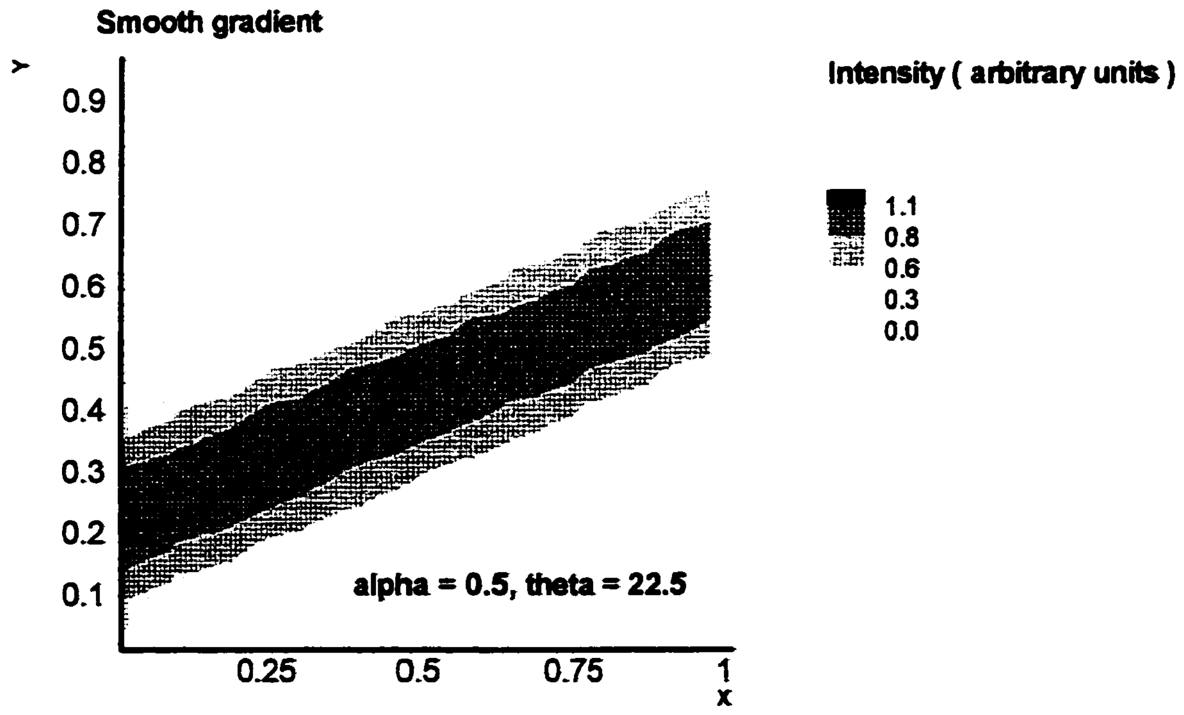

Figure 3.19 False oscillations in sharp and smooth intensity gradients

This dependency is shown by repeating the Chai, Lee and Patankar experiment (Figure 3.17) with $\alpha = 0.5$. This particular value of alpha reduces false scattering to a minimum. Referring to Figure 3.17 this means that the rms error produced in such a case is mostly due to the false oscillations. In particular it should be noted that the oscillations reach their maximum value when $\theta = 90$ and $\theta = 0$ and there are almost no oscillations at $\theta = 45$. For a particular angle, there is also a relation between the oscillations and the value of alpha. In constrast to false scattering, these false oscillations reach their maximum when $\alpha = 0.5$ and are not present at $\alpha = 1$.

Table 3.2 summarizes these results.

Table 3.2 Dependence of false scattering and false oscillations on θ and α

Effect	Maximum error alpha, α	Maximum error theta, θ	Minimum error angle, θ
False scattering	alpha = 1	45	0 , 90
False oscillations	alpha = 0.5	0, 90	45

These results suggest that there is an optimal value of alpha to be used at each particular value of θ. In particular if the the beam is aligned with a coordinate axis alpha should be equal to one because in this case neither false scattering or false oscillations would appear in the result. If $\theta = 45$ alpha should be equal to 0.5 because in this case, also, no false oscillations and almost no 0numerical scattering would be produced. At all other angles, the Chai, Lee and Patankar (1993) experiment is repeated to find the alpha that minimizes the rms error for each angle. The results are shown in Figure 3.20. To obtain the same results for the 3-D case, an

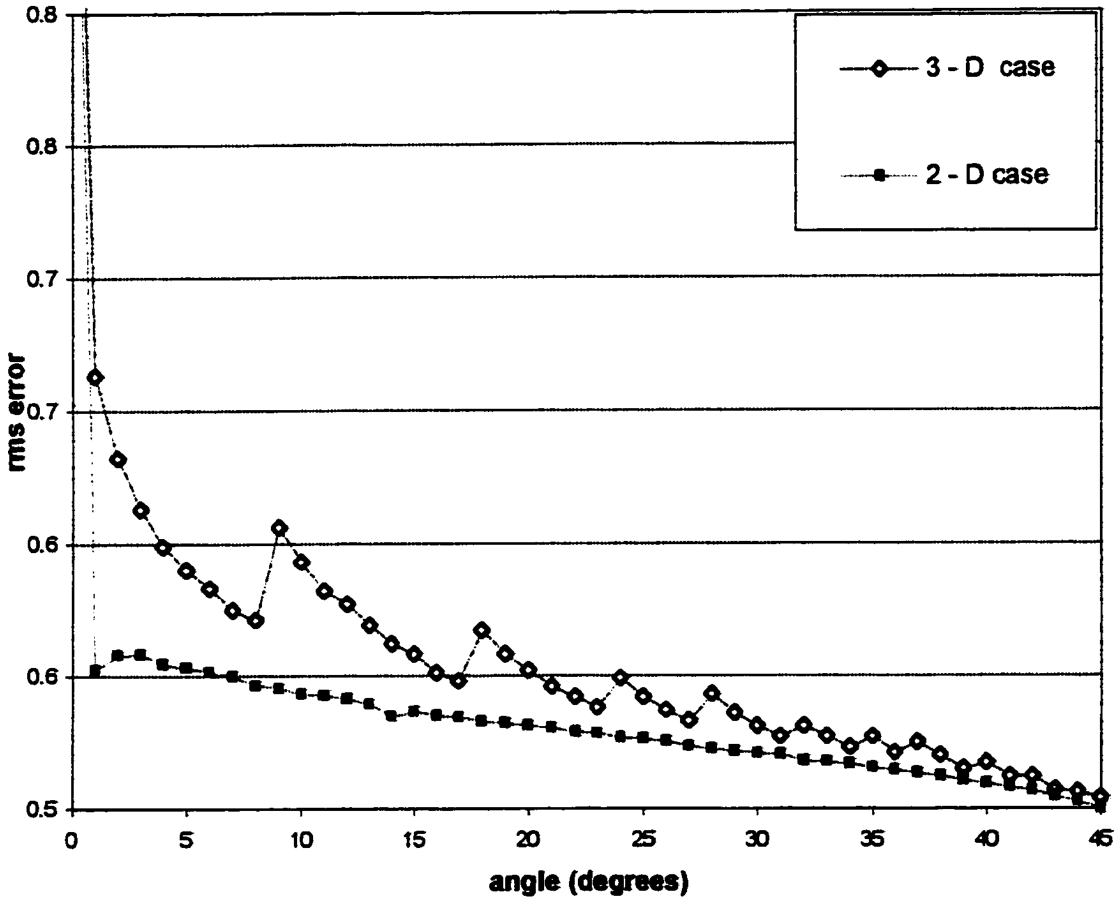

Figure 3.20 Optimal alpha as a function of theta

experiment similar to the one discussed above, can be made. In this case a beam with I = 1, would be launched from the bottom of a cube as shown in Figure 3.21.

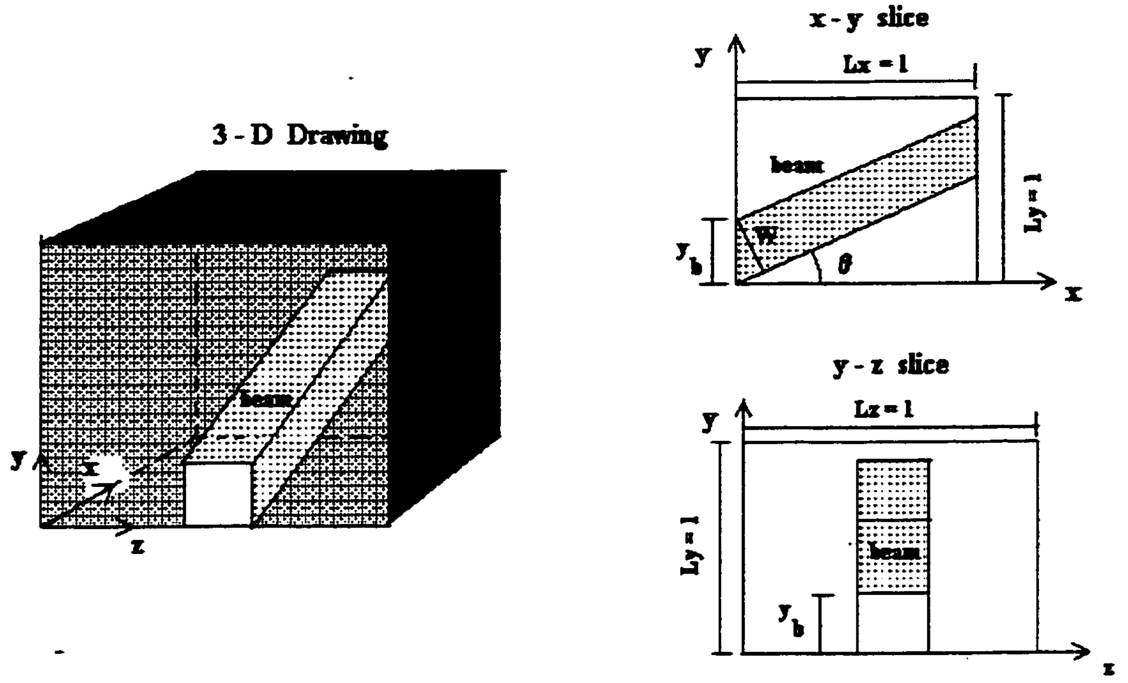

Figure 3.21 Rms error calculation 3 - D

The results are shown in Figure 3.20. In Chapter five the these findings will be used to improve the performance of Discrete Ordinates Method.

3.5 TEST CASES

The DOM was used to calculate the radiation heat flux along the floor midline in cases one and two shown in Figures 1.2 and 1.3. The first case represents a classical example of the kind of problems that were tackled with the method. It is a cube with constant temperature walls. Neither hot nor cold spots, as would be represented in buildings by heat panels or windows, appear in this example. Case 2 was chosen to represent a typical room, with normal boundary conditions.

Several values of alpha were used with a fixed quadrature set (the performance of different quadrature sets is discussed in chapter 4). The results for the first case are shown in Figure

3.22. Although each wall is at a constant temperature, there is still a ray effect produced by the change in intensity at the corners of the room. This is the reason why the oscillations do not completely disappear even using an alpha equal to one. Any other oscillation is due to the spatial scheme. That is why these are more pronounced near alpha equal 0.5 . Even when the oscillations are evident, if all that is needed is an average value for the heat flux on the wall, it could be argued that the results are within the accuracy limits desired.

However, if the experiment is repeated with case number two (Figure 1.3), the results are completely different as shown in Figure 3.23. In this case for an alpha equal to 0.5 the true shape of the heat flux line is lost in the oscillations produced by the spatial differential scheme. If alpha is chosen to be one, although most of the oscillations disappear (those due to the spatial scheme), the accuracy of the result is poor. This is so even if an intermediate value of alpha is chosen in an attempt to diminish both false scattering and false oscillations.

3.6 SUMMARY

One approach to the problem of solving radiative interchange within enclosures is to discretize the equation of transfer. After this equation is discretized, different sets of boundary conditions can be applied depending on the region of the spectrum where the heat fluxes are needed. Normally, in buildings two wavebands are distinguished. These two wave bands give rise to two different sets of boundary conditions.

The DOM is the result of a double discretization process. First a discretization in angular space is made. The transformation of the continium where all angular directions are possible to the discrete angular space produces a numerical error called the ray effect. Although several attempts had been made to reduce the ray effect, the best method at present is to increase the number of angular directions as much as possible. In Chapter 4 the advantages and disadvantages of some quadrature sets will be investigated.

The second discretization is a discretization of the equation of transfer itself. Spatial discretization produces the numerical errors of false scattering and false oscillations. This implies that every time a new angular direction is added to a quadrature set, a new source of false scattering and false oscillations is also added. Therefore, if a new angular direction is added, the ray effect will be reduced but false scattering and false oscillations will increase. This may limit the capability of the DOM to produce an accurate answer. It also means that these two numerical problems have to be solved in a simple manner in order not to increase without proportion the CPU time spent in a radiation exchange calculation. In Chapter 4 some partial solutions are suggested to mitigate false scattering and false oscillations.

In practice it is difficult to separate the effects produced by the ray effect, false scattering and false oscillations. If $\alpha = 1$ the oscillations due to the spatial scheme are eliminated and, because of the numerical scattering produced, the oscillations produced by the ray effect are mitigated. However the accuracy of the solution is sacrificed by producing a result that is too smooth and cannot capture sharp gradients. If α is different from one, it will be difficult to distinguish those oscillations caused by the ray effect from those caused by the alpha term.

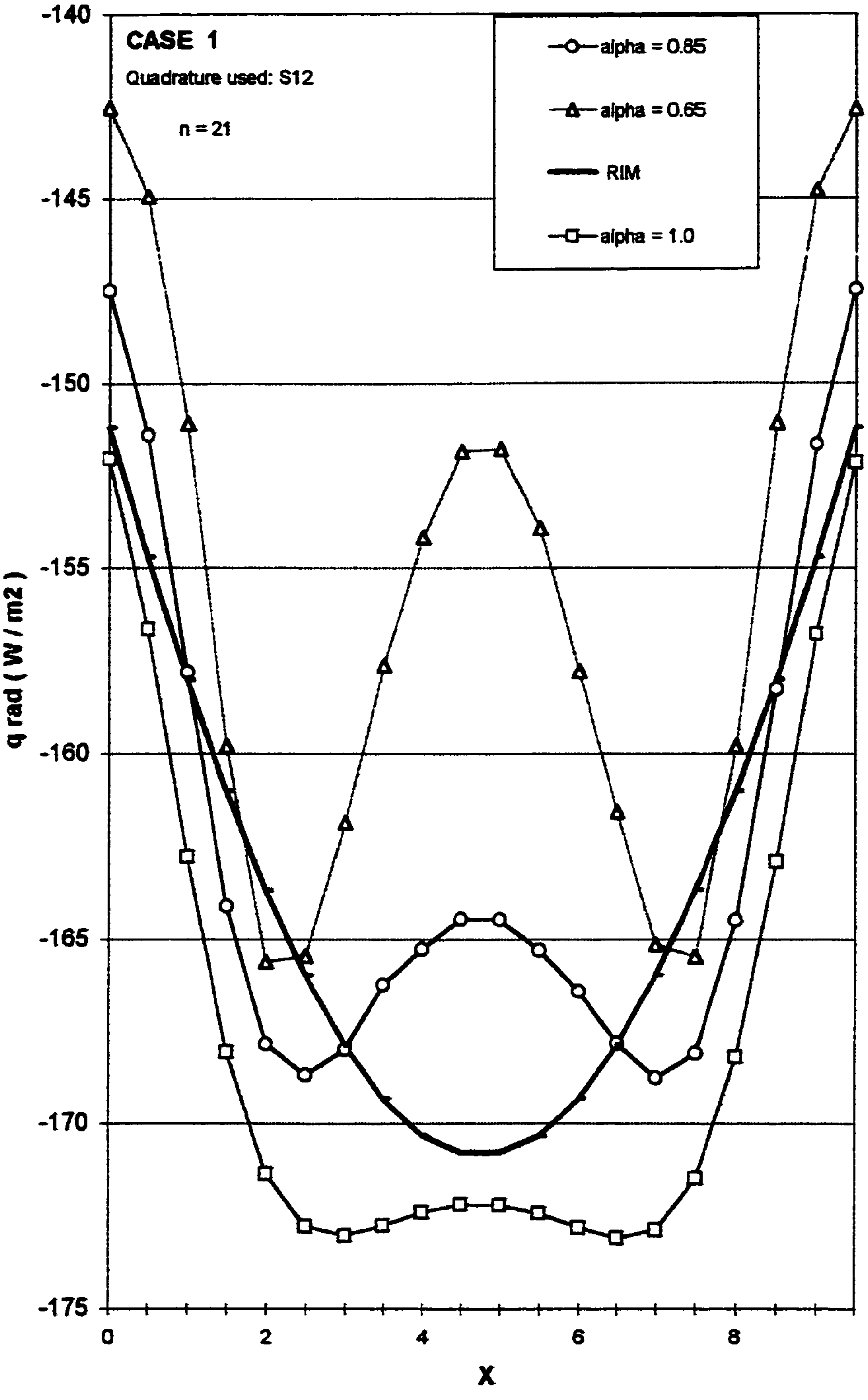

Figure 3.22 Effect of alpha on heat flux

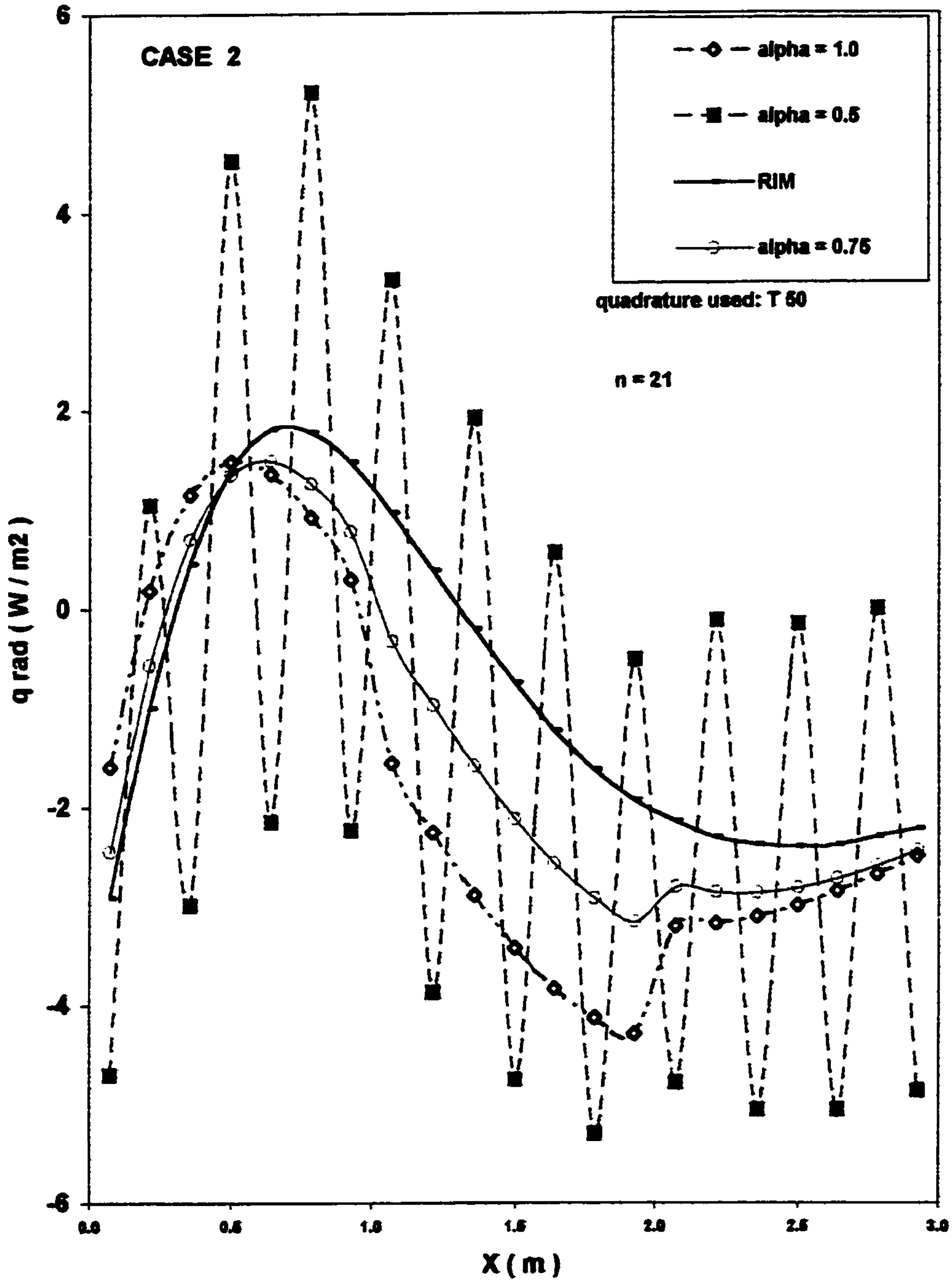

Figure 3.23 Effect of alpha on heat flux

Chapter 4

ANGULAR DISCRETIZATION SCHEMES.

4.1 INTRODUCTION

This chapter begins by describing the principles upon which angular quadratures are constructed. Then a description of the different quadrature families is presented.. Finally, these families are compared using quantitative and qualitative criteria. Their capacity to deal with the ray effect discussed in Chapter 3 is also examined.

An angular quadrature is a set of M directions and weights, {Ω_i, ω_i where i = 1... M. } Each direction is represented by Ω_i (μ_i, ξ_i, η_i) and by an associated weight ω_i. A visualization of the set can be obtained by inspection of a unit sphere. The Cartesian coordinates of Ω_i : μ_i, ξ_i, η_i, are a point on the surface of the sphere. When all the components of the set are represented in this way we have an image of the entire angular quadrature. A 2-D example is shown in Figure 4.1.

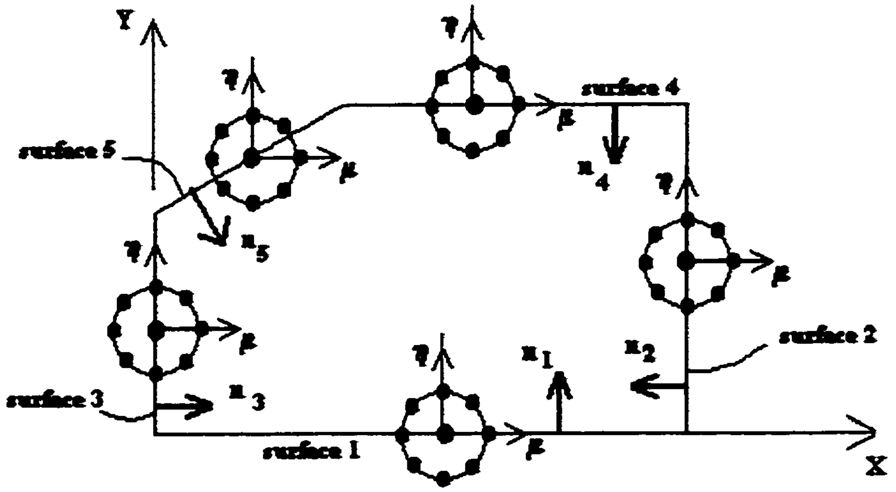

Figure 4.1 A 2-D example of a 90° symmetric angular quadrature set

4.2 QUADRATURE CONSTRUCTION CRITERIA

SYMMETRY

Obviously the heat flux on an enclosure surface, the mean radiant temperature, or any other quantity calculated by a discretization method such as the DOM should not depend on the coordinate system used. Suppose, for example, that the heat flux on surfaces 1 and 3 in Figure 4.1 are computed. We expect that the orientation of these surfaces would not introduce any bias in the results. In particular note that the angle between normal $\mathbf{n}_1$ and any of the angular directions at surface 1, (0, 45 or 90 degrees) is the same as the angle between normal $\mathbf{n}_3$ and the angular directions at surface 3. As apparent from Figure 4.1, a quadrature set symmetric to 90-degree rotations would also ensure the same treatment for surfaces 2 and 4. In the same manner, a symmetric angular quadrature set with respect to reflections would ensure consistency for surfaces 2 and 3 on the one hand and surfaces 1 and 4 on the other.

However note that, for surface number 5, the relative angle between $\mathbf{n}_5$ and the angular directions of the set are not the same as in the other cases. Therefore in the case of this surface, the heat flux will be calculated in a way not consistent with the rest of the surfaces of the enclosure. Since the majority of DOM applications occur inside rectangular enclosures, the quadrature sets developed so far use as a criteria this " Ninety Degree symmetry " also called "Complete Symmetry " by Lathrop and Carlson (1965). It should be stressed that these quadratures will not ensure consistency in a non – rectangular enclosure such as the one shown in Figure 4.1. This will become clear in Chapter 6, when a DOM calculation is attempted in such an enclosure.

Ninety- Degree Symmetry

Due to angular discretization it is impossible to have a completely symmetric quadrature set. However, as mentioned above, most of the radiation exchange applications occur in rectangles where a ninety-degree symmetry is enough. What is meant by a ninety-degree symmetry is shown in the following example: Suppose that the heat flux on surface 1 in Figure 4.2 is calculated two times. The first one, it is calculated with frame 1 where μ is aligned with $-y$, ξ with $-x$ and η with z.. The second time frame 2 is used. Now μ is aligned with x, ξ with y and η with -z. If the angular quadrature set is chosen appropiately, the results of both calculations should be equal. In fact every time the frame of reference is changed in such a way that the line AB is parallel to either coordinate axis x, y or z, the heat flux calculation should not change. If these is true, let us say that our quadrature set has a ninety-degree symmetry. In this way no axis is privileged.

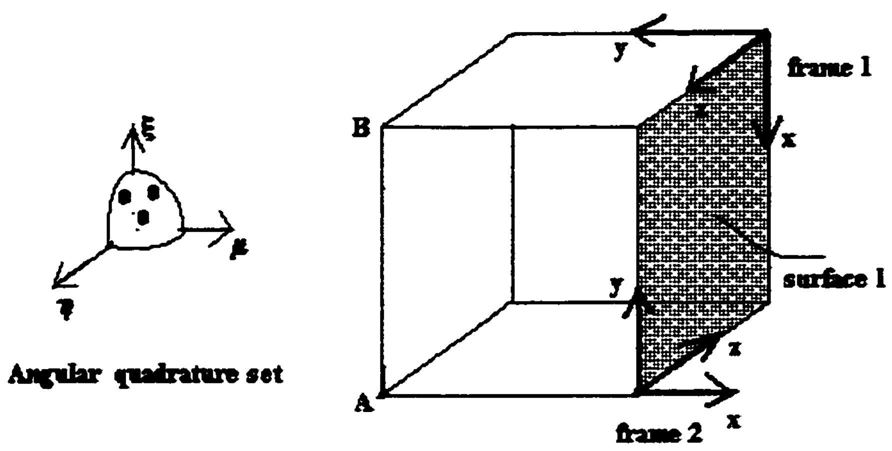

Figure 4.2 Ninety degree symmetry: the heat flux in any wall should have the same value whether frame 1 or frame 2 is used

Ninety-degree symmetry can be divided into two cases: Reflection Symmetry and Interchange symmetry as discussed in Lee (1961), Lathrop & Carlson (1968) and Thurgood (1992).

a) Reflection symmetry. As shown in Figure 4.3, if a mirror were placed on the x- y plane the direction of the z-axis would be reversed. To have reflection symmetry, if the angular direction

(μ, ξ, η), with weight ω_l, belongs to the original quadrature, then the point $(\mu, -\xi, \eta)$ should also belong to the quadrature and it should have the same weight ω_l. By similar arguments, if (μ, ξ, η) belong to the quadrature, any point $(\pm\mu, \pm\xi, \pm\eta)$ should also belong to the quadrature set with the same weight.

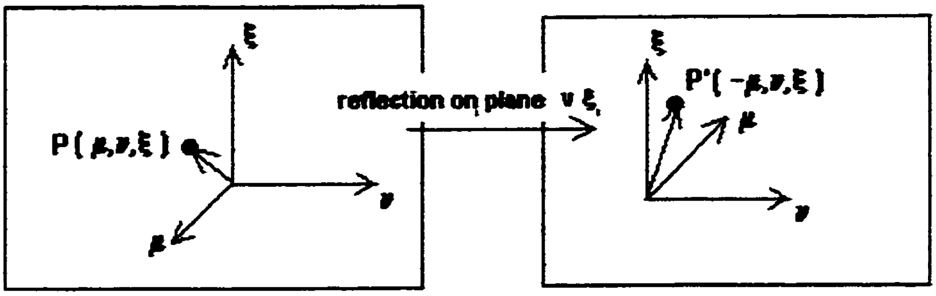

Figure 4.3 Reflection symmetry on a typical case: If P is a direction in the quadrature set so is P' and both have the same weight

b) Interchange symmetry. This refers to the reflection of the axis in one of the main planes plus a 90 degree rotation about any axis. As illustrated in Figure 4.4

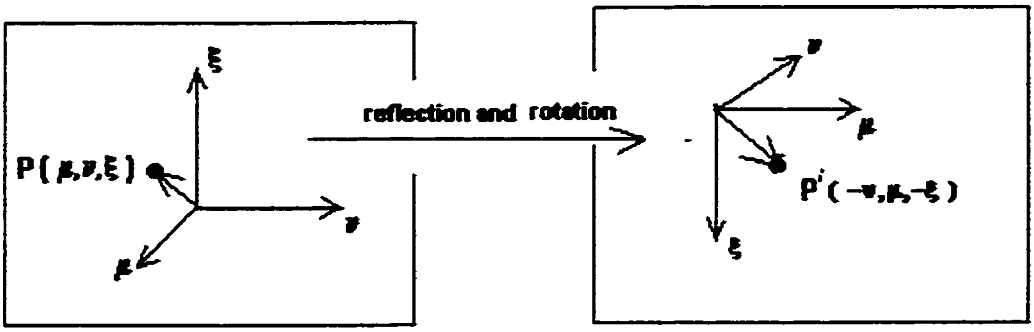

Figure 4.4 Interchange symmetry: Equivalent to rotations plus reflections

This implies that if direction (μ, ξ, η) is in the quadrature set with weight ω_l then all of the following points should, also, belong to the quadrature and have the same weight.

(μ, η, ξ) (μ, ξ, η) (ξ, μ, η)

(η, μ, ξ) (η, ξ, μ) (ξ, η, μ)

MOMENT MATCHING CRITERIA

If $\xi = \cos\theta$ in Figure 4.5, it is a mathematical fact that:

$$\int_0^{\frac{\pi}{2}}\int_0^{4\pi} \xi^r d\Omega = \frac{4\pi}{(r+1)} \tag{4.1}$$

Where r is any integer and the rest of the literals are explained in Figure 4.5. In discrete form, equation 4.1 is :

$$\sum_{j=1}^{8N_{octant}} \omega_j \xi_j^r = \frac{4\pi}{(r+1)} \tag{4.2}$$

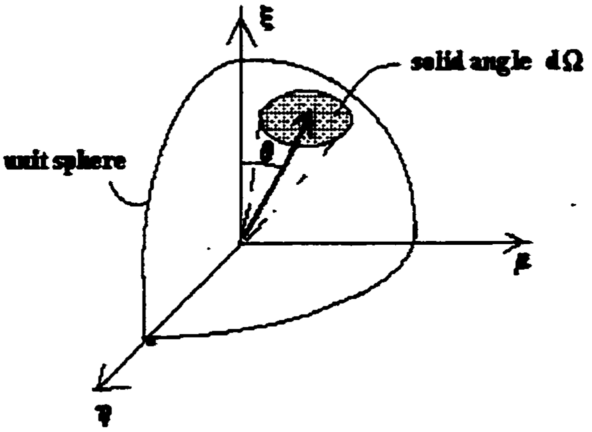

Figure 4.5 Nomenclature for moment integrals

The family of equations represented by equation 4.2 are called the moment equations. Although they represent a purely mathematical requirement, some of them also have a physical interpretation. If r = 0, for example, this integral should give 4π, that is, the solid angle sustained by a sphere. In 1992 Thurgood suggested a more general criteria. The following equalities are well known to mathematicians:

$$\int_0^{2\pi} \mu^a \eta^b \xi^c d\Omega = \frac{\Gamma\left(\frac{a+1}{2}\right).\Gamma\left(\frac{b+1}{2}\right).\Gamma\left(\frac{c+1}{2}\right)}{\Gamma\left(\frac{a+b+c+3}{2}\right)}.$$

$$\Gamma\left(n+\tfrac{1}{2}\right) = \frac{1\cdot 3\cdot 5\ldots(2n-1)\sqrt{\pi}}{2^n} \qquad (4.3)$$

$$\Gamma(n) = (n-1)!$$

$$\Gamma(\tfrac{1}{2}) = \sqrt{\pi}$$

As in the case of the single moment equations, the angular quadrature should mimic the above equations. While equation 4.2 was used to construct some quadrature sets (Lathrop, Fiveland, Truelove) equations 4.3 has been used by Thurgood (1992) to compare different families of quadratures.

4.3 DIFFERENT FAMILIES OF QUADRATURE SETS

The more popular quadratures used in DOM are shown in Figure 4.6 below:

Quadrature sets

- Angular segmentation S_n
  - Half range 2π (LSO)(LSH)
  - Complete range 4π (LSE)
- Equal weights
  - Even moments (EWE)
  - Odd moments (EWO)
- Thurgood T_n

Figure 4.6 Some quadrature sets

It is a common practice to represent the order of the different quadratures by a subscript. For example: S_n represents the angular segmentation quadrature of order n in the same way that T_n represents Thurgood quadrature of order n. This, however, is not a good practice when different quadrature families are being compared. The order of the quadrature is really represented by N_{octant}, the total number of angular directions that the quadrature has in an octant. For the case of the angular segmentation quadrature as well as for the Equal Weights quadratures, $N_{octant} = n(n+2)/8$. In the case of the Thurgood quadrature, however, $N_{octant} = n^2$. For instance the quadratures represented by S_{16}, EWE_{16} and T_6 are of the same order since in all these cases $N_{octant} = 36$.

THE ANGULAR SEGMENTATION QUADRATURE (S_n)

It was proposed by Lee (1962) and Lathrop & Carlson (1965). It is the more popular one for DOM users. To build the S_n quadrature set each axis in the unit sphere is divided into n/2 segments. To satisfy the requirements of ninety-degree symmetry, corresponding points on each axis should have the same value, so no axis is different from another. That is:

$$\mu_1 = \eta_1 = \xi_1 \qquad \mu_2 = \eta_2 = \xi_2 \quad etc. \tag{4.4}$$

These points are used to construct "latitude" circles. The idea is shown in Figure 4.7 for the S_6 member of the family. Since ninety-degree symmetry applies also to the weights, these should be distributed as shown in Figure 4.8 in which each line represents one " latitude ".

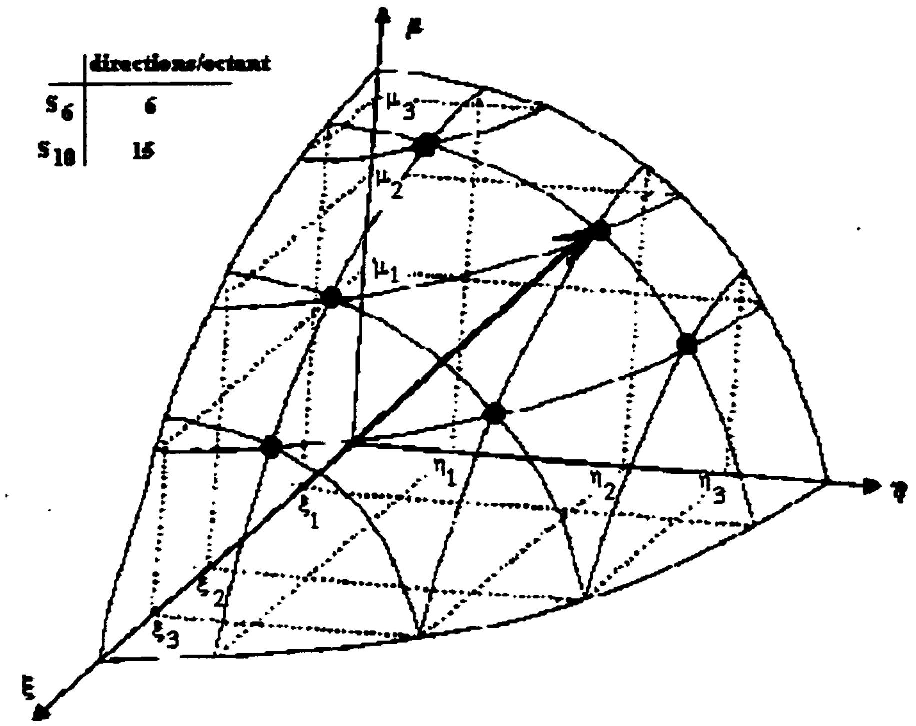

Figure 4.7 The directions of the S6 quadrature scheme as seen on a unit sphere

n

8

1
2 2
2 3 2
1 2 2 1

μ latitude levels

10

1
2 2
3 4 3
2 4 4 2
1 2 3 2 1

ξ latitude levels

Figure 4.8 Equal weight points for some Sn quadrature sets

As the last requirement of ninety-degree symmetry, Lathrop and Carlson (1965) showed that the position of the μ_i's that belong to the quadrature can be calculated as:

$$\mu_i^2 = \mu_1^2 + (i-1)\Delta \qquad \Delta = \frac{2\left(1-3\mu_1^2\right)}{(n-2)} \tag{4.5}$$

The term μ_1 can be chosen arbitrarily. Hence, if no other criteria besides symmetry were used, the system would have one degree of freedom. To calculate μ_1 as well as the n/2 – 1 weights, n/2 equations are needed. There are three alternatives:

The equations could be obtained by using the moment equation 4.2 with even values of r. Fiveland (1992) calls this the Level Symmetric Even (LSE) moment's quadrature. It should be noted that the moment equation is automatically satisfied for odd values of r. The highest degree quadrature available with this option is S_{22}. If n > 22, negative weights are obtained which are not recommended.

As an alternative to matching even moments, all half-range moments where equation 4.2 is integrated for just half a hemisphere (from 0 to 2π instead of from 0 to 4π) could be used. Fiveland calls this the Level Symmetric Odd (LSO) moment quadrature. In 1987 Truelove recommended this version of S_n showing that it gives better results. In this case some of the moment equations acquire physical significance: if r = 0, the integral in equation 4.1 represents the hemisphere solid angle. If r = 1, then the integral represents the heat flux received in a surface with uniform intensity $I = 1$. Higher order moments represent the scattering integral in equation 2.1. In this case negative weights values are obtained for n > 10.

The third alternative was suggested by Fiveland (1992). It is a combination of the previous ones. It is called the Level Symmetric Hybrid set (LSH). In this case, the moment equation is solved for r = 0, 1, 2, 4, 6....n −2. The highest degree quadrature available with this set is S8. In his paper Fiveland shows that this quadrature successfully represents many phase functions associated with scattering media.

EQUAL WEIGHTS QUADRATURES

This was proposed by Carlson in 1971 and further developed by Fiveland in 1991. First, it is assumed that all points in the quadrature have the same weight ω. If M is the total number of angular directions in the quadrature, this weight has to be:

$$\omega = \frac{4\pi}{M} \tag{4.6}$$

However, once this is done, it is not possible to keep the points on latitude levels as in Figure 4.7. In order to calculate the position of the points, equation 4.2 is used again together with 4.6 and the fact that, since the points are represented in a unit circle:

$$\mu_i^2 + \xi_i^2 + \eta_i^2 = 1 \tag{4.7}$$

This kind of equal weights quadrature comes in two varieties: The Equal Weights Even moment quadrature (EWE) and the Equal Weights Odd moments quadrature (EWO) depending on the parity of r chosen to solve equation 4.2.

Fiveland (1991) compares the S_n quadrature with EWE and EWO regarding its ability to integrate equation 4.2. In this paper Fiveland suggested the use of EWO and LSH . Ehlert and Smith (1994) found for a 3-D rectangle with uniform surface temperatures that EWO produced the most accurate results. However, as I will show later, my own numerical experiments suggest that this is not generally true.

THURGOOD QUADRATURE SET

Lee, Lewis & Miller and Thurgood (1992) noted that equation 4.5, obtained by assuming that the quadrature points had to be positioned in latitude levels, greatly restricted the choice of quadratures. The reason for this lies in the single degree of freedom that it allows. In 1992 Thurgood introduced a new family of quadratures, the T_n family. Apart from the three criteria that these quadratures should follow, this new family has the advantage that the number of directions can be incremented indefinitely and the weights remain always positive. To create a Tn quadrature the first step is to draw an equilateral triangle between the points (1,0,0), (0,1,0) and (0,0,1) on the x y and z axis as shown in Figure 4.9. Any point in this triangle can be easily projected into the unitary sphere. After choosing a local reference frame for the triangle (Figure 4.10), it needs to be divided into n parts to make n^2 equilateral triangles. These triangles can be projected into the unitary sphere, their area are the weights of the quadrature points and the points themselves are represented by the centroids of each of these triangles. In Figure 4.10, a tessellation for a T_4 quadrature set is shown. Thurgood worked with a 2-D rectangular enclosure (and with HEART, a spatial discrete scheme of his own invention) to probe his method. As I will try to show, his quadrature works very well for 3-D geometry as well. Because of its high order capability, it can mitigate the ray effect in an effective way.

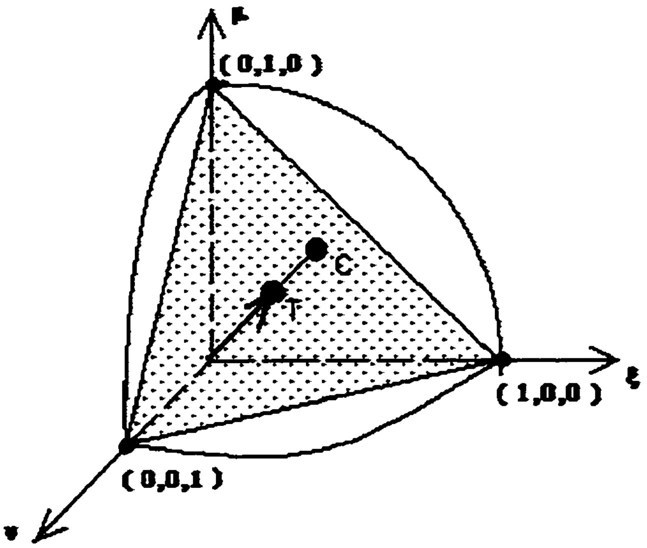

Figure 4.9 Basal triangle for the construction of the Tn quadrature set

dir / octant

T_3	9
T_4	16
T_9	81
T_{12}	144

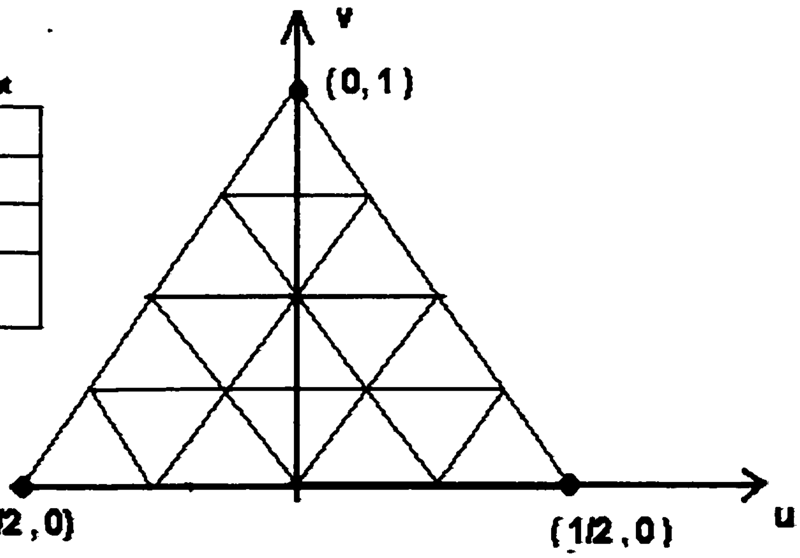

Figure 4.10 Tesselation of the basal triangle to generate the T_4 quadrature set

4.4 COMPARISON BETWEEN QUADRATURE SETS

Fiveland (1991) compares the S_n, and Equal Weights quadratures regarding their moment matching capability, i.e, their ability to integrate equation 4.1. Based on this, he recomends the LSH and EWO quadratures. Using equation 4.3 as a more general criteria and with various values for a, b and c , Thurgood (1995) concludes that, up to the limit attainable by the S_n quadrature, it had a better ability than the T_n quadrature of the same order to match the moments of equation 4.3. However the great advantage of the T_n quadrature is that it can work with any value of n.

In addition to be able to solve equations 4.1 and 4.3 adequately, there are a number of additional criteria that a quadrature set should meet in order to deal effectively with the ray-effect.

The first of these criteria were suggested by Thurgood (1992) and deals with the distribution of angular directions on a particular set. Suppose that f is an unknown function and that the integral $\int f\,dx$ is going to be calculated as $\sum f(x_i)\ \omega_i$. In that case a uniform spacing of the x_i is recommended. Otherwise a large variation in f in a region where the subdivisions are coarse may result in a gross miscalculation. Since nothing is known about the intensity in the angular integral $\int I\,d\Omega$ a uniform distribution of angular directions would be the optimum in this respect. A clustering of angular directions is undesirable since it implies that some directions are more important than others. A clustering of angular directions in one region also implies a lack of angular directions in other regions. This could create a large ray effect. Figure 4.11 represents the angular directions of S_{16} and T_6 as projected on the basal triangle used by Thurgood for his T_n quadrature. Both of these quadratures have 36 directions per octant. However the distribution of rays is very different among them. The consequences of this will be discussed later.

The second criteria is the angular distribution of weights. As mentioned in Chapter 3, a large gradient in the distribution of weights as the angular directions are changed could cause an

S_{16} and the T_6 quadrature is shown. Near the middle of the basal triangle, a strong angular weight gradient appears in the S_{16} quadrature.

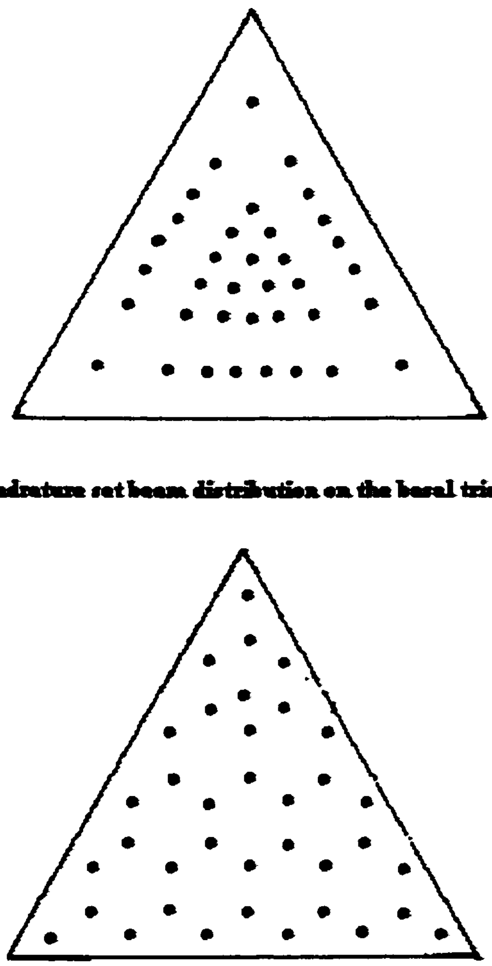

S_{16} quadrature set beam distribution on the basal triangle

T_6 quadrature beam distribution on the basal triangle

Figure 4.11 Distribution of angular directions for the T6 and S16 quadrature sets

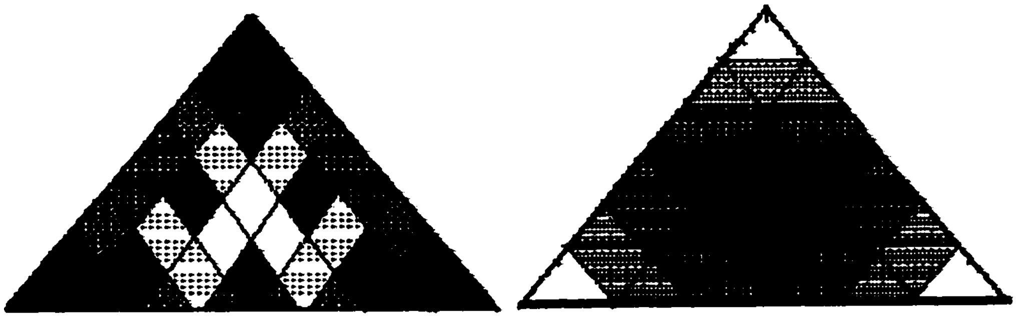

Weight intervals (10^{-2})

1.33 - 1.97	4.51 - 5.14
1.97 - 2.60	5.14 - 5.78
2.60 - 3.24	5.78 - 6.42
3.24 - 3.87	6.42 - 7.05
3.87 - 4.51	7.05 - 7.69

Figure 4.12 Angular distribution of weights in quadratures S_{16} and T_6

In order to illustrate the effects of these two qualitative criteria in practice, The DOM was used twice to calculate the heat flux on the floor of the room for case number 3 (Figure 1.4). The first time the DOM was used with a S_{16} quadrature. This set contains 36 directions per octant as mentioned before. The second time the T_6 quadrature, also with 36 directions per octant was used. In both cases an alpha equal to one was used in order to avoid false oscillations due to the spatial difference scheme. The results appear in Figure 4.13. Note that the S_{16} quadrature produce spurious heat flux patterns, which are not seen in the T_6 quadrature.. This effect is also seen in Figure 4.15, where the same quadrature order used for EWE and EWO, and they have very different flux profiles.

In summary, these results suggest that the ray effect is not just a function of the number of rays but also of the quadrature set used. The pattern of oscillations will be different for different angular quadratures even if they have the same number of angular directions.

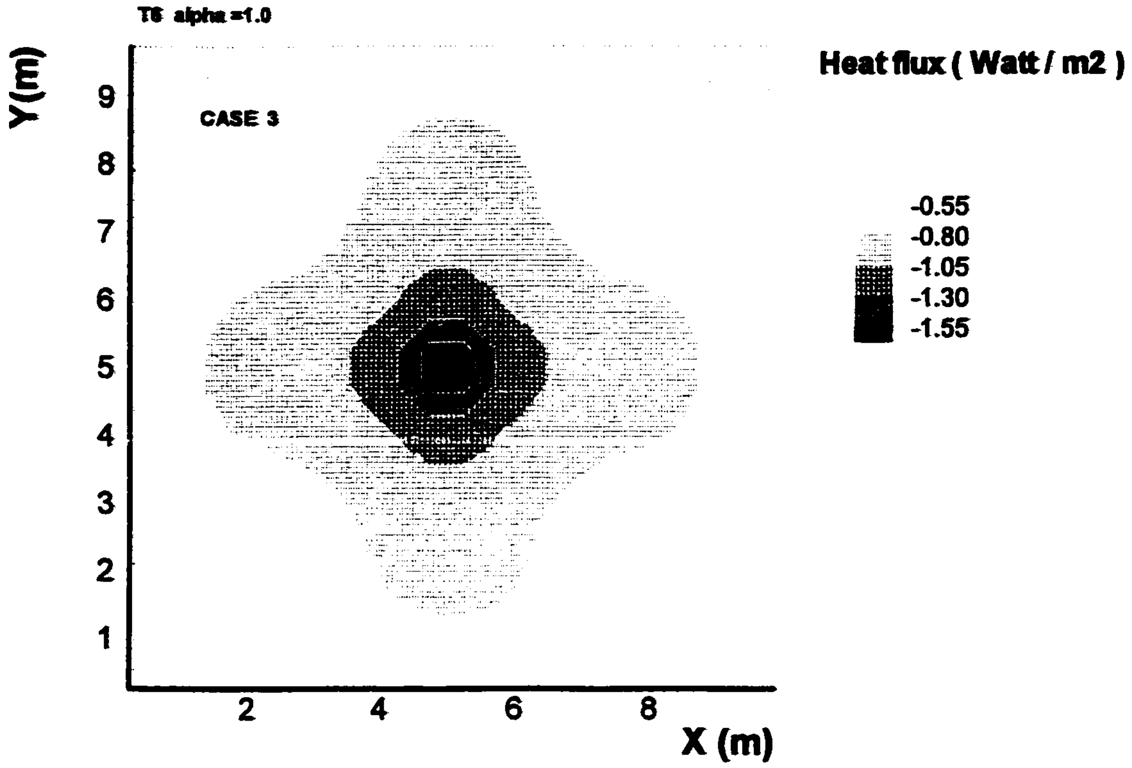

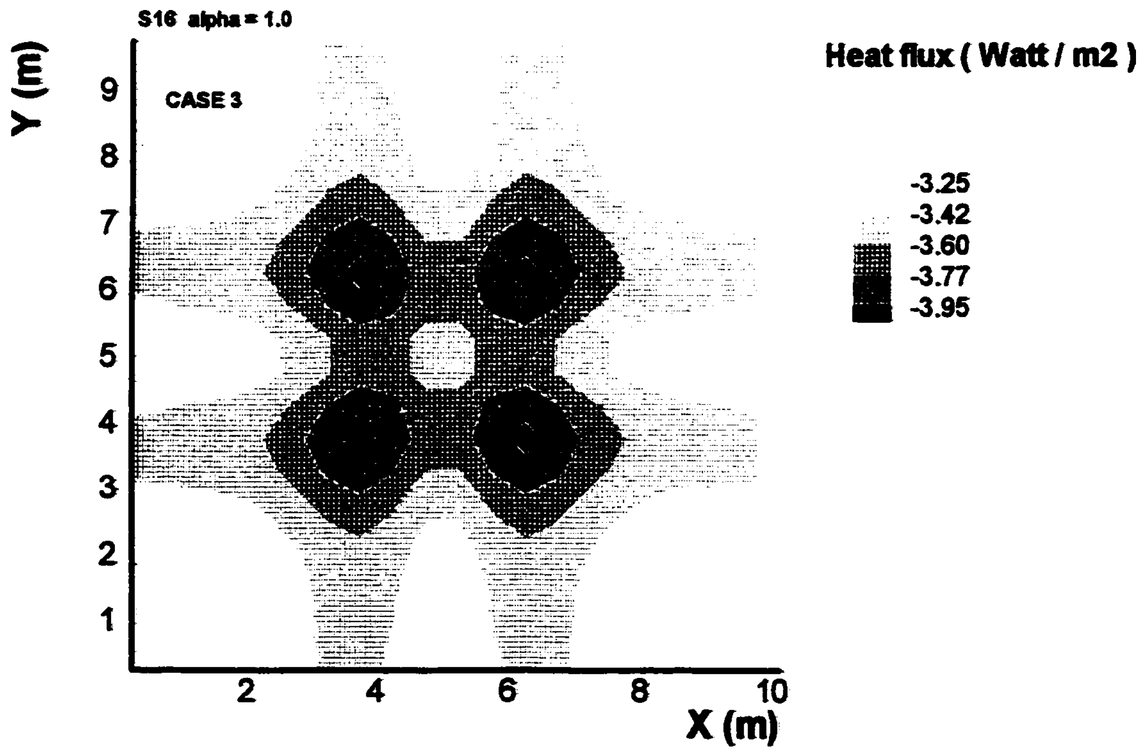

Figure 4.13 Ray effect in two different quadrature sets

4.5 TEST CASES

The same test cases chosen in Chapter Two, case 1 and case 2 were used to show the performance of different quadrature sets. For case 1 the midline heat fluxes at the floor (Figure 4.14) are computed with some of the more used high order quadrature sets. Although the oscillations are evident the calculations give good average results considering the relative coarse mesh used (n = 20). Figure 4.15 represents the same calculations for case 2. The quadratures used in the figure were EWE_{15}, EWO_{15} and S_{16}, which have the greatest precision possible within those particular quadratures. The sources of error in Figure 4.15 are false scattering and the ray effect. Increasing the mesh size reduces the error due to false scattering but not change the shape of the curves. In short, the graph shows the inability of the angular quadratures shown to deal with sharp intensity gradients. In particular the angular quadrature scheme used by Chapman (1995) for radiation exchange, produces poor results when the local heat fluxes are calculated as shown in Figure 4.16.

Figure 4.17 shows the local heat fluxes calculated at the floor midline of case 1 using Thurgood quadrature. Although for a similar number of directions the T_n quadrature does not seem to do better than the other ones, it has the great advantage of been able to have as many quadrature points as desired. Figure 4.18 shows the convergence of the T_n set as the number of angular directions is increased. There is still some difference between the benchmark RIM value and the DOM calculation as performed with a high order Thurgood set. The difference can be attributed to false scattering. In Chapters five and six some suggestions are made to reduce false scattering and the false oscillations that result from the spatial differential scheme.

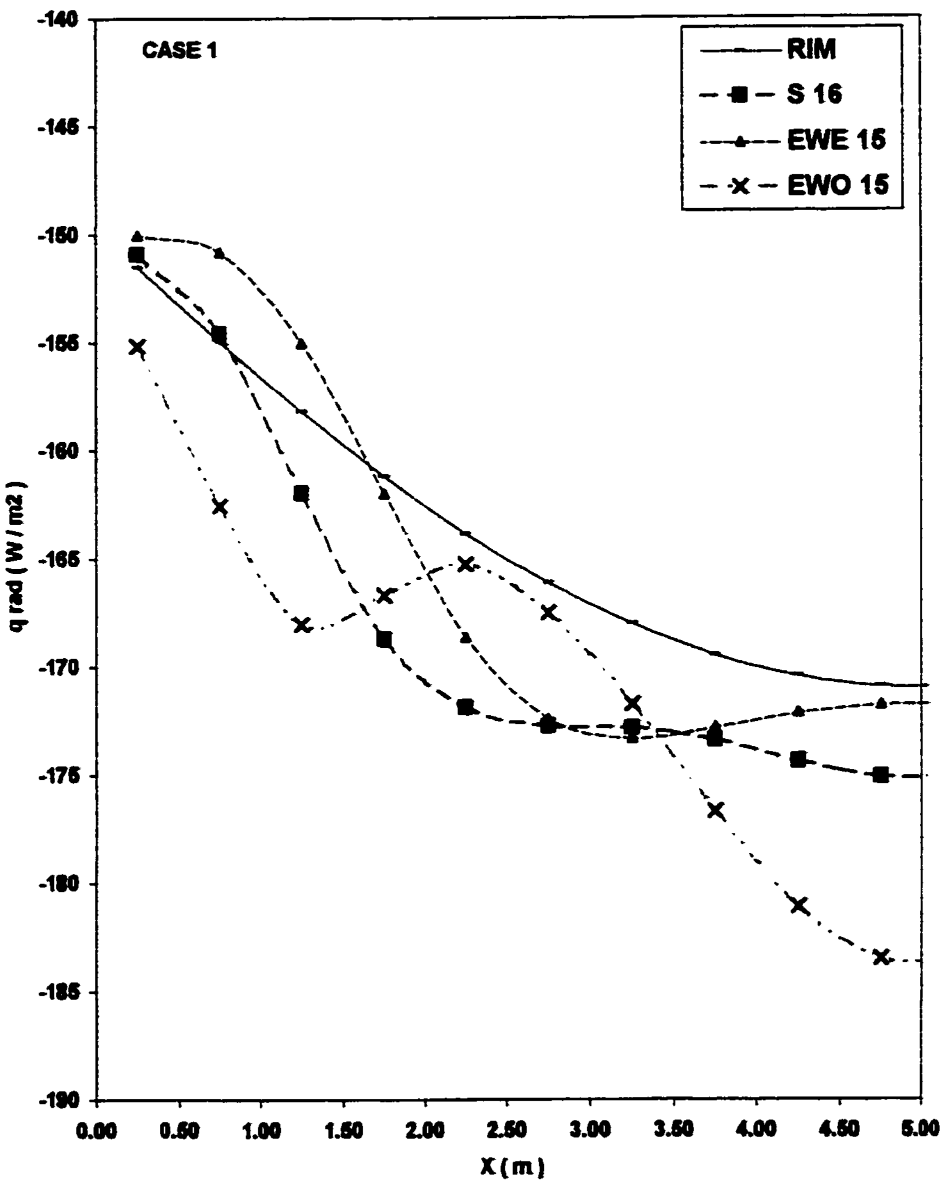

Figure 4.14 Heat flux. comparison of angular schemes.

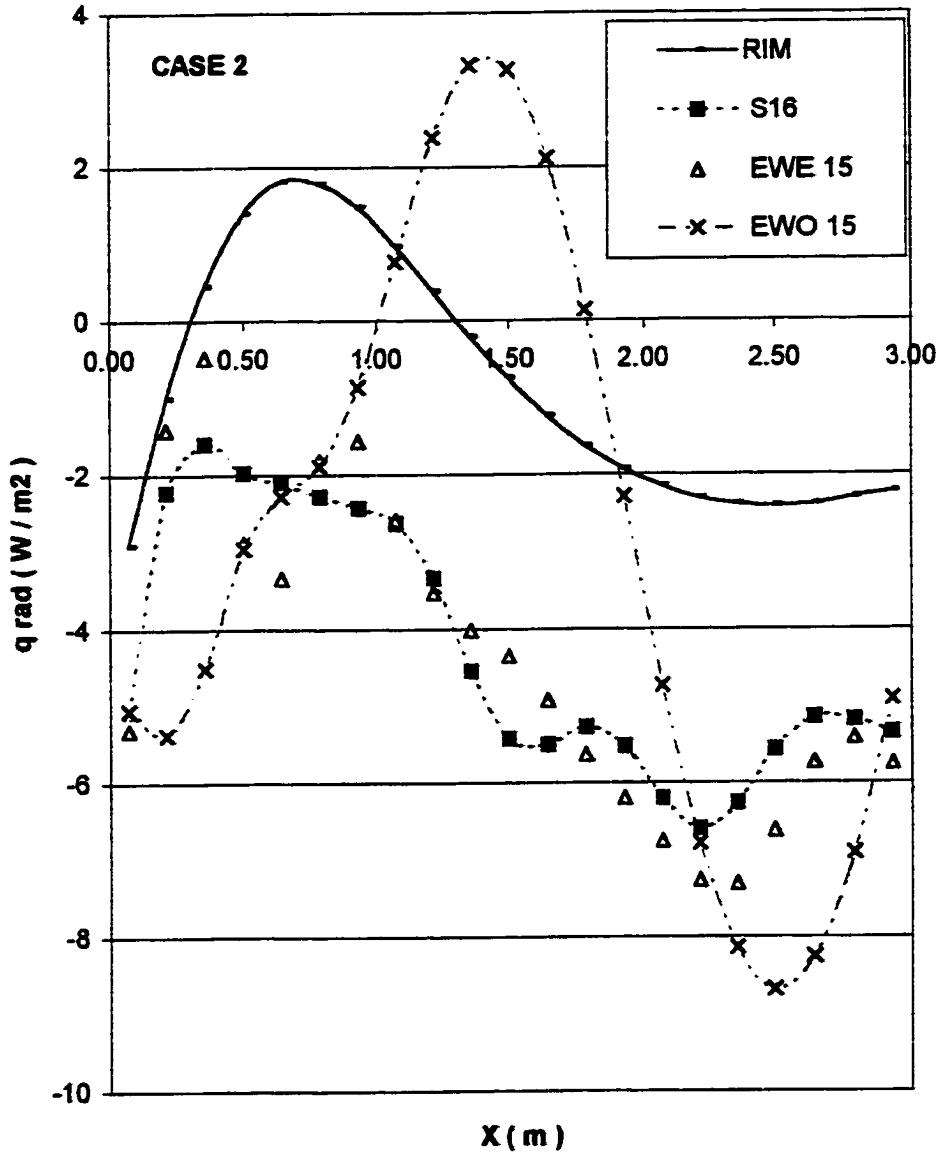

Figure 4.16. Heat flux. comparison of angular schemes

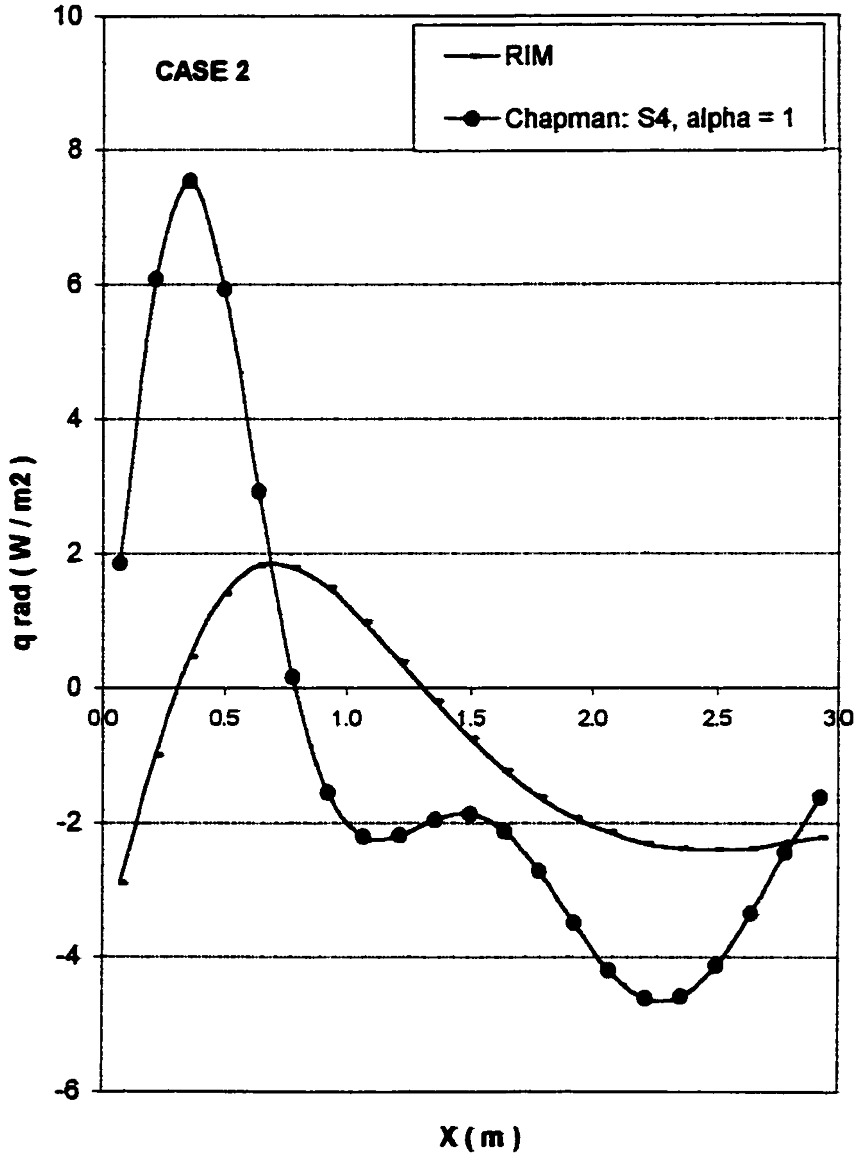

Figure 4.16 Heat flux. RIM and Chapman DOM calculation

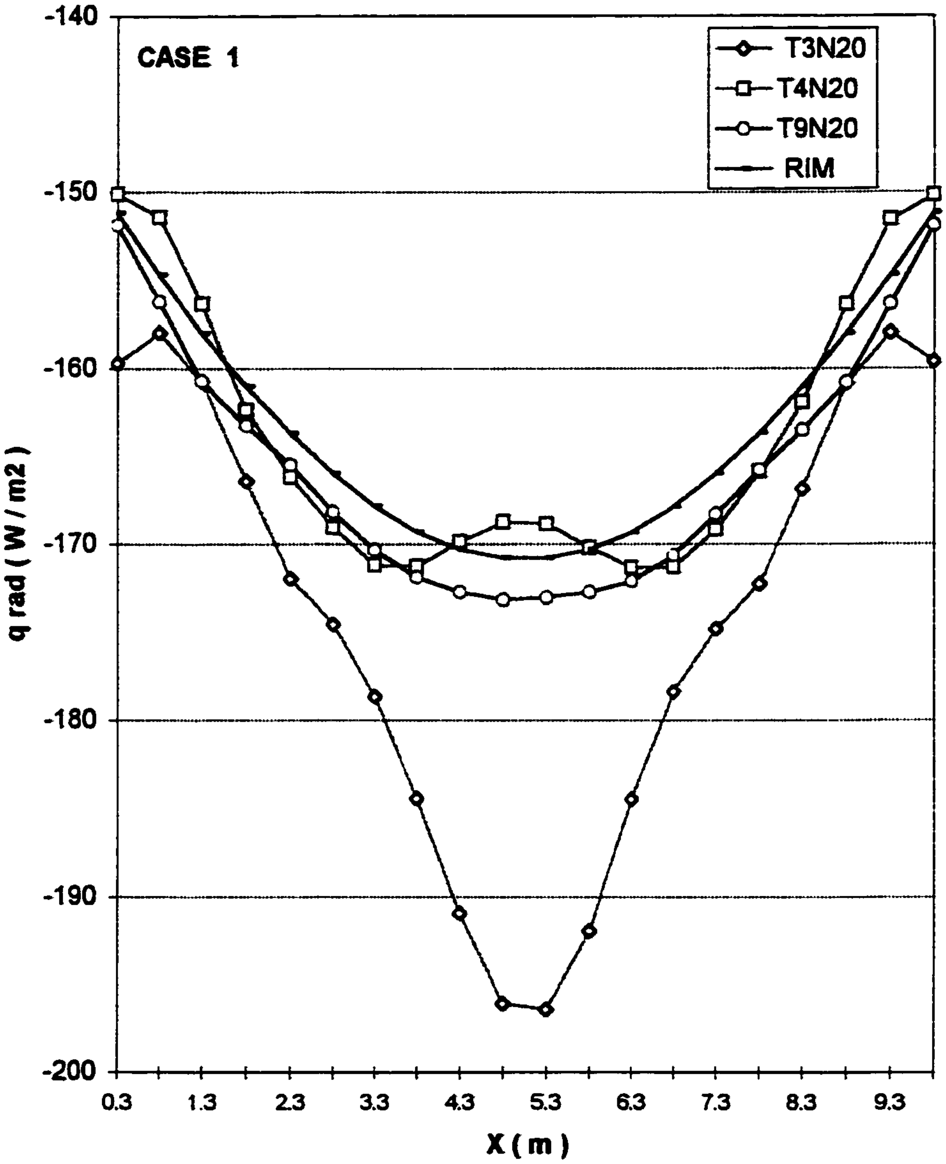

Figure 4.17. Local heat flux. Tn convergence

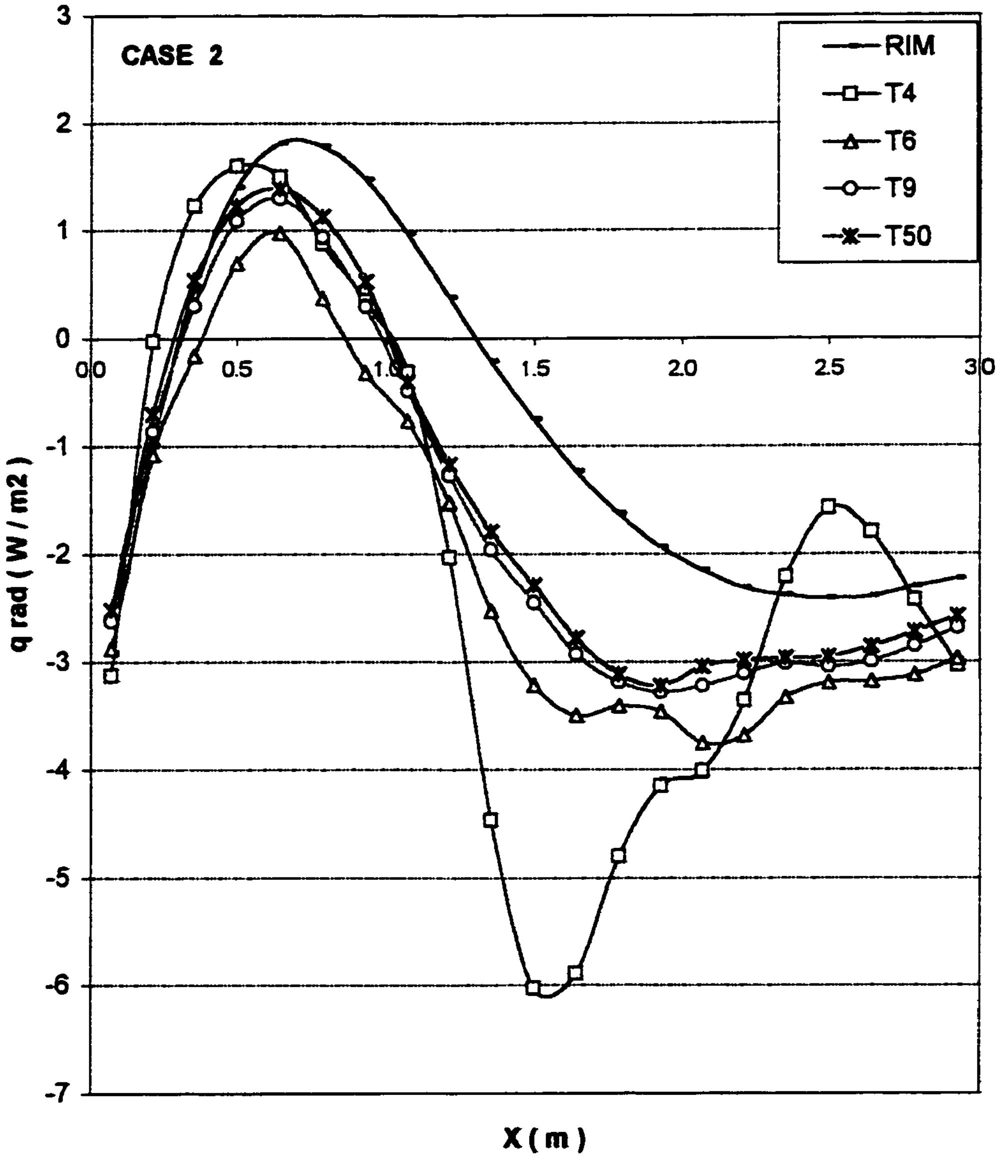

Figure 4.18. Local heat flux. Tn convergence

4.6 SUMMARY

If radiation heat exchange is calculated in an enclosure where there are no sharp gradients in intensity on the boundaries due to windows and heat panels, then angular quadratures such as S_n, EWE and EWO will be able to produce acceptable results. In the majority of the DOM applications, such as in furnaces, this is the case. On the other hand, if sharp intensity gradients are present, such as those produced by windows or heat panels, and if the medium is transparent, the above quadratures fail completely to produce a realistic profile of heat flux on a wall. This is mainly because of their inability to deal with the ray effect. The ray effect does not only depend on the number of rays. It has been shown that two sets with the same number of directions (EWE_{15} and EWO_{15}) produce heat flux curves that have completely different profiles.

The Tn quadrature has been compared to a benchmark solution given by the radiosity method. The invention of this quadrature partially rescues the DOM method so that it can be a valuable tool to calculate detailed, radiant heat exchange within a building enclosure. The T_n quadrature, however, as the other ones discussed in this thesis, has only ninety-degree symmetry. This means, as was shown at the beginning of this chapter, that it works properly for rectangules or cylinders but it does not work quite as well with sloped surfaces. This problem will become evident in Chapter 6.

Chapter 5

MINIMIZATION OF DISCRETE ORDINATES METHOD ERRORS

5.1 INTRODUCTION

As it was mentioned in Chapter 3, the Discrete Ordinates Method (DOM) is composed of two discretization processes: an angular discretization and a spatial discretization. Equations 3.24 and 3.25, reproduced here for convenience, govern the spatial discretization process.

$$
\begin{aligned}
I_p^J &= \alpha\, I_{x+\Delta x}^J + (1-\alpha)\, I_{x-\Delta x}^J \\
I_p^J &= \alpha\, I_{y+\Delta y}^J + (1-\alpha)\, I_{y-\Delta y}^J \\
I_p^J &= \alpha\, I_{z+\Delta z}^J + (1-\alpha)\, I_{z-\Delta z}^J
\end{aligned}
\tag{3.24}
$$

$$
I_p = \frac{\mu \Delta y \Delta z\, I_{x-\Delta x}^J + \eta \Delta x \Delta y\, I_{y-\Delta y}^J + \xi \Delta y \Delta z\, I_{z-\Delta z}^J}{\mu \Delta y \Delta z + \eta \Delta x \Delta y + \xi \Delta y \Delta z}
\tag{3.25}
$$

These equations provide the values of the intensities for a cell in the interior of the enclosure at a particular direction. They provide a simple set of equations involving just one cell of the internal mesh. This form of discretizing the equation of transfer allows a fast solution. However, equations 3.24 and 3.25 are the cause of two of the major numerical problems of the DOM, false scattering and false oscillations. In this Chapter an attempt to reduce these problems without involving more interior cells will be made.

5.2 THE RMS EXPERIMENT

In the following paragraphs extensive use will be made of the results of the rms experiment explained in Chapter 3 in relation with false scattering and false oscillations. For this reason a brief description of the experiment is repeated here. The original idea comes from Chai and Patankar (1992) in order to show the phenomena of false scattering and false oscillations, Chai et al. proposed an empty square with walls emitting no radiation. In this 2 – D enclosure a beam with I = 1 enters from the bottom-left corner of the square (Figure 3.14). Using the Discrete Ordinates Method (DOM), the intensities in the interior of the square are calculated. These intensities ought to be equal to one at the points that the beam intersects and zero otherwise. The beam can enter the enclosure at different angles, θ, and the error in the DOM calculation can be measured using the rms error defined as:

$$rms\ error = \sqrt{\frac{\left(I_{real\ at\ nodal\ point} - I_{DOM\ at\ nodal\ point}\right)^2}{n}} \qquad (3.33)$$

The rms error shows the combined effect of false scattering and false oscillations. The experiment can be repeated, as will be done in this chapter, with variable mesh sizes, with different angles and with different values of the interpolation constant.

5.3 FALSE SCATTERING & FALSE OSCILLATIONS

The causes of false scattering has been attributed to the lack of coincidence between the direction of the beam and the coordinate axis. Several attempts have been made to reduce the error arising from false scattering (Carey, Scanlon and Fraser, 1993, Satoru and Yamanaka,1991). The majority of these attempts use more than one interior cell. While in some cases this has proven to be a successful approach to reduce false scattering, the CPU time needed increases by a considerable amount. In many fluid dynamics situations this is not a cause of concern since the equations involved have to be solved just for one particular direction. However in the Discrete Ordinates Method (DOM) the equation of radiative transfer is solved M times where M is the total number of angular directions in the quadrature set chosen. For a typical quadrature set used in this thesis, a T_{20} for example, M could be as much as 3200. Hence, if the DOM is to work, a fast solution that involves only one cell needs to be found. The following paragraphs are an attempt to find this simple partial solution to the problem of false scattering.

The first idea is to refine the mesh. Hopefully false scattering decreases rapidly as the size of the cell diminishes. If this were true the only thing that would be necessary is to increase the number of spatial divisions. To probe this idea the rms experiment of Chapter 3 was repeated with a variety of mesh sizes. The experiment was performed with the beam inclined at an angle of 45 degrees where the worst case of false scattering is present. The results are shown in Figure 5.1 in terms of CPU time. In parenthesis the size of the mesh is shown for each point in the graph. As can be seen in this Figure, a fine grid performs just slightly better than a coarse one. After some point the rms error does not seem to decrease any further.

The second attempt is an attempt to adjust the interpolation factor, α, used in equations 3.23 to calculate the intensities at the boundaries of an internal cell. In Chapter 3, the value of this interpolation parameter had been shown to have a considerable influence on the accuracy of the method. In particular the phenomena of false scattering and false oscillations depend in an opposite manner, on the value of alpha as Table 5.1, another way of writing Table 3.1, shows.

Table 5.1 Dependence of false scattering and false oscillations on alpha

	False scattering	False oscillations
Alpha = 1	Large	No
Alpha = 0.5	Small	Large

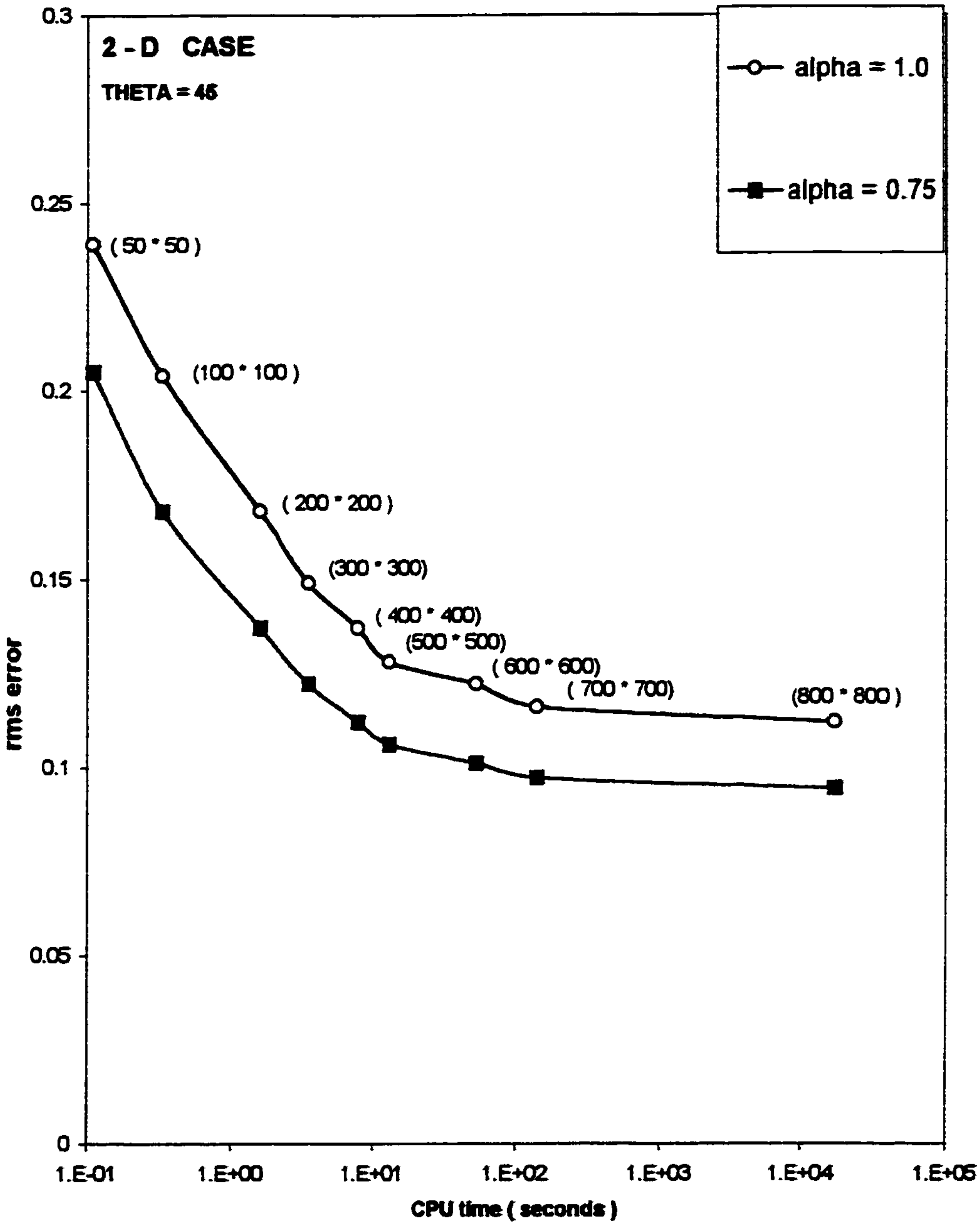

Figure 5.1. Rms error vs CPU time for a beam

This table, as well as Figure 3.21, suggests that for every angle there exists an alpha that minimizes the combined effect of false scattering and false oscillations. Specifically, it can be suggested, that by using a curve to approximate the experimental results of Figure 3.20, a DOM that uses the alpha suggested by this curve would produce the best possible DOM in terms of false oscillations and false scattering. The rms experiment was repeated changing the width of the beam and the mesh size and no significant changes were observed. The results are tempting since most of the alpha values are near 0.5 and their use promises to significantly diminish false scattering. However, since sharp intensity gradients cause false oscillations it can be argued that the results just shown are not going to be the same if they are repeated with more beams present.

Figure 5.2 shows a modification of the rms experiment. This modification allows for multiple rays. If the experiment to obtain an optimal alpha is repeated for this new situation, Figure 5.3 is obtained.

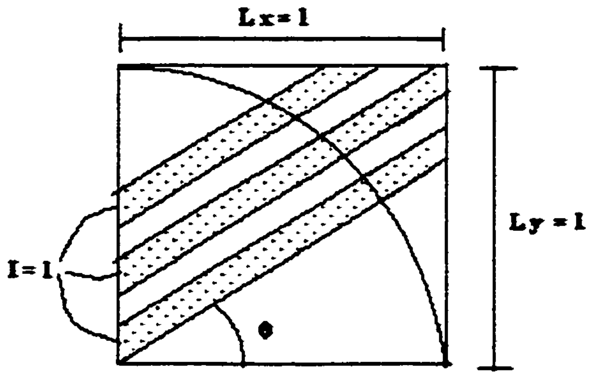

Figure 5.2 Rms error experiment for three beams

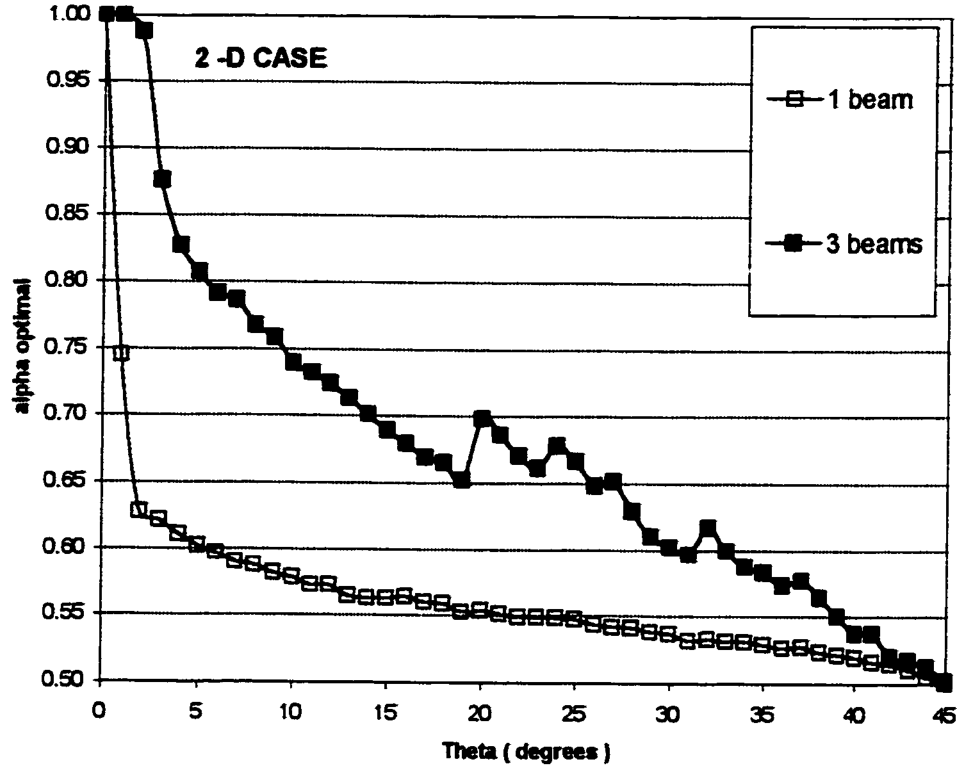

Figure 5.3 Optimal alpha with multiple beams

Therefore there is not a unique value of alpha that would minimize the combined effect of false oscillations and false scattering.

5.4 MODEL TO EXPLAIN FALSE OSCILLATIONS

As in the case of false scattering, to solve the problem of false oscillations, spatial schemes involving the use of downstream as well as upstream cells has been proposed. This group of spatial discretization schemes has been called High-Resolution (HR) schemes. Fiveland (1992) found that by using them, false oscillations were eliminated in a 2-D enclosure, Liu, Becker and Pollard (1996) suggested the use of SMART, one of these HR schemes, to eliminate false oscillations in 3 – D enclosures. However the use of these HR schemes in 3- D enclosures consume an enormous amount of CPU time.

In this thesis, the proposed procedure departs from a physical explanation of false oscillations in 2-D. As in the case of false scattering, the idea is to use just one cell. According to Table 5.1 the smaller the value of alpha the less false scattering there is. Therefore the following question emerges: Is there a minimum value of alpha for each value of theta that would ensure that we do not have false oscillations? . For $\theta = 45$ degrees that value is 0.5. In the case of $\theta = 0$ or $\theta = 90$ degrees that value is 1. In this section we will search for a theoretical answer and we will attempt to probe it experimentally. Let us return to an interior cell inside the volume of the enclosure. For the purpose of the following explanation assume that the beam comes from West to East and from South to North. Further assume, without lost of generality, that $I_w > I_s$.

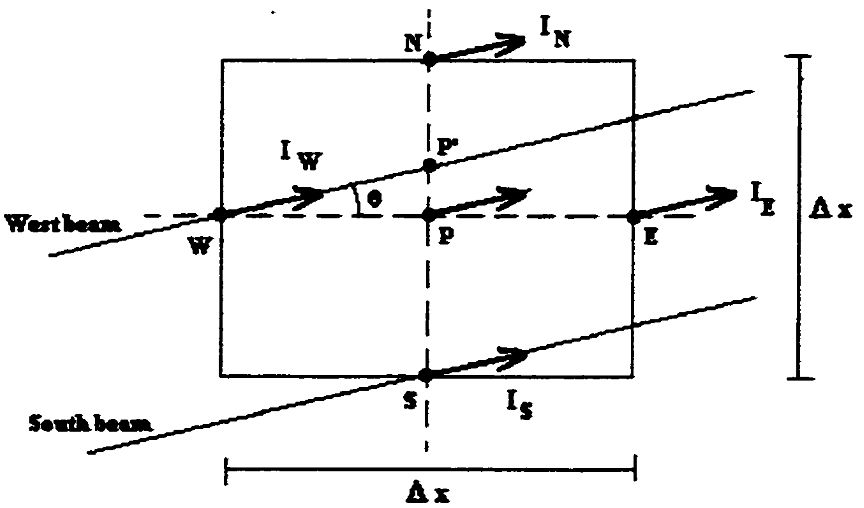

Figure 5.4 Average intensities inside a cell

Recall that equation 3.23 was obtained by assuming that I_w , I_s , I_E and I_N were constant over their respective faces. In practice the values of these intensities can be thought as average values for each particular face. It is also important to remark that the known values, the inputs, are I_w and I_s . If the medium is transparent, the second law of thermodynamics assures us that $I_S < I_N < I_W$ and $I_S < I_E < I_W$. That is, in the absence of sources, the intensity outputs have to be bounded by the inputs.

As an analogy the cell can be thought as a 2- D empty room in which the West and South walls are kept at constant temperatures such that I_S and I_W are emitted by these walls. In this case even if the North and East surfaces were black, adiabatic walls, their temperature would have to be between the temperature of the "sources" (the West and South walls).

Although I_w , I_s, I_E and I_N are the average intensities at each wall, the DOM assumes that all the intensity field inside the cell is concentrated at 5 points: I_w , I_s, I_E, I_N and I_p .

Assume that we desire to obtain I_E and I_N in the most possible accurate way without involving other cells. In this circumstances, the best possible choice is linear interpolation, $\alpha = 0.5$, From Figure 5.4 it can be seen that it would be adequate to do this for I_E since the beam that crossed at E is between the beams crossing at S & W. Thus, in this situation, if the intensity I_E is obtained by linear extrapolation from I_W and I_P it cannot be larger than Iw. The situation is different in the case of I_N . If we obtain I_N from a linear extrapolation involving I_S and I_P it would end with a value larger than I_W.

Figure 5.4 and Figure 5.5 illustrate what would be the best possible choice of I_N , and therefore of alpha in this case. This is the minimum value of alpha that would not produce oscillations:

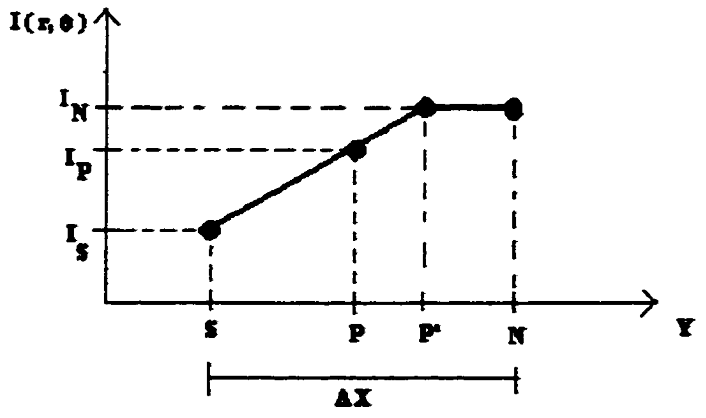

Figure 5.5 Best posible extrapolation for I_N

If P' is the intersection of the West beam and the line that joins S with N, we could say that it is " safe" to linearly interpolate between I_s, I_p and $I_{p'}$. However this would be the limit. If the linear interpolation were continued $I_N > I_W$ would be obtained, which would violate the second law within the cell. Thus from Figure 5.5:

$$I_N = I_{P'} = \left(\frac{I_P - I_S}{\Delta x/2}\right)\left(\frac{\Delta x}{2} + s\right) + I_S \tag{5.1}$$

But from Figure 5.4 and some trigonometry:

$$s = \tan\theta\left(\frac{\Delta x}{2}\right) \tag{5.2}$$

Substituting in Equation 5.1 and rearranging:

$$I_P = \left(\frac{1}{1+\tan\theta}\right) I_N + \left(1 - \frac{1}{1+\tan\theta}\right) I_S \tag{5.3}$$

By comparing equation 5.3 with 3.24 it is obvious that this equations are equivalent if:

$$\alpha = \left(\frac{1}{1+\tan\theta}\right) \tag{5.4}$$

In summary, a formula that shows us the non-oscillatory optimal alpha has been obtained. A couple of remarks need to be made:

In the paragraph above it was said that in the case of I_E we were free to make a linear interpolation all across the cell. That would mean $\alpha = 0.5$ for this direction. However equation 3.25 was obtained by assuming the same value of alpha for the N-S and the E-W interpolations.

Therefore, the maximum alpha would have to be chosen. That is, the alpha calculated by equation 5.4.

In equation 5.4, θ is always an angle $\theta < 45$. If $\theta > 45$ the same analysis would show equation 5.4, to be true except that " θ " in this case, would mean the angle between the y axis and the beam.

The numerical experiment to verify this theoretical formulation is similar to the rms experiment (Figure 5.2). This time, however, instead of measuring the rms error within the beam, a flag was introduced that turned on whenever an $I < 0$ or $I > 1$ was found. Using this procedure, the minimum value of alpha that produced no oscillations, $\alpha_{osc}(\theta)$, was found.

The experiment was repeated with multiple unitary intensity beams. The results are shown in Figure 5.6. The results confirm our expectations regarding the elimination of false oscillations.

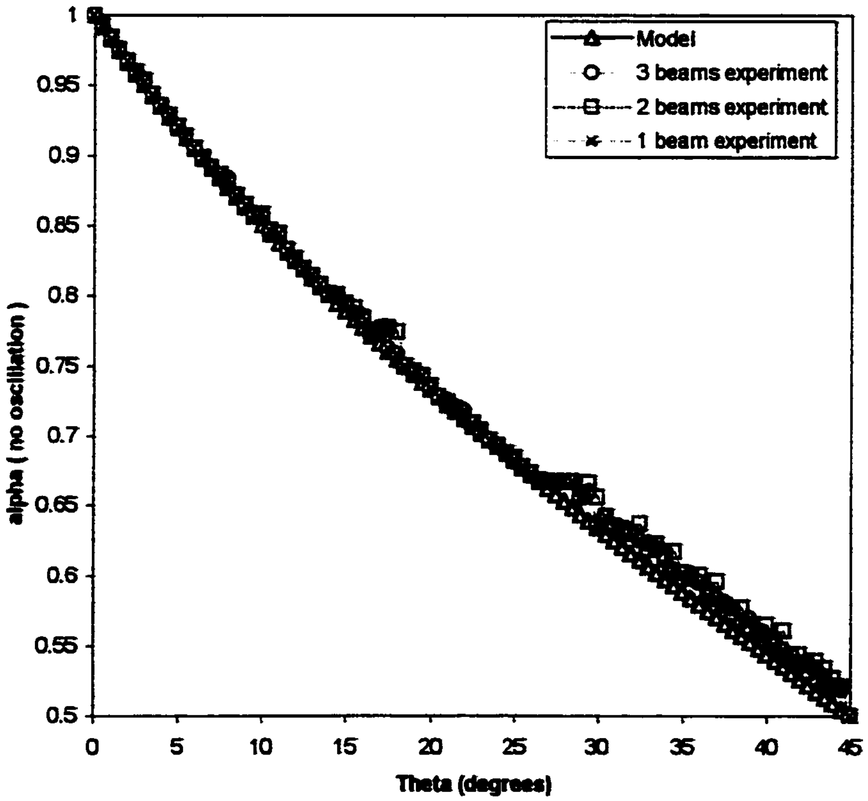

Figure 5.6 No oscillation value for alpha

Figure 5.7 shows the rms error measured using $\alpha_{osc}(\theta)$ with multiple beams. Notice that as more and more sharp gradients appear in the scene, the rms error continues to grow. This may be a signal of the limits of the DOM method to perform accurate calculations.

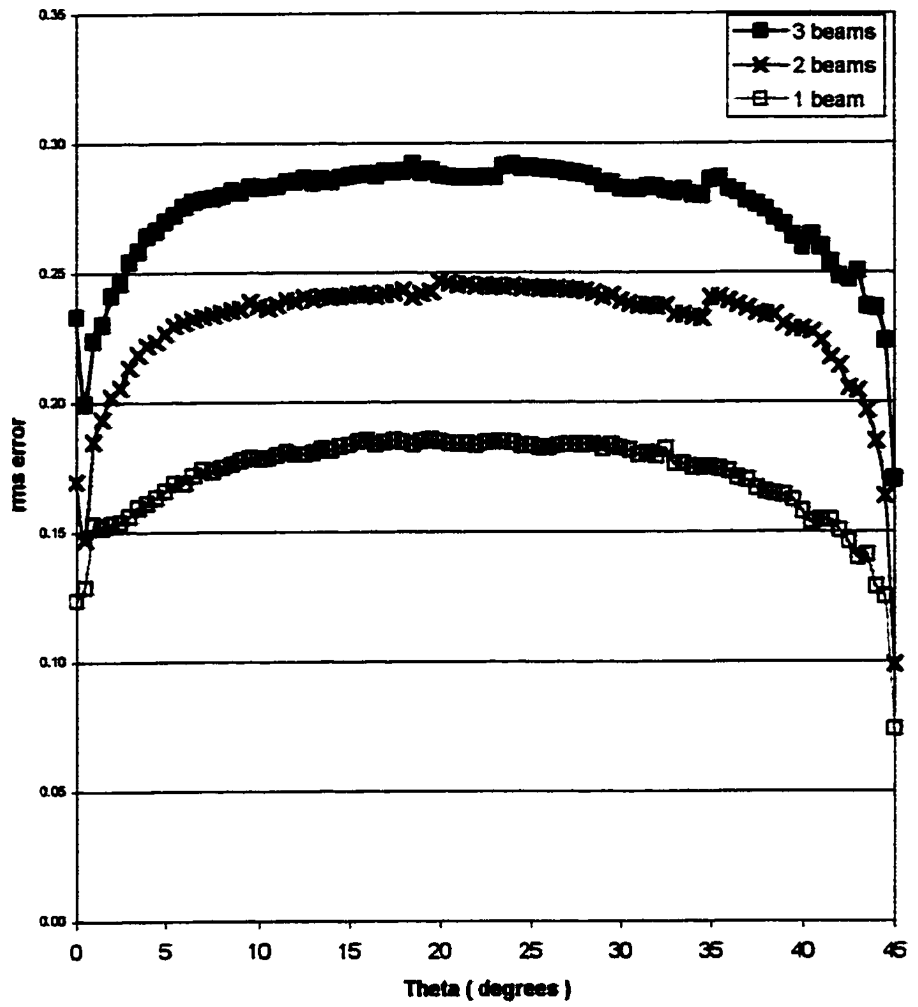

Figure 5.7 No oscillation alpha rms error

5.5 SUMMARY

In this Chapter an attempt was made to minimize the effects of false scattering combined with false oscillations. This was done working just within one cell and thus without significantly increasing the CPU time.

In particular we intended to use an alpha dependent on the direction cosines as opposed to a constant alpha. This was done in two ways. The first method used numerical experiments where the objective was to find the alpha that minimizes the rms error. It was found that no such single alpha exists. The alpha with the minimum rms errors depends on the number of intensity sources and sinks.

The second method involves the use of physical arguments and the second law, the minimum non oscillatory alpha was calculated for each angle θ.

Although the experiment suggests that we were successful in this attempt, the implementation of the idea has not produced any practical benefits. It was noticed that the performance of the DOM decreases with every new intensity gradient (windows or heat panels). The attempts to reduce false scattering & false oscillations had limited results. Therefore, if a method with capabilities comparable with the DOM can be found that outperforms the DOM it would be preferable. The Discrete Transfer method (DTM) is such a method; it completely eliminates false scattering and false oscillations by eliminating its source: the volume still mesh, as discussed in the next chapter.

Chapter 6

The Discrete Transfer Method as Applied to Transparent Enclosures

6.1 INTRODUCTION

In Chapter three, the equation of radiant transfer for nonparticipating media was written as:

$$\frac{\partial I_\lambda}{\partial S} = 0 \tag{6.1}$$

In this equation, S represents the distance along the beam direction. The DOM uses equation 6.2, which is a Cartesian version of equation 6.1. expressed in terms of coordinate axis, x, y, and z.

$$\mu\frac{\partial I_\lambda^j}{\partial x} + \eta\frac{\partial I_\lambda^j}{\partial y} + \xi\frac{\partial I_\lambda^j}{\partial z} = 0 \tag{6.2}$$

However two of the main numerical problems of the DOM, false scattering and false oscillations, mentioned in Chapter 3 and Chapter 5, come from the lack of coincidence between the coordinate axis and the direction of the beam. The aim of this chapter is to present an alternative to the DOM. The new method shares with the DOM the same basic idea: solve the equation of radiative transfer for a finite number of angular directions. With this method, however, it is solved along the beam direction. This method was proposed by Saha in 1979 and was named the " Discrete Transfer Method " (DTM).

In this chapter a version of the DTM for transparent enclosures will be presented first. The DTM has also been used to solve problems in participating media, but not previously for transparent media. The DTM and the DOM methods will then be compared in terms of speed and accuracy. The relative advantages and disadvantages of the two methods will be discussed.

6.2 THE DISCRETE TRANSPORT METHOD FOR NONPARTICIPATING MEDIA

In the original formulation including participating media, the physical domain is discretized with a global uniform rectangular mesh with boundary segments as shown in Figure 6.1 for the 2-D case. We first initialize the intensities leaving each boundary segment. The intensities along each ray are determined by using a recurrence relation obtained by integrating the general equation of radiative transfer, equation 3.1 which includes absorption, along a ray distance s and assuming no scattering:

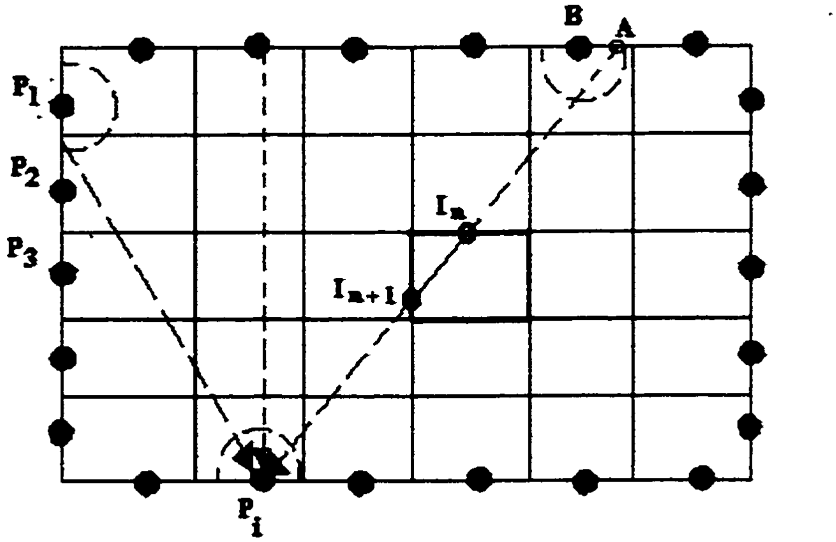

Figure 6.1 The original Discrete Transfer Method idea

$$I_{n+1} = \frac{\sigma T^4}{\pi}\left(1-e^{-ks}\right)+I_n e^{-ks} \tag{6.3}$$

The intensity impinging upon point Pi from a particular direction is found then by following the ray backwards through each mesh interior cell and using equation 6.3 to find point A, where the ray originates. The intensity at point A in Figure 6.1 is assumed to be equal to the intensity at the center of the respective boundary segment, point B in this case.

For transparent media, equation 6.1 implies that the intensity of a beam does not change while it is traveling between two surfaces. In particular this means that the intensity impinging upon point Pi in Figure 6.1 is equal to the intensity leaving point A. Therefore no interior mesh is needed.

As in the case of the DOM, the boundary conditions are written for an opaque uniformly reflecting wall as:

$$I_{\lambda,boundary} = \varepsilon I_{b,\lambda} + \frac{\rho_\lambda}{\pi}\int_{n.\Omega\leq 0} |n.\Omega|\, I_\lambda(\Omega')d\Omega' \tag{6.4}$$

Therefore, as in the case of the DOM, in order to calculate equation 6.4, it is necessary to make an angular discretization and to choose a quadrature set. The same rules regarding symmetry and moment matching should be applied and, therefore, the same quadrature sets are available for both methods. As in the case of the DOM and for similar reasons, the Thurgood quadrature is chosen in this case. Therefore as was done before, equation 6.4 takes the following form:

$$I_{\lambda,boundary} = \varepsilon I_{b,\lambda} + \frac{\rho_\lambda}{\pi}\sum_{n.\Omega<0} |n.\Omega|\, I_\lambda^j\, \omega_j \tag{6.5}$$

6.3 SOLUTION SCHEME FOR DTM

The process described below is represented in the block diagrams of Figures 6.2 and 6.3. In contrast with the DOM method, this version of the DTM method does not use any mesh and therefore the volume inside the enclosure is not divided into cells. The procedure can be divided in two parts. In the first, the heat fluxes (or temperatures) at the surfaces of the enclosure are calculated without using any interior points at all. In Figure 6.4 a 2-D example is shown. In the picture, n_a, n_b, n_c and n_d are the normal vectors at the respective surfaces. The different angular directions used are represented by j =1 through j = 8 and the weights by $\omega_1 \ldots \omega_8$.

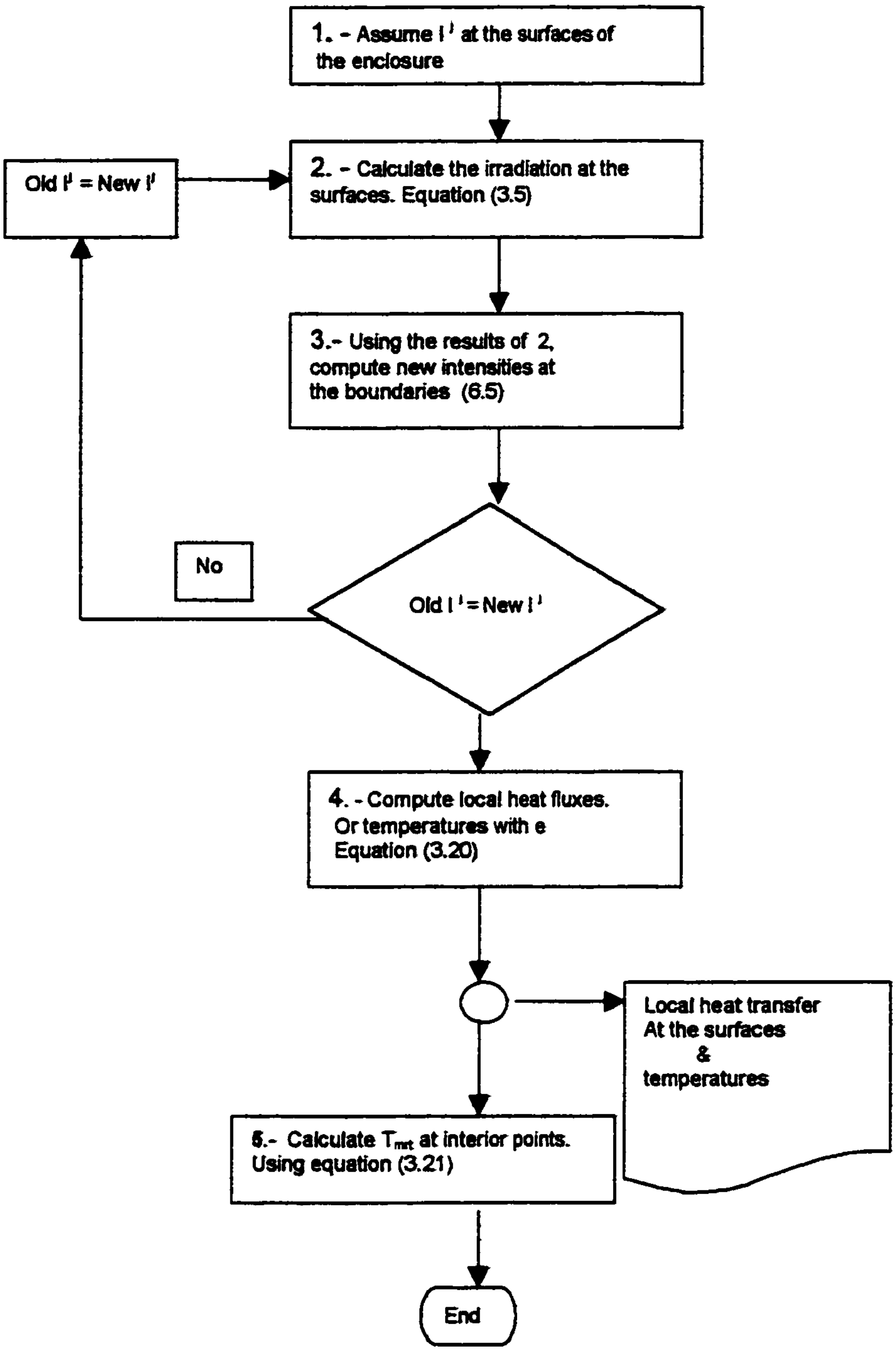

Figure 6.2 Block diagram for the Discrete Transfer Method for transparent enclosures

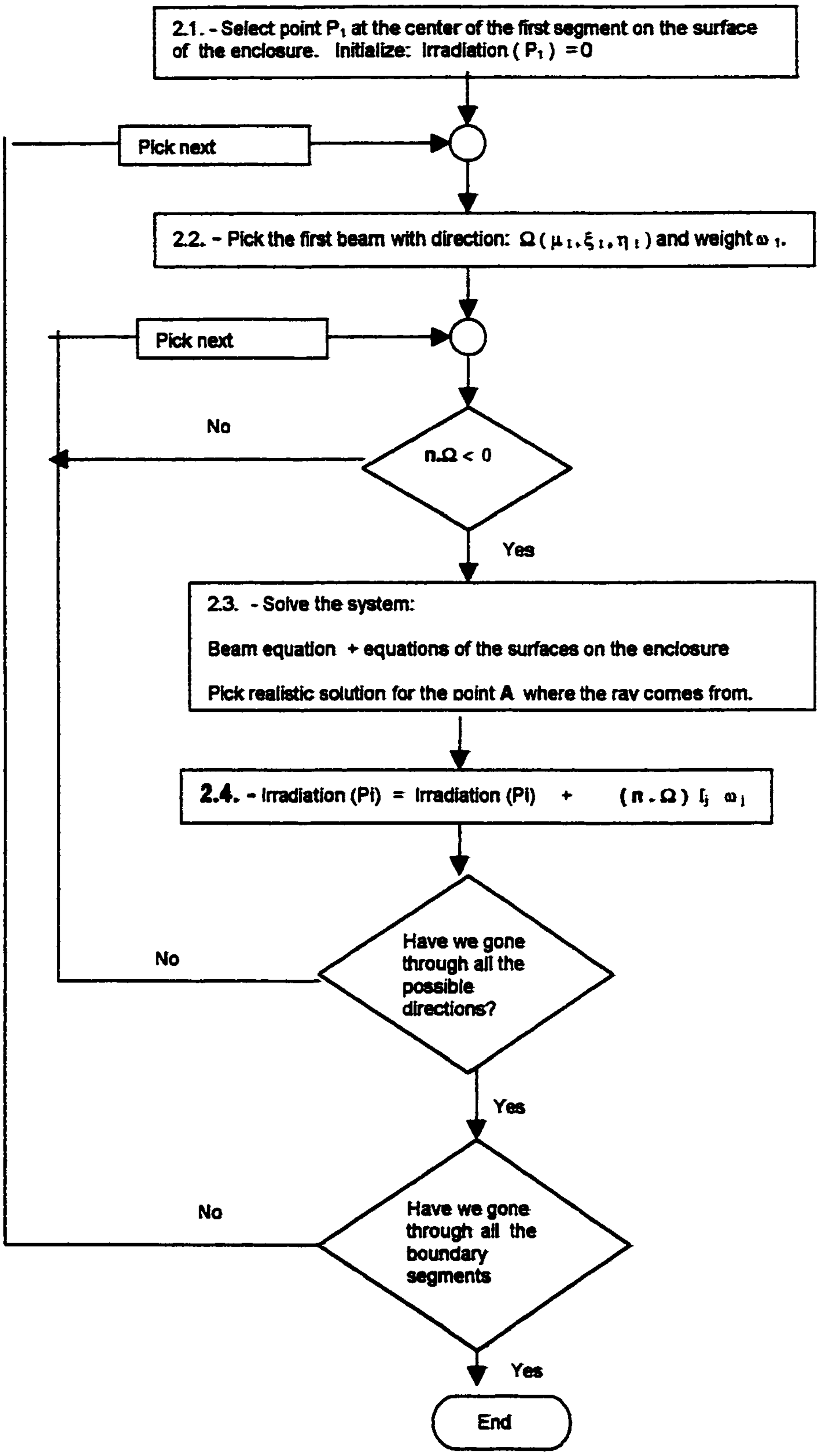

Figure 6.3 Step 2: Irradiation calculation for the Discrete Transport Method

For this example the intensity distribution on each wall is divided in two segments. In the following description all reference are made to this Figure .

PART A: Heat flux or temperature calculation at the boundary points

A.1 .- Assume the intensities at the discretized boundary segments. In this example, the center of the segments are labeled P1 through P8. Normally these intensities are initialized by making them equal to the intensities emitted by gray bodies at the specified temperature

$$I(P_i)_{\lambda,boundary} = \varepsilon I_{b,\lambda} \tag{6.6}$$

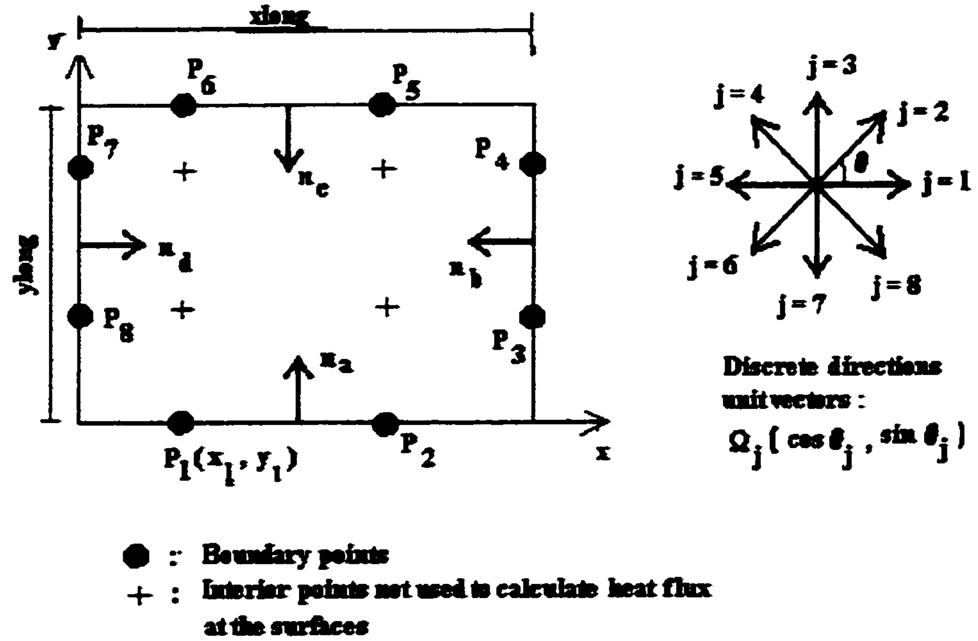

Figure 6.4 A 2-D example of the DTM in transparent enclosures

A.2. - <u>Calculate the irradiation at the boundary points</u>. Recall that, at any particular point, the irradiation can be approximated by:

$$G(P_i) = \sum_{n.\Omega<0} |n \bullet \Omega| I_j \, \omega_j \tag{6.7}$$

In Equation 6.7, i represents a segment on the surface of the enclosure and j represents an angular direction. Note that from the four multipliers in equation 6.7 just I^{j}_{λ} needs to be calculated; n, Ω, ω_j are given either by the geometry of the enclosure or by the angular quadrature chosen The process described below is shown in Figure 6.3 as a block diagram

2.1. - Select the center of the first segment on the surface of the enclosure, P_1 in Figure 6.4. Initialize the irradiation at that point to zero.

2.2. - Select the first direction on the angular quadrature (j = 1). Calculate the product $\mathbf{n}_i . \Omega^j$. If it is positive, pick the next angular direction, continue the process until $\mathbf{n}_i . \Omega_j < 0$.

2.3. - Calculate the point where the beam impinging point P_1 originated. In order to do this the beam equation is solved simultaneously with the equations of the surfaces of the enclosure. For a rectangular enclosure there is only one realistic solution. If the result is point A and if point B is the center of the segment where point A belongs then: then $I_{\lambda}^{j} = I_B$. Figure 6.5 represents the process for a two dimensional case. Figure 6.6 illustrates a method to calculate the equation of the beam in a 3 – D case.

2.4. - Recalculate the irradiation at the point:

$$G(P_1) = G(P_1) + (n.\Omega_j).I_j \, \omega_j \tag{6.8}$$

2.5. - Select the next angular direction in the quadrature set (j = j + 1) and repeat steps 2.2 to 2.4 until all the available angular directions are used.

2.6. - Pick the next segment on the surface of the enclosure (i = i + 1) and repeat the process until all the segments on the surface of the enclosure are considered. At the end of the process the irradiation at the center of all of these segments is now calculated.

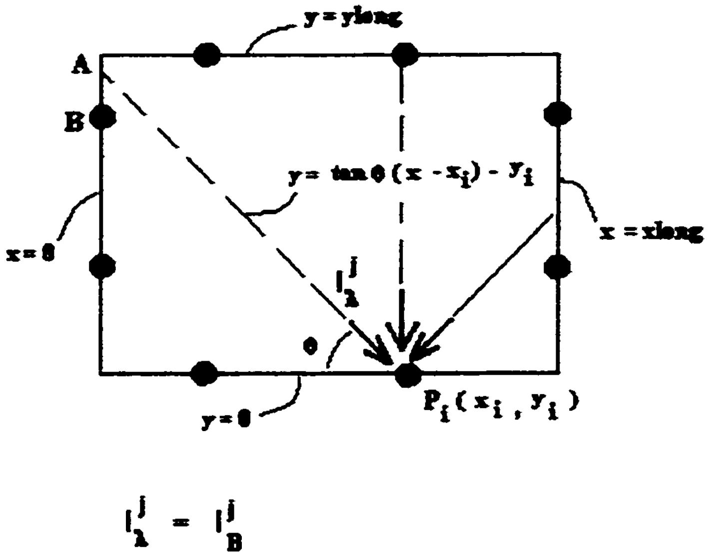

Figure 6.5 Step 2: Calculating the intensity of the impinging ray

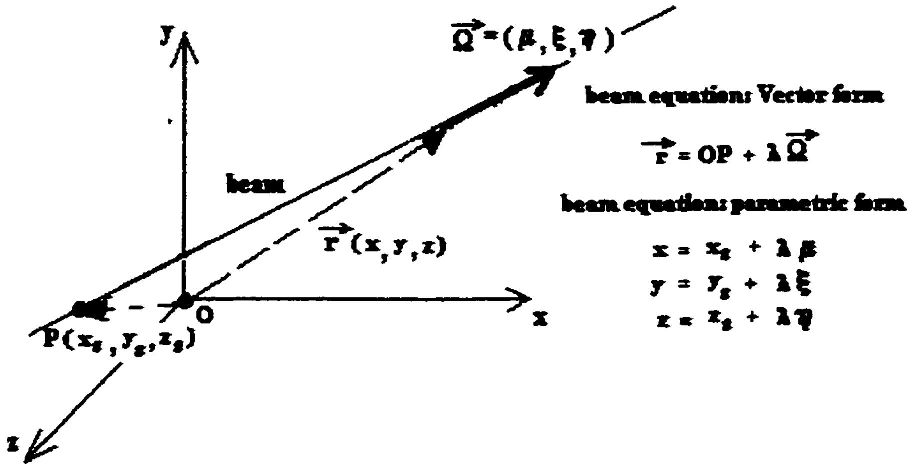

Figure 6.6 Equation of the beam in three dimensions

A.3. - Recalculate the intensities at the boundary points. Using the results of step 2. equation 6.5 is applied at the center of each segment on the surface of the enclosure to find a new value for the intensities at those points. If the difference between the old and the new values of intensity at the boundaries are not small enough, step # 2 & step # 3 are repeated again until the solution converges.

$$I(r)_{\lambda,boundary} = \varepsilon I_{b,\lambda} + \frac{\rho_\lambda}{\pi} G(r) \tag{6.5}$$

A.4. - Compute the heat flux at the boundary segments. Now the distribution of intensities along the boundary segments in every possible direction is known. Therefore, equation 6.9 is applied directly at each point to obtain the heat flux for each segment.

$$q(r) = \varepsilon I_b \quad - \quad (1-\rho)G(r) \tag{6.9}$$

PART B. Mean radiant temperature calculation at interior points

B.1. - Selection of interior points. Select the interior points where the mean radiant temperature value is desired. They do not have to be arranged in any particular pattern.

B.2. - Mean radiant temperature calculation. Recall that:

$$T_{mrt}^4 = \frac{1}{4\sigma} \sum I^j \omega_j$$

Therefore, at each of the selected interior points, direction by direction as was done in step 2, follow the beam backwards until the segment of the surface where it was originated is detected. The intensity at the center of this segment is used in equation 6.8 to calculate mean radiant temperatures.

A TWO-DIMENSIONAL EXAMPLE:

Assume that the enclosure in Figure 6.4 is a square and that the temperature at surface A is T_A = 200 K. Assume, further, that in the rest of the enclosure surfaces are at T = 100 K. Suppose, also, that the emisivitties at all the walls are equal to 0.9. The steps outlined above will be followed to calculate the heat flux at each segment on the enclosure.

For a three dimensional example, the weights ω_i, would be chosen in accordance with the angular quadrature set selected. In the two dimensional case, Smith and Sanchez (1992) proposed the use of equal weights chosen with the formulae given below. In the following equations, M is the number of angular directions per quadrant:

$$\omega = \omega_1 = \omega_2 = \cdots = \omega_i = \frac{\pi}{2\sum_{i=1}^{M} \cos \phi_i} \tag{6.11}$$

$$\phi_i = \frac{\Delta\phi}{2} + (i-1)\Delta\phi \tag{6.12}$$

In our 2-D example, $\Delta\phi = 45$, therefore:

$$\omega = 1.202$$

It should be remarked that Smith and Sanchez proposed the angular directions given by equation 6.12 along with the weights calculated with equation 6.11. However, since the purpose of this example is just to illustrate the DTM technique, that advice is not been followed.

1. - Assume intensities:

Suppose that the irradiation is equal to zero at every point, then the intensities for each segment can be calculated by:

$$I_{P1} = \frac{\varepsilon \sigma T^4}{\pi} \tag{6.13}$$

The results for each point are shown in the first column of Table 6.2

2. - Calculate the irradiation at each point on the surface:

In order to apply equation it is necessary to compute **n.Ω** for the eight different directions applied at four different surfaces. The results of these computations are shown in Table 6.1

Table 6.1. Dot product for 2-D example

	n.Ω							
	J = 1	J = 2	J = 3	J = 4	J = 5	J = 6	J = 7	J = 8
Surface A	0	0.707	1	0.707	0	-0.707	-1	-0.707
Surface B	-1	-0.707	0	0.707	1	0.707	0	-0.707
Surface C	0	-0.707	-1	-0.707	0	0.707	1	0.707
Surface D	1	0.707	0	-0.707	-1	-0.707	0	0.707

Therefore equation applied to point one would be:

$$G(P_1) \;=\; 0.7071\omega_6 I^6 + 1\omega_7 I^7 + 0.7071\omega_8 I^8 \tag{6.14}$$

In this equation I^6, I^7 and I^8 are the intensities impinging upon the first segment of the enclosure coming from directions j = 6, 7 and 8. To find the values of these intensities, the beams arriving at point P1 from these directions need to be followed back to the segment where they come from. In this particular case:

$$I^{6} = I_{leaving\ at\ segment4} = 1.624\,\frac{watts}{sr.m^{2}}$$

$$I^{7} = I_{leaving\ at\ segment\ 6} = 1.624\,\frac{watts}{sr.m^{2}}$$

$$I^{8} = I_{leaving\ at\ segment\ 8} = 1.624\,\frac{watts}{sr.m^{2}}$$

Therefore, applying equation

$$G(P_1) \quad = \quad 4.713 \quad \frac{Watts}{m^2}$$

Applying the same procedure, the irradiation at every segment can be calculated, the results are shown in the second column of Table 6.1

3. - Recalculate the intensities at each segment.

Since the irradiation falling upon every segment of the enclosure is known, equation 6.4 can be applied to recalculate new intensities for every segment. At point 1 for example:

$$I(P_1) \; = \varepsilon I_{surface\ A} + \frac{\rho_\lambda}{\pi} G(P_1) \qquad (6.5)$$

$$I\,(P_1) \quad = \quad 26.086\,\frac{Watts}{m^2\,sr}$$

The intensity at other segments is recalculated in the same manner. The results are shown in the third column of Table 3.2. Since the intensities calculated differ substantially from the intensities assumed in step 1, steps two and three need to be repeated until the difference in the intensities between iterations is below a predetermined level. The computed intensities and irradiations at each segment are shown in Table 6.1.

Table 6.2 Surface intensities for 2-D example

	Iteration 1		Iteration 2		Iteration 3	
Segment	Intensity ($W/sr.m^2$)	Irradiation (W/m^2)	Intensity	Irradiation	Intensity	Irradiation
1	25.988	4.713	26.138	7.389	26.223	7.558
2	25.988	4.713	26.138	7.389	26.223	7.558
3	1.624	25.421	2.433	27.441	2.497	27.633
4	1.624	25.421	2.433	27.441	2.497	27.663
5	1.624	33.998	2.706	35.554	2.756	35.766
6	1.624	33.998	2.706	35.554	2.756	35.766
7	1.624	25.421	2.433	27.441	2.497	27.633
8	1.624	25.421	2.433	27.441	2.497	27.633

4. - Compute the heat flux at each segment.

Recall that:

$$q(r) = \varepsilon \pi I_b \quad - \quad \varepsilon G(r) \qquad (6.9)$$

The last column in Table 3.2 represents the final approximation of the irradiation obtained at every segment. Therefore a straight-forward computation produce the following results.

Table 6.3 Heat fluxes for the 2-D example

Segment	Heat flux (W / m2)
1	74.84
2	74.84
3	-19.77
4	-19.77
5	-27.087
6	-27.087
7	-19.77
8	-19.77
Total heat	16.441

The lack of accuracy of the results is due to the small number of angular directions used. In particular it should be noted that equation 6.1 is the energy conservation equation for a particular direction. As the number of directions is increased, the accuracy increases.

6.4. - DISCUSSION OF CHARACTERISTICS OF THE DTM ALGORITHM

The algorithm has some interesting features that should be mentioned. The computation of the irradiation at point Pi is independent of the same computation made at point Pi+1. This suggests, as was noted by Cumber (1998), that these calculations could be performed by different processors and, therefore, the algorithm could easily be adapted on a parallel computer architecture. In the limit, there could be one processor for each point Pi at the surface of the enclosure. Another feature noted by Cumber (1995) is worth mentioning. According to him, approximately 70 % of the execution time needed by the DTM method was accumulated tracing rays through the domain. Since the angular directions are fixed, it is possible to calculate the point of departure of a beam (step 2.3) only during the first iteration. In subsequent iterations, the stored values of these departure points can be used rather than recalculating them. In this way, the speed of the calculation could be increased by as much as 3.5 times. As he noticed, the disadvantage of this procedure is the huge amount of memory needed, however, maybe in the near future, as the computer systems advance, this " once and for all ray implementation " would be feasible.

The version of the DTM method that we are implementing has the same geometric capabilities as a Monte Carlo code since the DTM method borrows from the latter the idea of following the rays. The same shading algorithms, for example, could be implemented in the DTM method, However, contrary to what happens in the Monte Carlo Method, in the DTM method, the rays need to be followed just once. It is also important to note that part A and part B can be uncoupled. That is, if all that is desired are the heat fluxes on the walls of the enclosure then just part A needs to be used. In fact the interior points in part B do not need to have any relation to the way the surfaces of the enclosure are divided. For instance if a 30 by 30 grid was used on the surfaces of the enclosure and the mean radiant temperature is desired just in 5 specific interior points, then those five points can be computed without having to calculate the mean radiant temperatures anywhere else.

6.5. - TEST CASES AND RESULTS

A convergence test was implemented for the DTM method using case number One. The results are shown in Figure 6.7. It is instructive to compare it with graph 4.17 (page 87) where the same experiment was done for the DOM (In both cases Thurgood quadrature was used). Two observations come to mind: In general the DTM method tends to show more oscillations and it needs more angular divisions to converge. However, it does converge to the RIM benchmark solution . In contrast, as shown in Figure 4.17, the DOM converges to a heat flux value slightly more negative than the one predicted by the RIM. As it was mentioned in Chapter 3, the lack of accuracy of the DOM method can be attributed to false scattering. The smoother nature of the curves predicted by the DOM can also be attributed to false scattering. This is the case because, as was mentioned in Chapter 3, false scattering (or real scattering) tends to reduce the oscillations caused by the ray effect. In the case of the DTM method there is no false scattering present and

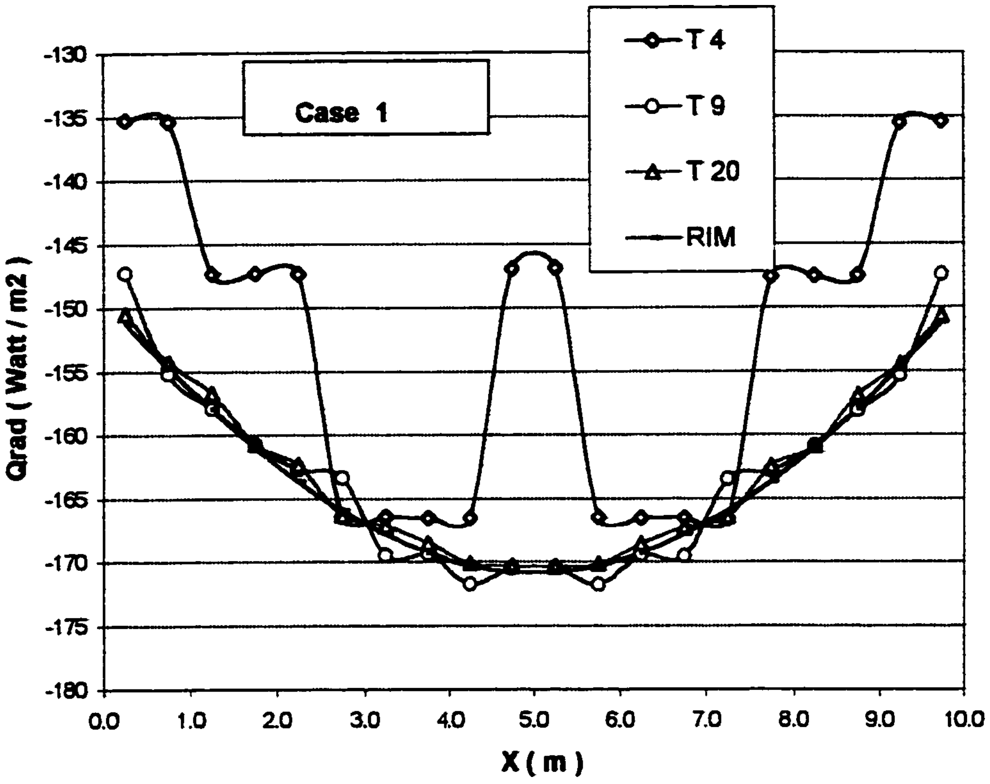

Figure 6.7 DTM convergence test

therefore, the oscillations caused by the ray-effect are not hindered. This could be explained, alternatively, by saying that the DOM partially converts its ray-effect to false scattering.

Case number 2 (Figure 1.3), with a cold window and a heat panel, should produce larger ray – effect oscillations in the DTM method and larger false scattering in the DOM. The results for the heat flux along the midline of the floor using the DTM method are shown in Figure 6.8.

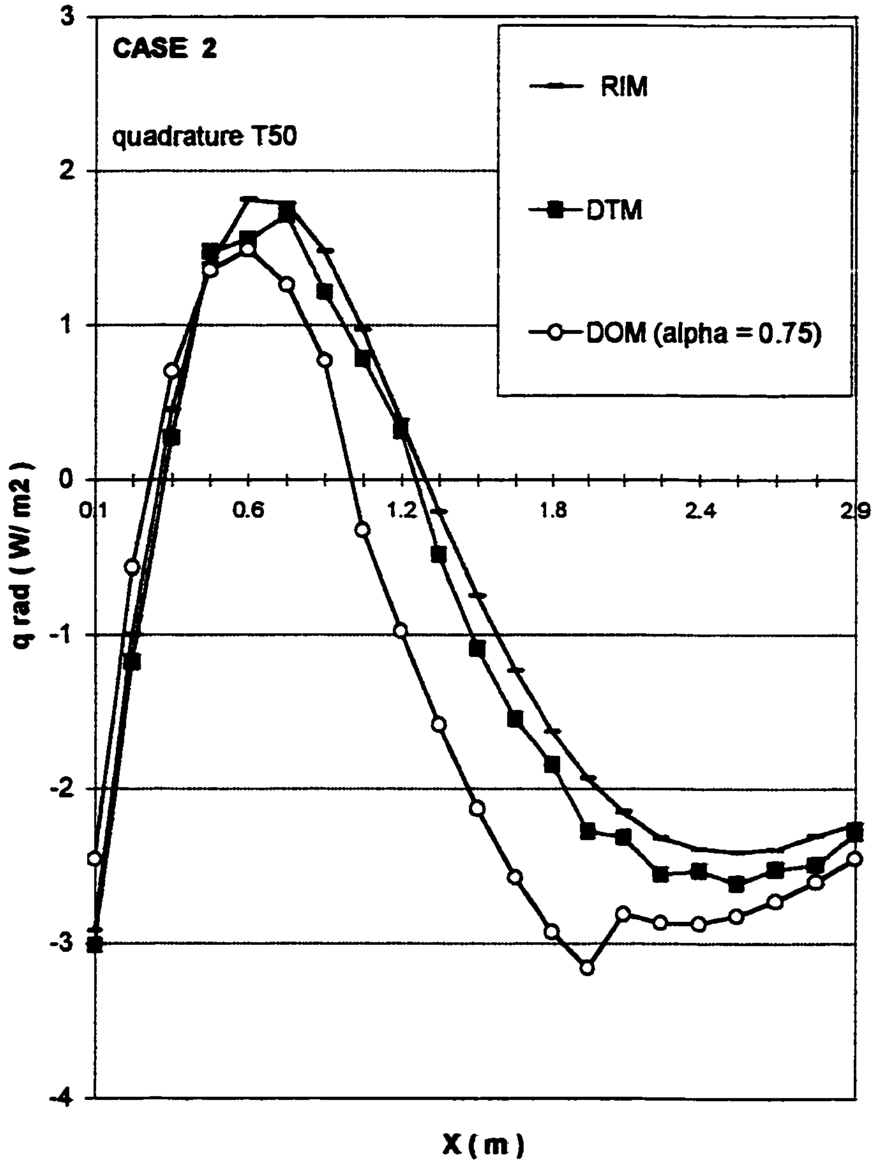

Figure 6.8. Floor midline local heat flux

As can be seen a large number of angular directions are needed to arrest the oscillations. The result, however, converges to the RIM benchmark value. In contrast, the heat fluxes calculated by the DOM depart, substantially, from the benchmark solution.

To compare both methods in terms of accuracy and CPU time needed, the heat fluxes in case 3, were calculated using both methods with different number of divisions (n = 9, 21, 36) and with different number of angular directions. The rms errors along the midline shown in Figure 1.3 were calculated with the following formulae:

$$rms\ error = \sqrt{\frac{\left(q_{RIM} - q_{DT}\right)^2}{n}}$$

Figure 6.9 is a graph of rms error vs CPU time. The ideal method would be located near the lower left corner of the graph, that is, it would produce results of great accuracy (small rms error) in a short time. The numerical experiment was done in a PC computer with a pentium processor at 333 Mhz. It is clear that for this kind of situations, the DTM method performs better in terms of accuracy and speed. Roughly speaking, if the same amount of CPU time is to be used, the DTM method give results approximately four times more precise.

As the number of windows and heat panels increase, i.e as the number of sharp gradients in intensity increase, the accuracy of the DOM should become worse and worse as the false scattering effects take its toll. For the DTM method, an increase of sharp intensity gradients means that it has to have larger and larger numbers of angular directions to arrest its ray effect. The total balance, however, appears to favor the DTM method.

Figure 6.10 is similar to Figure 6.9. This time the DTM is compared with the RIM. In this graph, as in the others, the benchmark used is the RIM with 21 divisions. The CPU time in the graph represents just the time needed to calculate heat flux on the walls. The time needed to estimate T_{mrt} is not considered in this figure since the RIM does not calculate these temperatures.

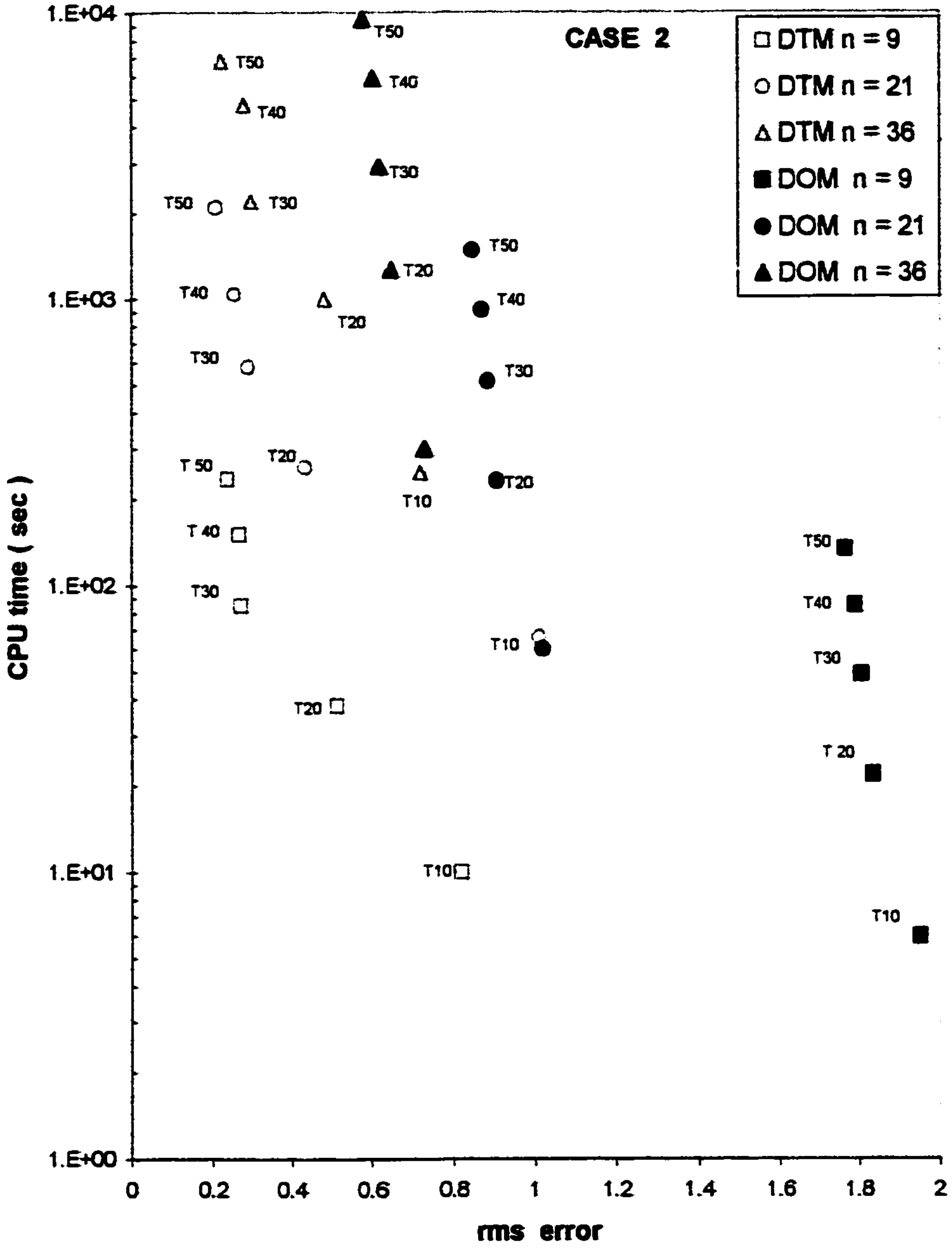

Figure 6.9 Comparison of DTM and DOM

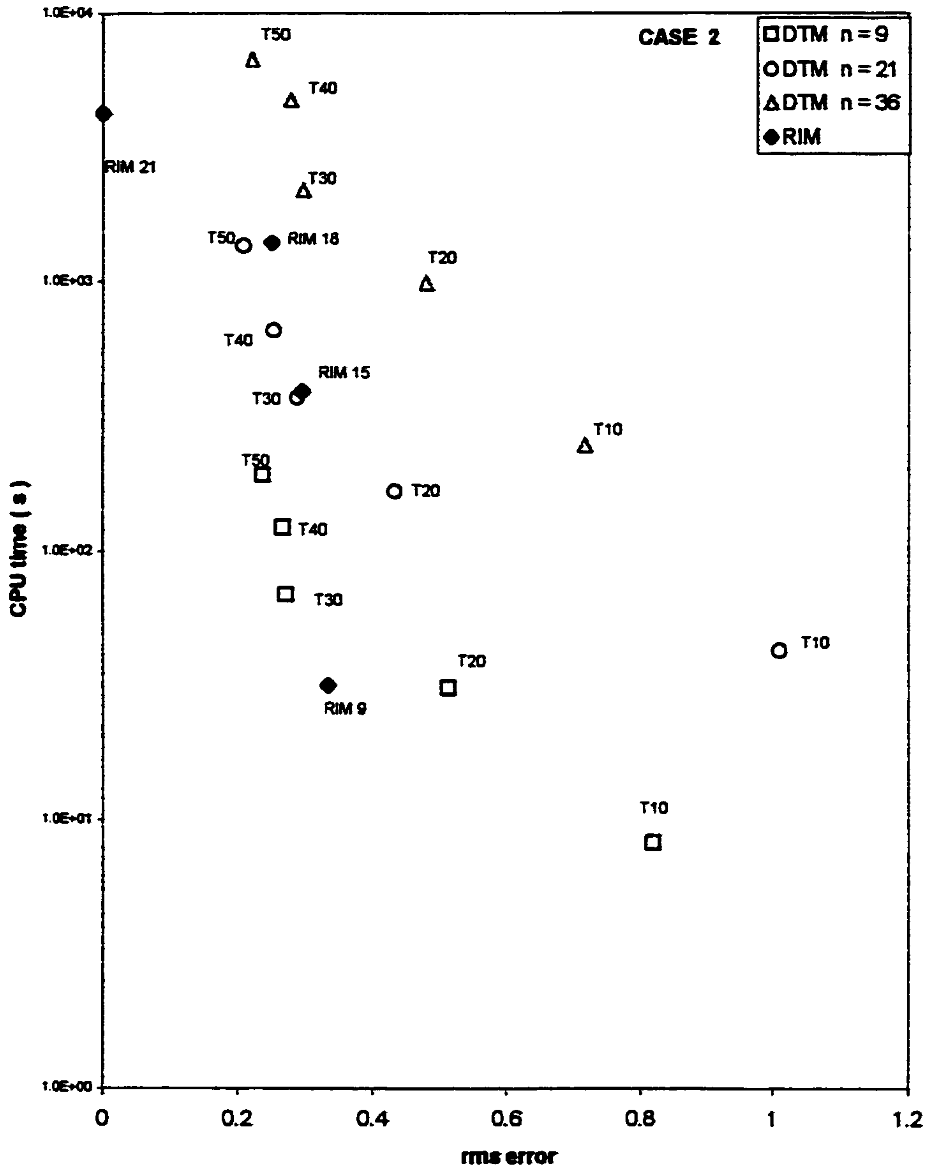

Figure 6.10 Comparison between DTM and RIM

MEAN RADIANT TEMPERATURE CALCULATION AND COMPARISONS WITH THE DOM.

The mean radiant temperature (T_{mrt}) was calculated for case 2 using both the DTM and the DOM. The noticeable differences in heat flux calculations between the DTM and the DOM apparently disappear in mean radiant temperature (T_{mrt}) calculations. . Even using Chapman's version of the DOM (an S_3 quadrature with alpha = 1.0) the T_{mrt} s obtained for case 2 are not very different from those obtained by the DTM as can be seen in Figure 6.11 This is the case even when the local heat fluxes computed with this Chapman version are in complete disagreement with the benchmark heat fluxes. (Figure 4.16). The computation of the T_{mrt} involves averaging the intensities over the whole enclosure so that methods such as the DOM Chapman formulation which have poor local heat flux accuracy , can compute acceptable values of the T_{mrt} It is expected that when the number of heat panels increases the accuracy of the DOM will decrease, as was explained in Chapter 5, due to increasing false scattering and ray effect.

In Figure 6.12 the 200 Watts heat panel of case 2 was substituted by two 100 Watts heat panels of Case 7. Notice that in both cases the total energy output from the panels is 200 Watts. In this case Chapman version of the DOM produces erroneous patterns in the T_{mrt} distribution. The DTM predicts a more uniform T_{mrt} distribution and it computes the T_{mrt} approximately ten times faster than this DOM version.

Figure 6.13 is a comparison of T_{mrt} between a rectangular enclosure and the non-rectangular one of case 5. The difference is not considerable because in this case the sloped surface is at the same temperature as the rest of the enclosure. If this temperature is changed the results would be different.

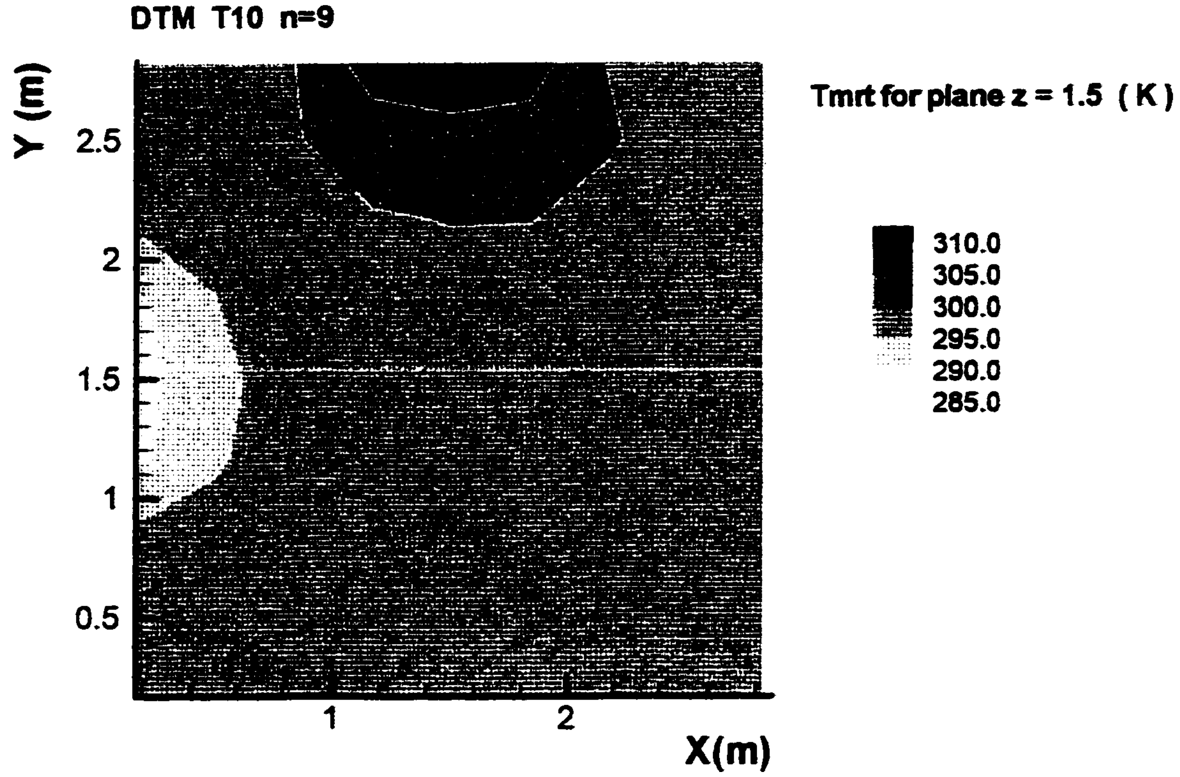

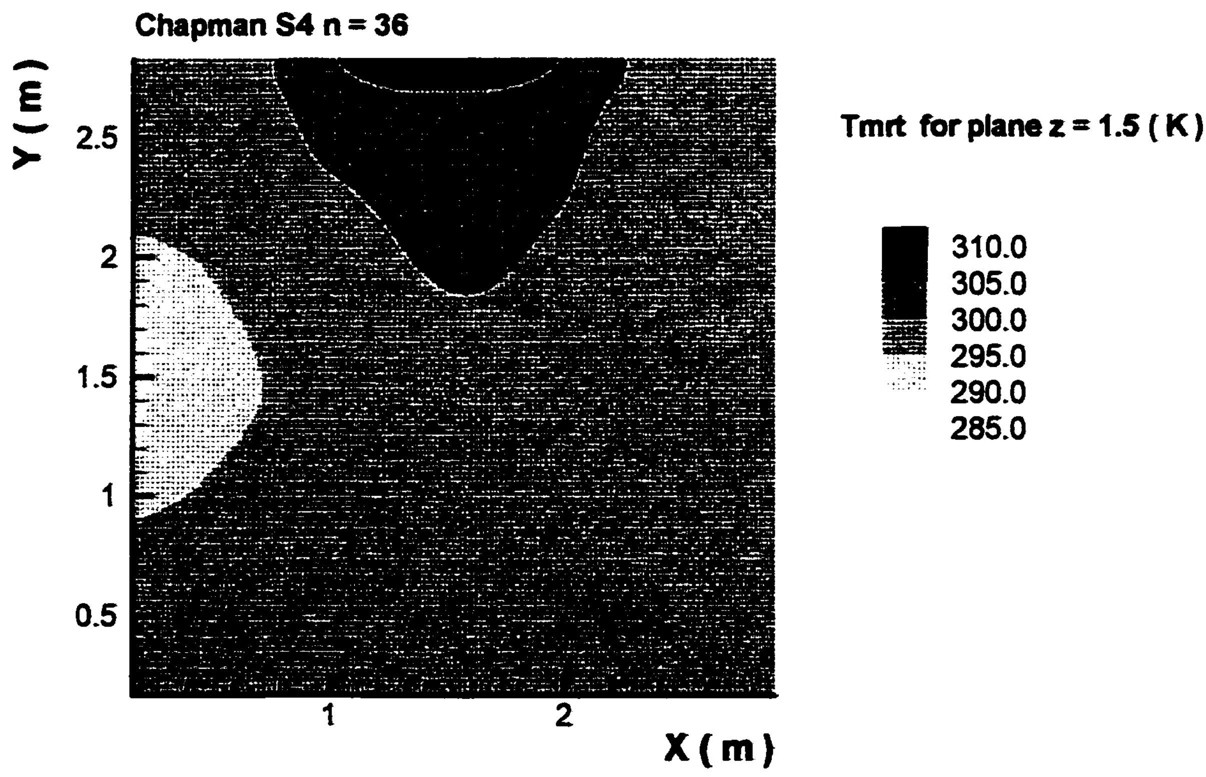

Figure 6.11 Case 2 Tmrt: Chapman and DTM

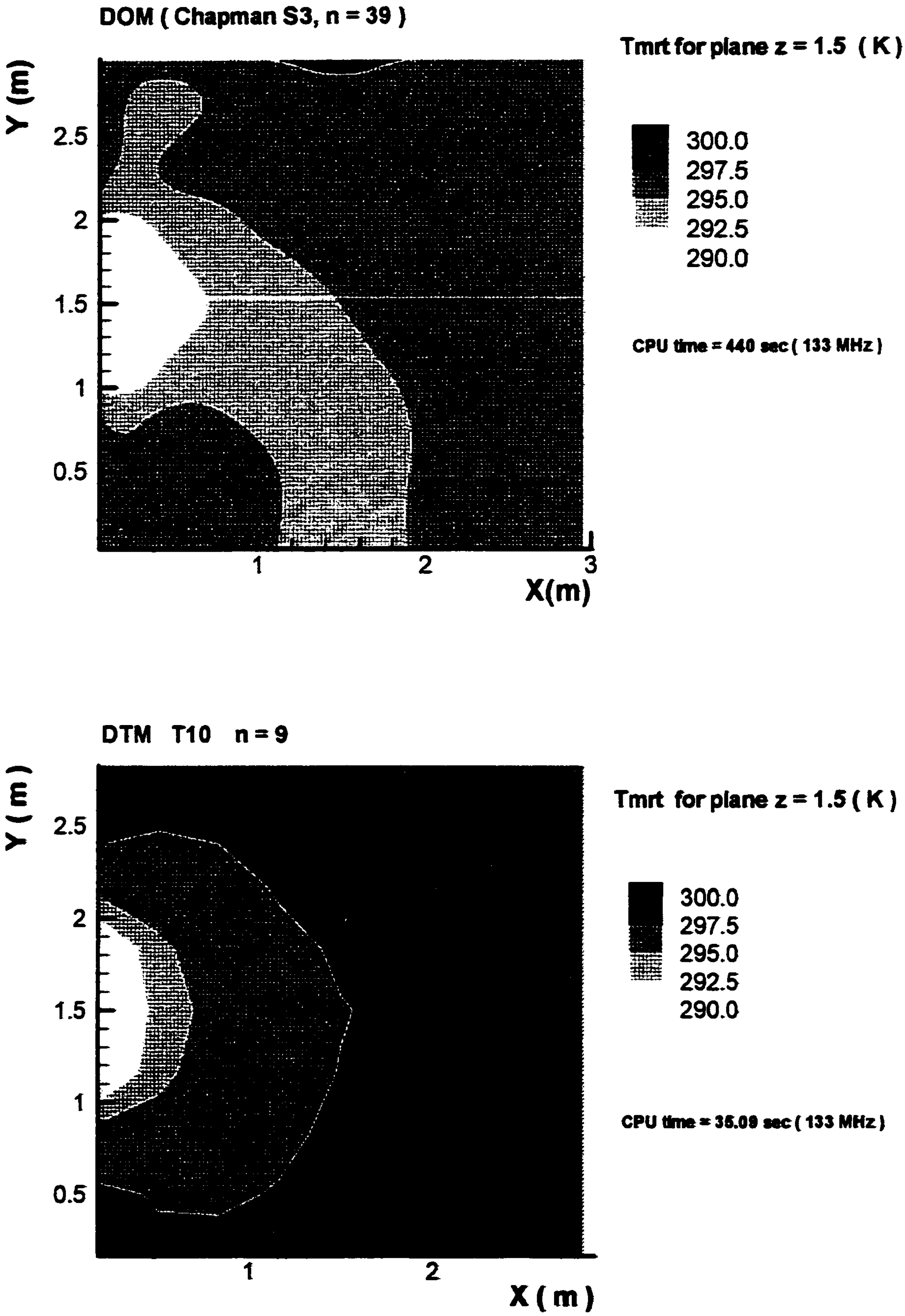

Figure 6.12 Case 7 Tmrt for 2 heat panels: DTM and DOM

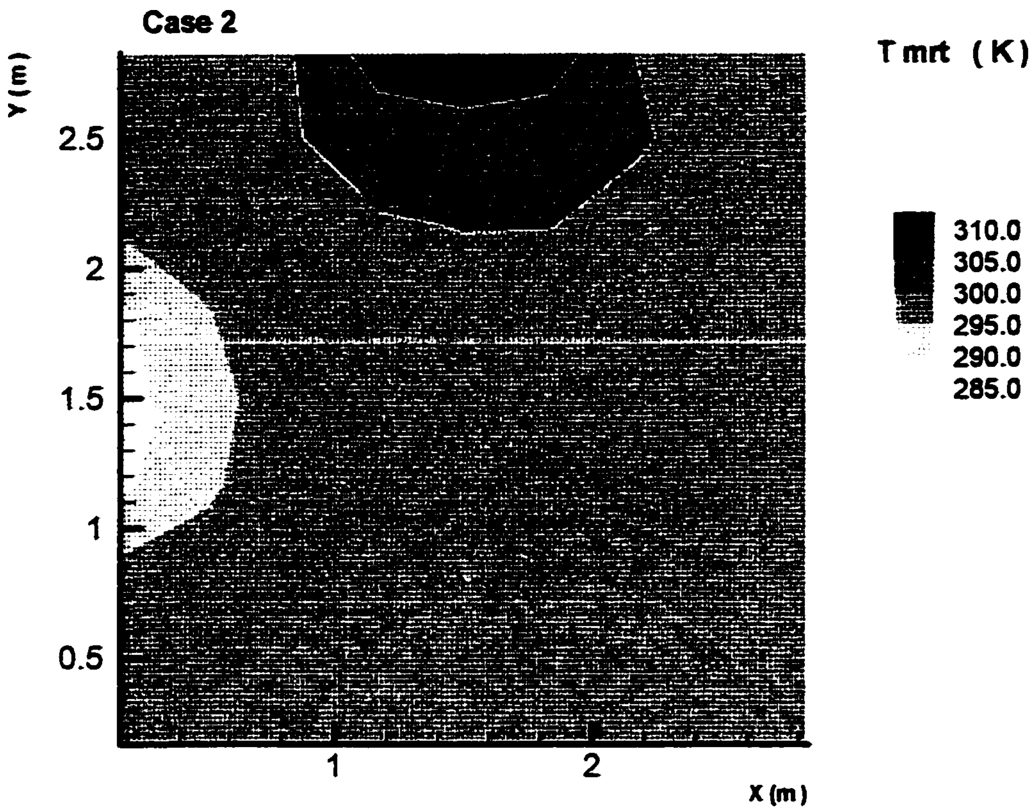

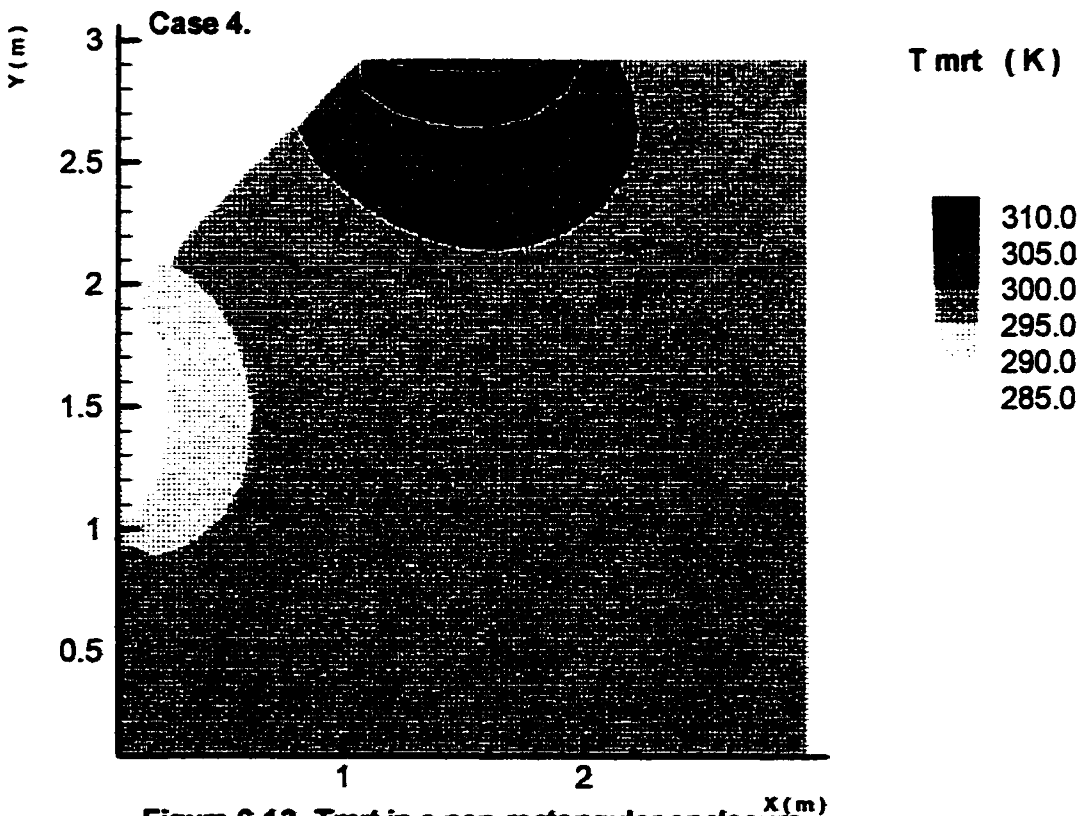

Figure 6.13 Tmrt in a non-rectangular enclosure

6.6 SUMMARY

The general DTM method was proposed in 1979 by Saha . The main idea of the method is to solve the equation of radiative transfer along the beam direction rather than using a rectangular mesh. Furthermore, in a transparent enclosure the intensity of the beam does not change along the beam direction. The version of the DTM method presented here (from now on referred only as the DTM method for brevity) uses this fact. Specifically this means that the mesh can be eliminated and with it, the principal source of two of the numerical problems of the DOM ; false scattering and false oscillations.

In enclosures with uniform wall temperatures, both methods give similar accuracy at comparable CPU times. However, as the number of sharp intensity gradients increases (windows, heat panels...etc) the DOM losses accuracy because of the increasing amounts of false scattering. The DTM method, on the other hand, needs to use more and more angular directions to arrest the oscillations caused by the ray effect. At the end, however, the DTM method produces results considerably more accurate than the DOM method. This fact can be explained in a simplified manner by observing that the DOM method has three numerical problems: false scattering, false oscillations and the ray effect, the DTM method suffers just from the last one.

In addition to the above, the following advantages and disadvantages were found among the DTM method and the DOM.

a) In the DOM method, the intensities in the entire volume should be calculated as many times as the number of iterations neccesary to obtain the final answer whereas in the DTM method the intensities at the interior of the enclosure, if desired, need to be calculated just once, when the final result for the radiosities on the surfaces of the enclosure are already known.

b)In the DTM method, the second part of the algorithm is completely independent of the first part. In particular this means that the interior points used to calculate mean radiant temperatures can be chosen at will. In a three dimensional rectangle, for instance, if each surface is divided in $n*n$ segments, we are not forced to have n^3 interior points. Since the mean radiant temperature calculation involves a ¼ th power, the number of internal points needed to obtain good accuracy for T_{mrt} calculation is less than the number of points needed to obtain good accuracy to compute local heat fluxes at a surface.

c)The DTM method borrows from the Monte Carlo method the idea of following the trajectories of the beams. Hence, the same geometric algorithms used in the Monte Carlo method can be applied here. In particular the same shading techniques may be used. Contrary to the Monte Carlo Method, the DTM method needs to follow the beam just once, from the location where it impinges a surface to the location where it was originated.

d) The major part of the CPU time used in the DTM method is spent following the rays. In parallel computers this CPU time could be greatly reduced since the method lends itself easily to parallelization.

e) In contrast with the DOM method, this version of the DTM method only works for non participating medium.

f) In rooms with protrusions or internal objects, the algorithms for tracing the beam become increasingly complicated in the DTM method (as well as in Monte Carlo). The DOM might work better in these conditions.

In the following Chapter the capabilities of the DTM method to work with sloping ceilings and beam radiation, particularly, solar radiation, will be explored.

Chapter 7

THE DISCRETE TRANSFER METHOD AS APPLIED TO PRACTICAL CASES

7.1 INTRODUCTION

The goal of this Chapter is to extend the capabilities of the Discrete Transfer Method (DTM). In particular, a short wave version will be developed and its performance will be compared to the Radiosity Intensity Method for short wave radiation which was developed in Chapter 2. The ability of the DTM to deal with non-rectangular enclosures will be investigated.

7.2.- SHORT WAVE SOLUTION PROCEDURE

The short wave boundary conditions within a radiative enclosure are given in Table 3.1. The following modifications to the Discrete Transfer Method solution scheme listed in Chapter 6 need to be made.

IN PART A :

A.1-- Assume the intensities at the discretized boundary segments. As in the case of the short wave Discrete Ordinates Method (DOM), the initial intensity leaving segment i on the boundary of the enclosure, $I_{boundary\,s}$, can be estimated by assuming that the total irradiation coming from the rest of the surfaces on the enclosure, and falling upon surface i, $G_{surf\,i}$, is equal to zero. Thus:

$$I_{boundary\,s} = \frac{\rho_s}{\pi}\left(G_s\right) \tag{7.1}$$

G_s is estimated as shown in Table 3.1

A.2 - Calculate the irradiation at the boundary points. As in the long wave case the irradiation coming from the rest of the segments on the surface of the enclosure falling upon segment i, $G_{surf\,i}$ can be approximated by:

$$G_{surf\,i}(r) = \sum_{n \bullet \Omega < 0} \left| n \bullet \Omega \right| I_j^s \, \omega_j \tag{7.2}$$

The technique used to calculate this irradiation is the same as the technique used in the long wave case: Choose angular direction number one in the quadrature set and follow the beam back from the center of segment i to the segment on the enclosure where it was originated. The intensity of the beam falling upon surface i is the intensity of the beam leaving surface j where this beam was originated. After $G_{surf\,i}$ is estimated, the total irradiation falling upon surface i, G_{si}, can be computed, depending on the type of surface that we have, using Table 3.1

A.3 - Recalculate the short wave intensities at the boundaries. This is a forward computation using the equations found in table 3.1. As in the long wave case, steps A.2 and A.3 need to be repeated until the solution reaches the desired accuracy.

A.4 - Compute the heat flux at the boundary segments. As in the long wave case, the distribution of intensities along the boundary segments is known for every available angular direction. Table 3.1 again tell us what is the equation that needs to be used depending on the type of surface that we have.

7.3 NON RECTANGULAR ENCLOSURES

As suggested in Chapter Four non-rectangular enclosures present special problems. The Angular Quadratures developed for the Discrete Ordinates Method (DOM) as well as for the Discrete Transfer Method have what we called "ninety-degree symmetry ". As explained in Chapter Four, this ninety degree symmetry means that exactly the same weights and angular directions are used to calculate the heat flux on an horizontal or a vertical surface of an enclosure. However if the wall has some inclination with the horizontal, the symmetry is lost.

One possible solution to this problem is to rotate the entire quadrature set in such a way that the relative position between the allowed angular directions and the normal remains the same for all the surfaces. This can be done by using a rotation matrix. In practice, due to the high number of angular directions used, the use of the rotation matrix produces almost the same results compared to the non-rotated regular quadrature used before. It remains to be seen, however, if the use of other quadrature sets with a more uniform distribution of weights would help to diminish the increased ray effect noted when dealing with non-rectangular quadrature sets.

7.4 BOUNDARY CONDITIONS FOR A COMPLETE SIMULATION

Figure 7.1 shows an energy analysis for two different kinds of surfaces: passive surfaces with no internal generation of heat, and active surfaces such as heat panels where a source of heat, q_{panel}, is considered. Following the same convention used for radiant heat transfer, the heat is considered positive when it leaves the control volume drawn around the inner surface of the surface segment.

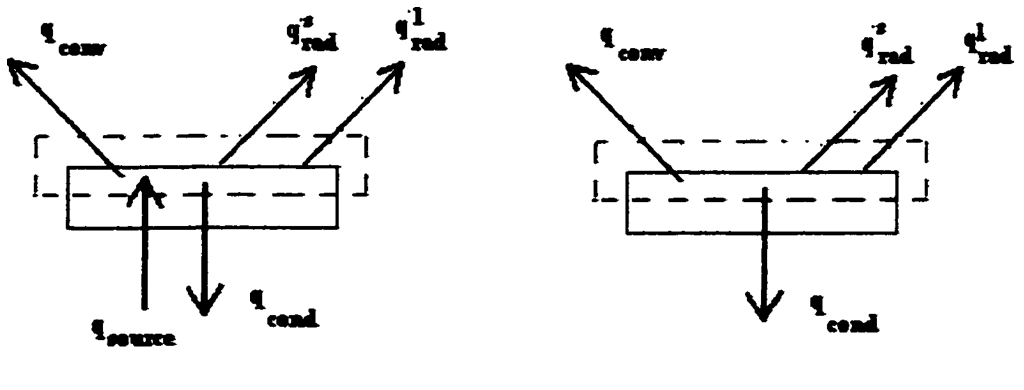

Element with a source of energy q_{source} **Passive element**

Figure 7.1 Energy balance in passive and active surfaces.

From the Figure it is clear that:

$$q^{l}_{rad} + q^{s}_{rad} = q_{source} - q_{cond} - q_{conv} \tag{7.3}$$

There are many possible boundary conditions: in passive buildings the temperature of the interior surfaces may be desired from known environmental data such as solar irradiation, wind velocity, etc. A simulation of this kind is beyond the scope of this work. It requires a simultanous calculation of conduction and convection heat transfer. On the other hand, if the interior temperatures of the enclosure are known, then the heat load might be required. In the following paragraphs a description of how this heat load can be calculated is shown.

In Chapter 6 it was shown how to calculate long-wave radiation heat transfer given a fixed surface temperature on a segment of the enclosure. On the other hand, short wave radiation heat fluxes are independent of the temperature of the enclosure. They only depend upon the solar heat flux, G_{beam} and $G_{diffuse}$, and the geometry of the enclosure. Therefore the procedure shown in Figure 7.2 is proposed to obtain the heat load on every segment of the enclosure.

Note that the short wave and the long wave heat flux calculation can be performed at the same time. In fact the same program could be used to calculate short and long wave heat fluxes. This procedure is recommended since it would cut the total CPU time needed to make the whole heat flux calculation approximately to a half. The reason for this is that around 70 % of the CPU time used by the DTM method is spent in the calculation of the place of origin of each of the beams. To calculate short-wave radiative heat flux it is not necessary to recalculate where the beam comes from.

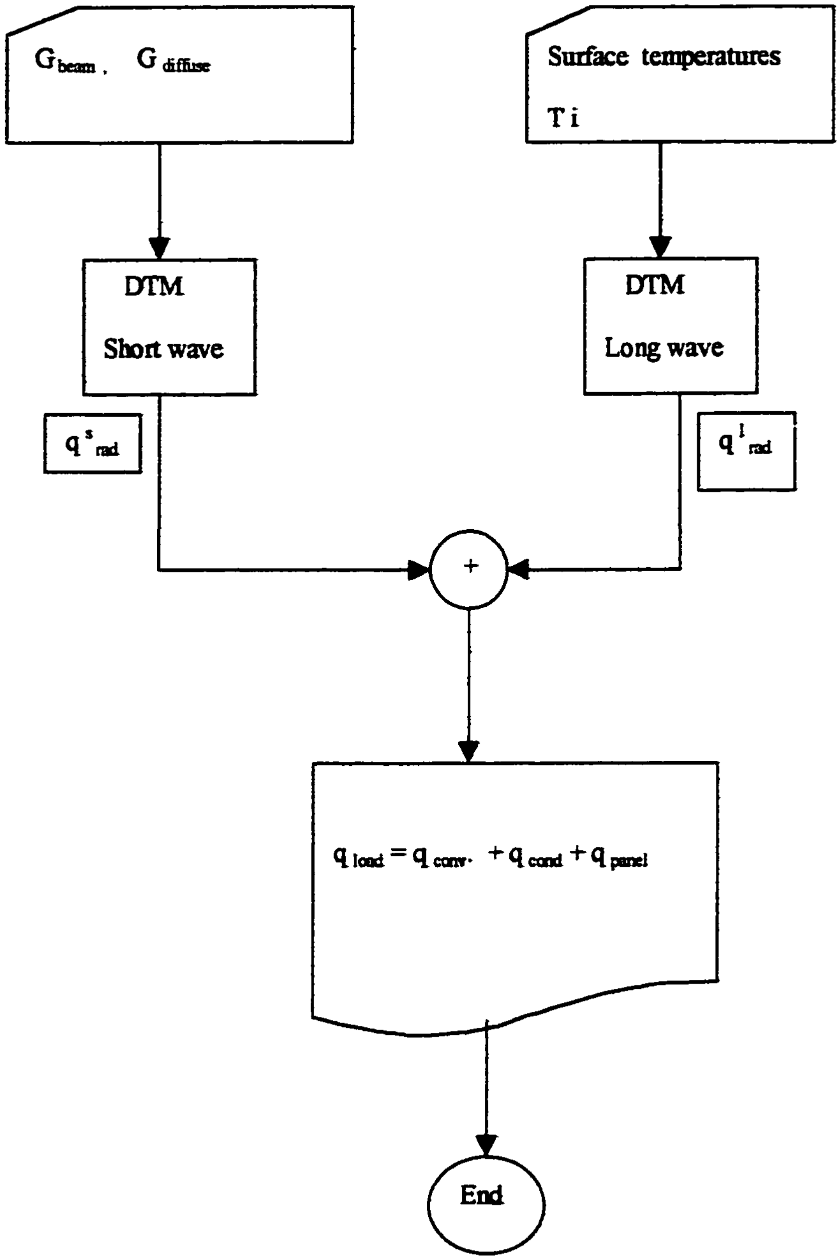

Figure 7.2 Complete simulation: temperature boundary conditions

7.5 TEST CASES

The short wave Discrete Transfer Method was tested using case 5 (Figure 1.6). The results shown in Figure 7.3 , 7.4 and 7.5 are compared with the results given by the short wave radiosity method developed in Chapter One. As can be seen, in general excellent agreement between both methods exists. It is remarkable that no ray effect is apparent in these Figures. The reason is that in the short-wave range just a few percent of the surfaces can be considered emitters (windows). That means that the radiosities involved are small compared with the radiosities involved in the long wave case. The ray effect, however, should appear as the number of angular directions is decreased. In Figure 7.6 the disappearance of the ray effect can be seen as the number of angular directions is incremented. This Figure shows the same calculations as the ones performed to obtain Figure 7.4. This time, however, T_6 and T_{10} quadratures are used instead of the T_{20} used before.

Figures 7.7 and 7.8 show the same calculations performed for case 6. This time the possibility of comparing it with the radiosity method is not present. For this effect, the Monte Carlo code can be used. In Figure 7.8 the sloping surface ray effect is shown by the irregular heat flux. To produce a smooth pattern in this figure, additional angular directions are needed.

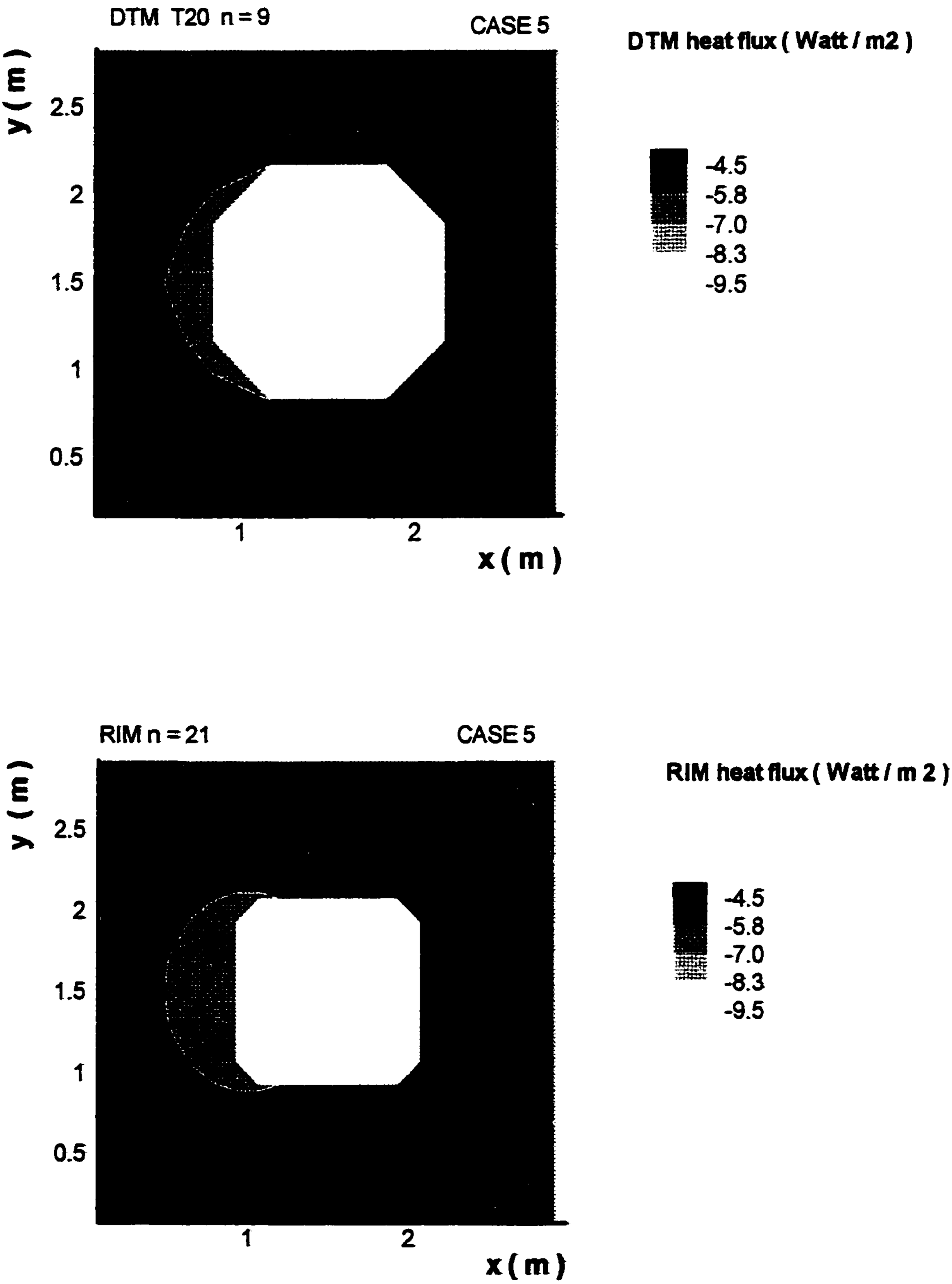

Figure 7.3 Comparison of floor short wave heat fluxes

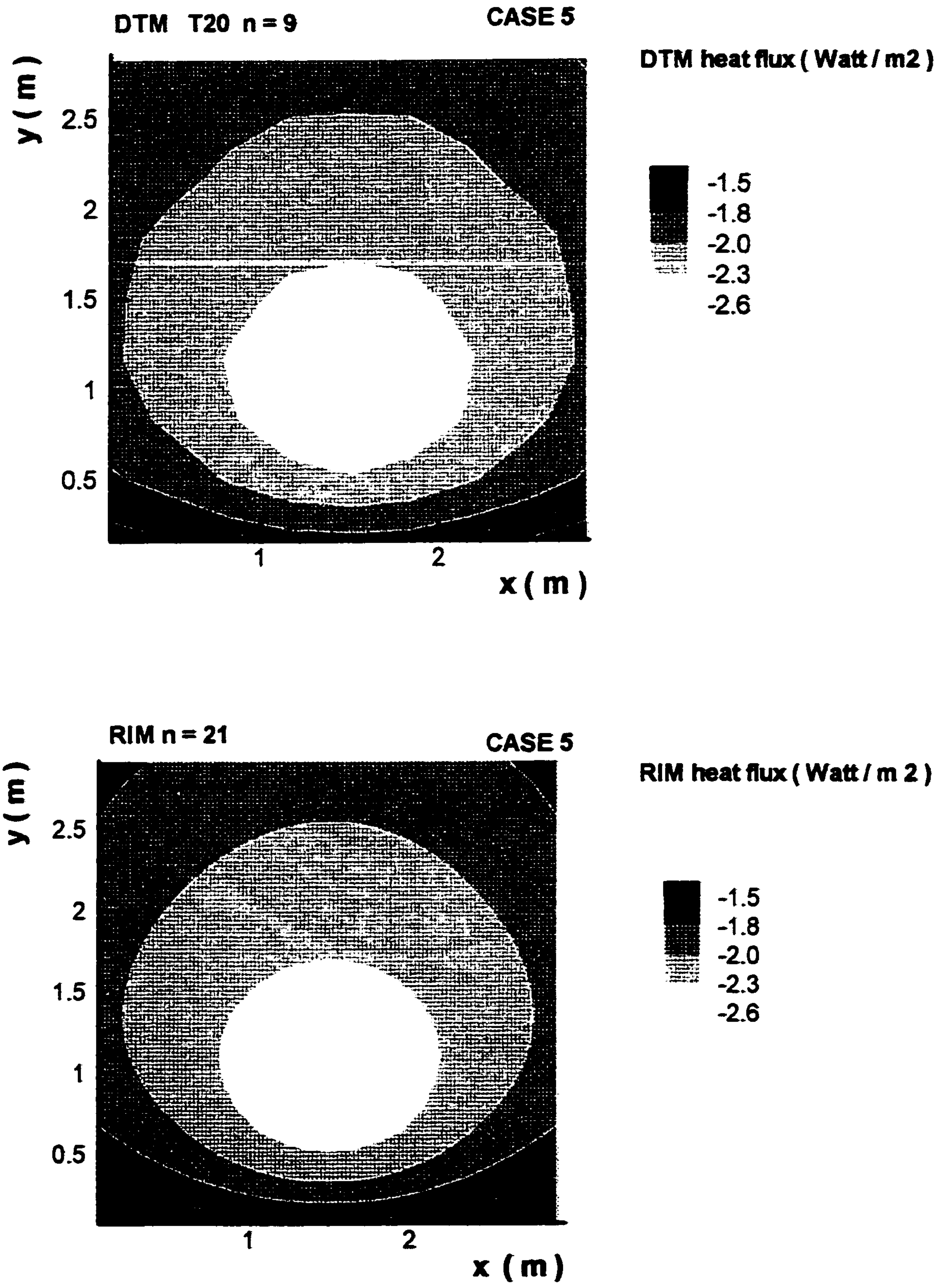

Figure 7.4 Comparison of wall 3 short wave heat fluxes

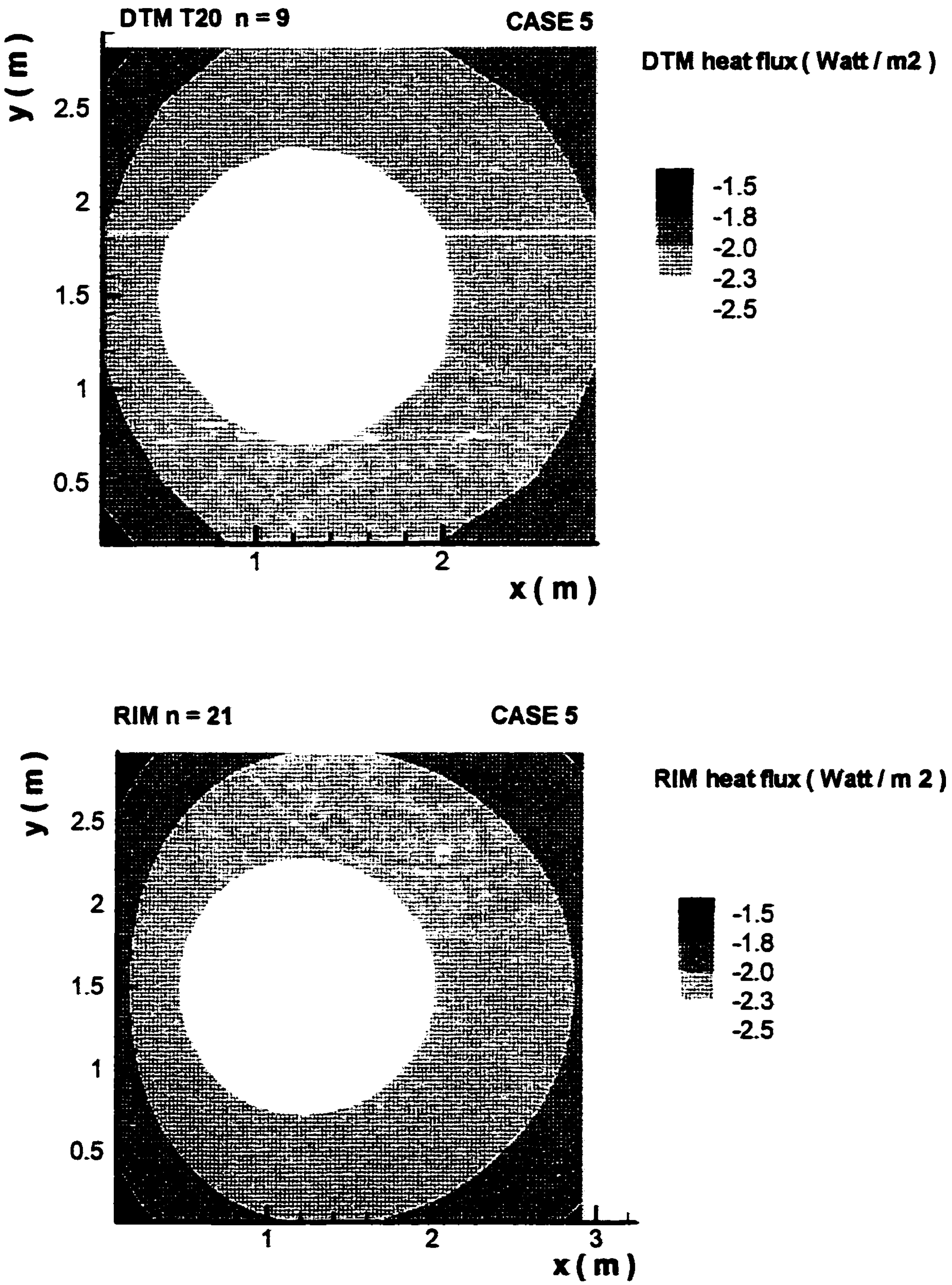

Figure 7.5 Comparison of ceiling short wave heat fluxes

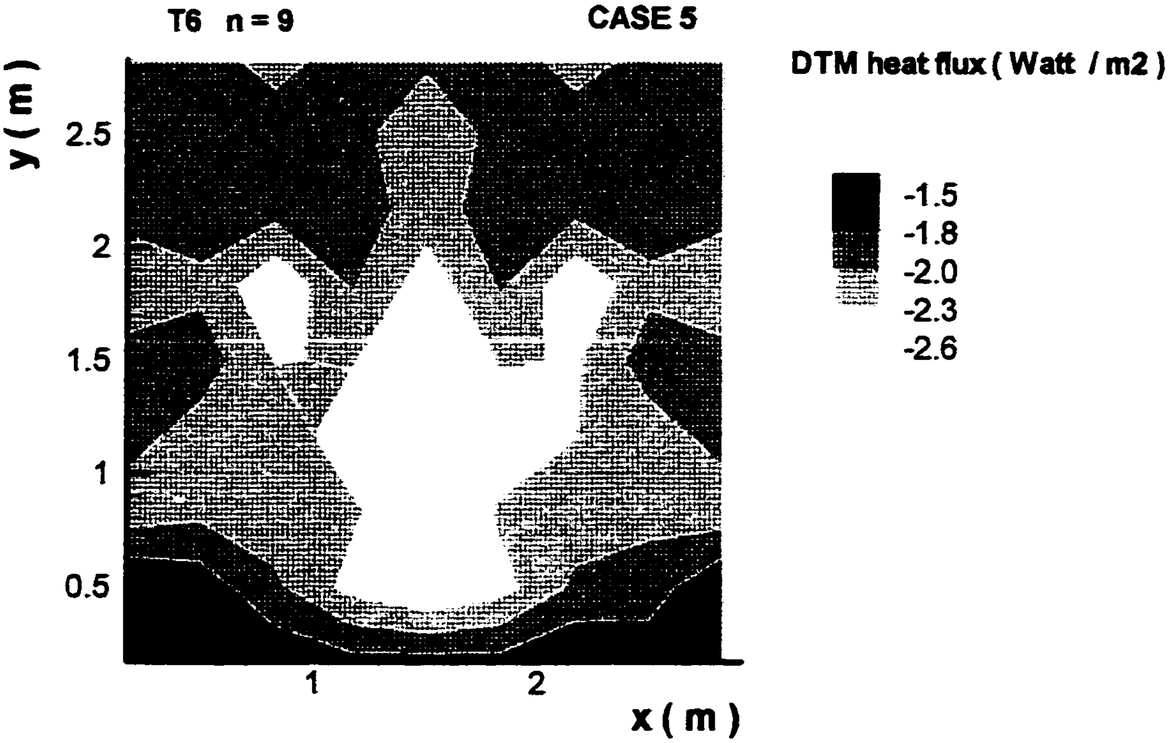

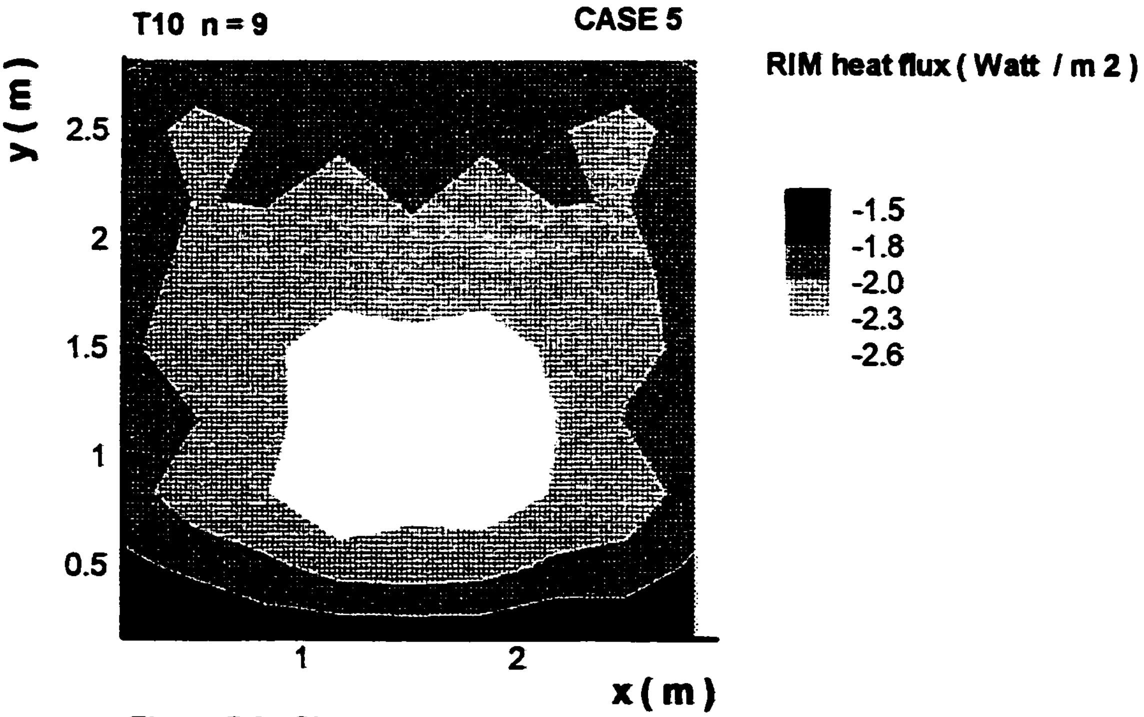

Figure 7.6 Short wave ray effect

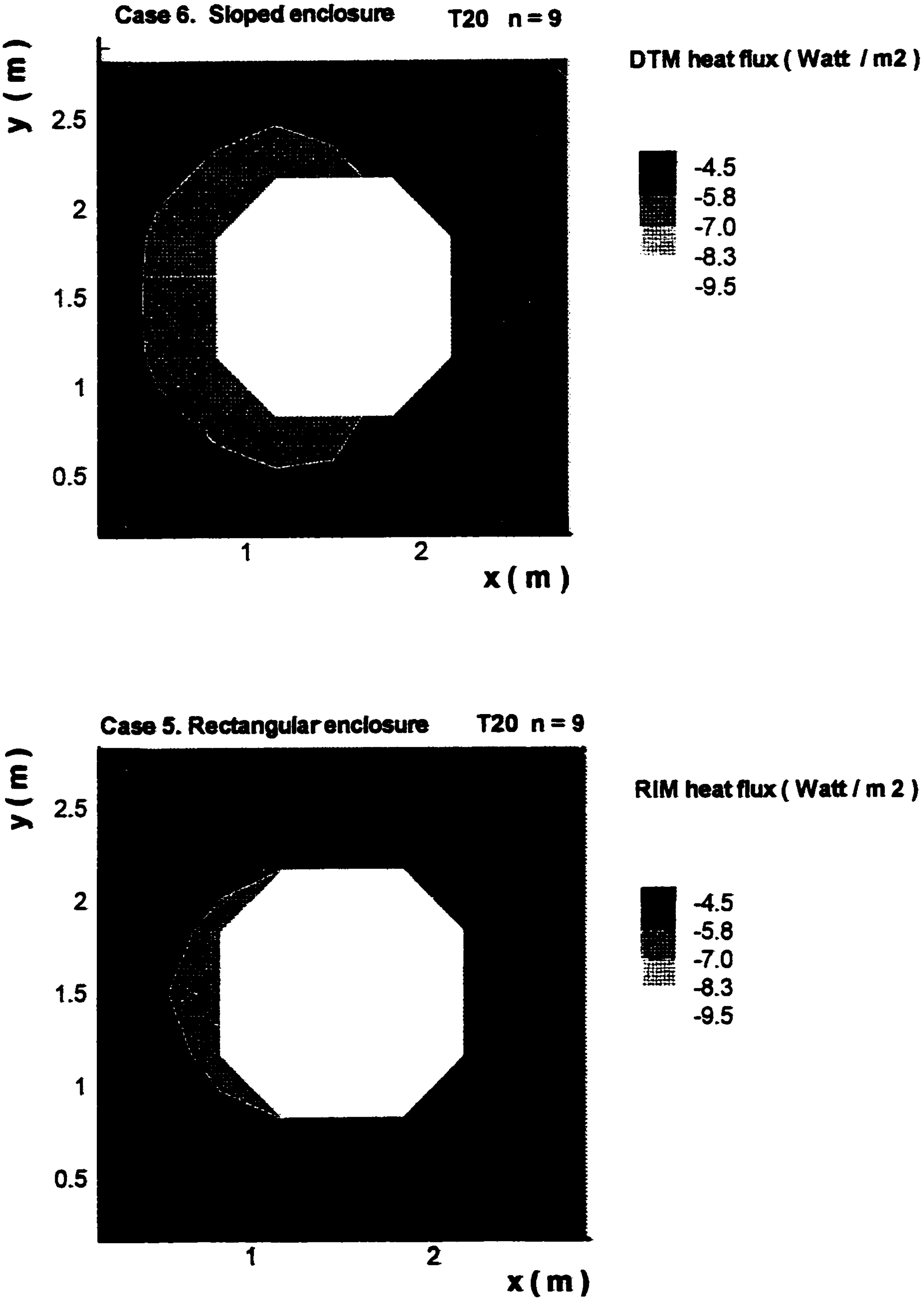

Figure 7.7 Sloped vs. non-sloped short wave floor heat flux

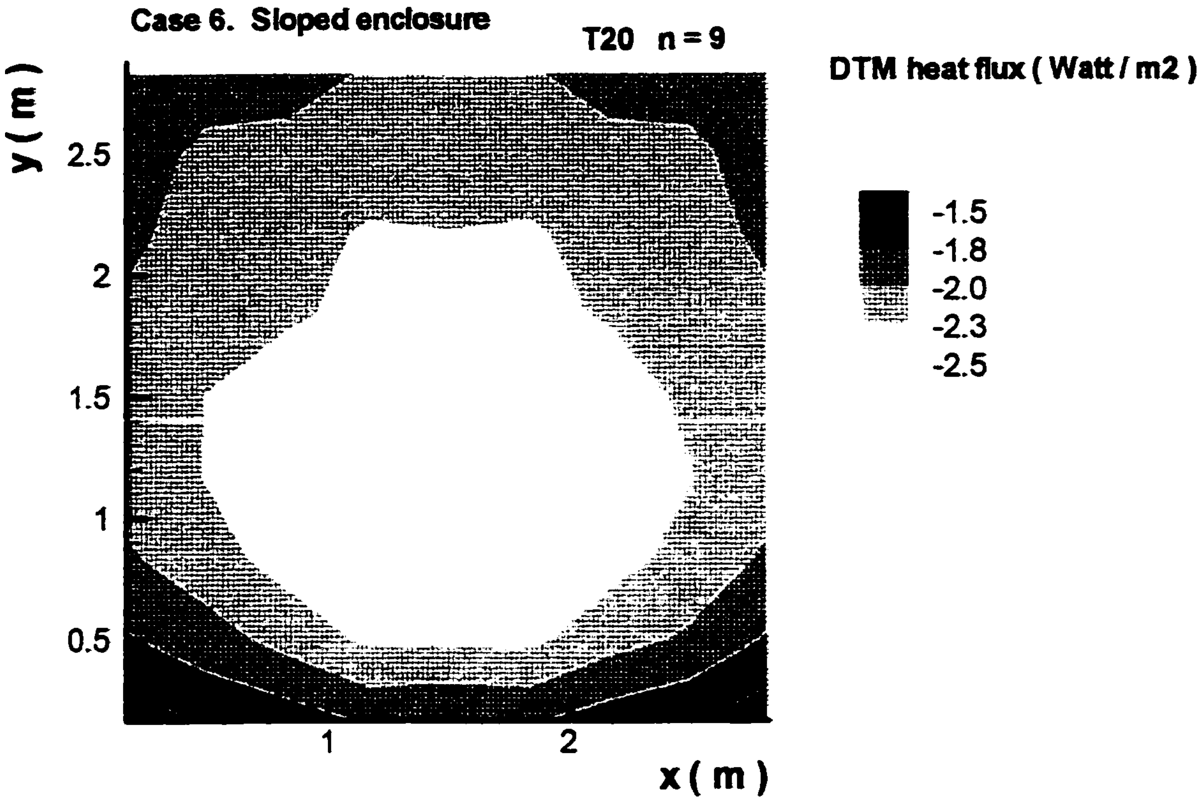

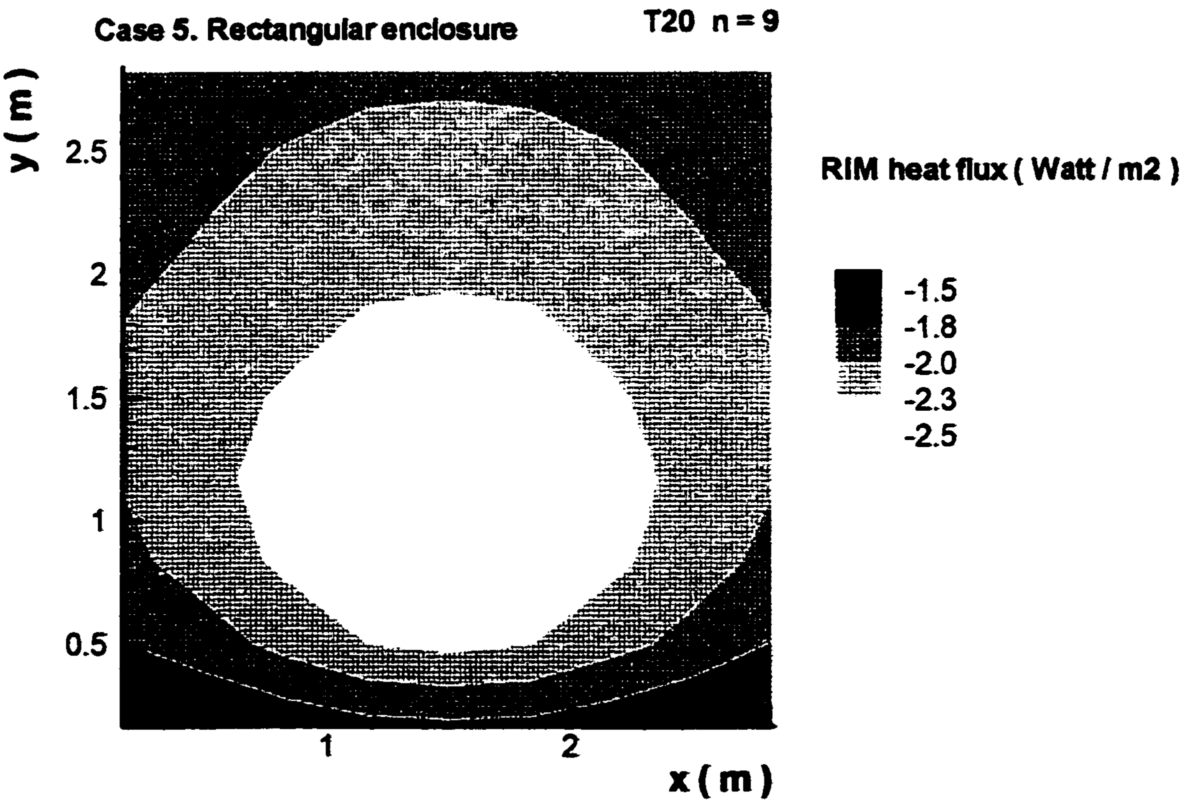

Figure 7.8 Sloped vs non-sloped wall 3 short wave heat flux

7.6 SUMMARY

As was already shown in Chapter 3, the discretization of the equation of radiative transfer can be solved with different sets of boundary conditions. In particular discretization methods such as the Discrete Ordinates Method (DOM) and the Discrete Transfer Method (DTM) can easily be adapted to short-wave boundary conditions. In this Chapter the steps needed to adapt the DTM to the short wave part of the spectrum were presented. These adaptations are shown to be successful by comparing the results produced by the DTM with the results given by the Radiosity Intensity Method (RIM) adapted, also, to short wave boundary conditions.

Although the results were successful, they also suggest that for rectangular empty rooms the Radiosity Intensity Method outperforms the DTM in terms of speed and performance. However, when the geometry becomes more complicated or, as shown in other chapters, when the mean radiant temperature is needed, the RIM cannot be applied and the DTM becomes a good alternative.

Chapter 8

SUMMARY AND CONCLUSIONS

8.1 SUMMARY & CONCLUSIONS

Two different methods to discretize the equation of radiative transfer in transparent media have been compared. First, in Chapters 3, 4 and 5 the Discrete Ordinates Method (DOM) was discussed and evaluated. The DOM is subject to 3 major numerical sources of error: the ray-effect, false scattering and false oscillations.

The ray effect is produced by the discretization of angular space. The most effective solution to reduce it is to increase the number of rays as much as possible. At least two angular quadratures are known that have good behavior: the Thurgood quadrature and the Bressloff et al. quadrature. In Chapter 4, it was shown that the ray effect is substantially reduced by the use of the first of these quadratures, and that the distribution of weights also contributes to the ray effect.

False scattering is produced by the lack of coincidence between the direction of the beam and the x, y and z-axes of a Cartesian mesh. False oscillations have a different origin; they are produced by allowing output intensities not to be bounded by the input intensities. Traditionally one of the solutions to minimize false oscillations, used in Computational Fluid Dynamics (CFD) is to set an interpolation factor, alpha, equal to one. However, this solution increases the amount of false scattering. False scattering, in turn, has been treated by increasing the number of upstream cells. There are many methods that proceed in this manner with various degrees of success. However, since the DOM has to address all of the numerical errors for all the angular directions contained in a set, a procedure of this type consumes an enormous amount of cpu time. False scattering presents a specially difficult problem for the DOM because it increases with the number of sharp intensity gradients present. In a building this means that with as the number of windows or heat panels increase, the less accurate the DOM method will be. As an extra complication it should also be pointed out that the more angular directions used in a set the more false scattering we have because of the increased number of beams considered. This means that by reducing the ray effect, false scattering is increased. These problems and complications limit the usefulness of the DOM.

As an alternative method, the use of the Discrete Transfer Method (DTM) as applied to transparent enclosures is proposed. Since no internal mesh is used by this method, it does not suffer from false scattering or false oscillations, therefore its performance is significantly superior to the that of the DOM, as was shown in Chapter 6. In Chapter 7 the capabilities of the Discrete Transfer Method for enclosures with transparent boundaries were further developed. In particular an adaptation of the method to include short wave radiation was performed. It was shown then that the Radiosity Intensity Method (RIM) and the DTM produced similar results.

In summary, for calculation of the heat flux on the surfaces of a rectangular enclosure with no internal objects, the Radiosity Intensity Method offers better performance that both the DTM and the DOM. However, if the mean radiant temperature inside the enclosure is also desired or if the room is not rectangular, or if it has embedded objects, then the Discrete Transfer Method would be the preferred method among the three mentioned.

From all of the above we conclude that the DTM as applied to transparent enclosures is a valuable tool to calculate radiant exchange between the surfaces of an enclosure. In particular, it outperforms the DOM at least in large empty spaces. It is also a valuable tool to evaluate the performance of radiant heat panels and the comfort conditions inside a room. For these purposes, its use is recommended as a substitute for the DOM.

8.2 RECOMMENDATIONS FOR FUTURE WORK

There are a number of topics for future work in this area. These are: specular reflection, non-rectangular enclosures, embedded objects, a comparison between the Monte Carlo Method and the DTM and a complete simulation.

SPECULAR REFLECTION

Although specular reflection has not been addressed in this work, both methods, the Discrete Ordinates Method (DOM) as well as the Discrete Transfer Method (DTM), have the capability of dealing with specular reflection. As a first step, we need to rewrite equations 3.13 and 3.16 in the following way:

$$I^{l}_{boundary} = \bar{\varepsilon} I_b + \frac{1}{\pi} \sum_{n.\Omega<0} \rho_j \left| n \bullet \Omega \right| I_j \, \omega_j \tag{8.1}$$

$$q_{rad}(r) = \bar{\varepsilon} \sigma T^4 - \sum_{n\bullet\Omega<0} \varepsilon_j \left| n \bullet \Omega \right| I_j \, \omega_j \tag{8.2}$$

The term ε is the hemispherical average of the emissivity on a given surface. In the above equations, diffuse emission and reflection are still assumed. However the reflectivity is considered a function of the incident angular direction. Therefore, for the directional-hemispherical problem outlined above, all that is needed is to replace equation 3.16 with equation 8.1, and equation 3.18 with equation 8.2 in the procedure outlined in Chapter 3. However a serious problem is anticipated from the application of the angular discretization scheme: In general different quadrature sets associate different weights to the same angular direction. It follows that for specular reflection the results will strongly depend on the quadrature set used. A possible solution to the problem would be the application of the "quasi-equal " weights quadrature developed by Bressloff, Moss and Rubini (1995) for the Discrete Transfer Method. As in the case of Thurgood quadrature, this quadrature is capable of increasing without limit the number of angular directions needed. However, contrary to what happens with the Thurgood quadrature (Fig 4.4) the weights assigned to all the angular directions are almost equal .

NON –RECTANGULAR SURFACES

As mentioned in Chapter 4 and Chapter 7, non-rectangular surfaces do not follow the ninety –degree symmetry under which the majority of the angular quadrature sets have been constructed. A possible solution would be the use of the Bressloff et al. (1995) quadrature since it gives approximately the same weights to the different angular directions and it can be divided in as many angular directions as desired. As mentioned above, the application of the Bressloff et al. quadrature could also solve the problem represented by specular reflection and it may present a relatively small ray effect compared with the Thurgood quadrature of the same order due to the more uniform distribution of weights that it presents.

EMBEDDED OBJECTS

As mentioned in Chapter One, although a general procedure has been developed for the Discrete Ordinates Method (DOM) to deal with embedded objects such as desks and bookcases, this procedure has not been applied to three-dimensional geometries. In the case of the Discrete Transfer Method the same techniques used by the Monte Carlo Method can be used. However the DTM also needs to be tested with embedded objects.

COMPARISON BETWEEN MONTE CARLO AND THE DISCRETE TRANSFER METHOD

As has been stated in this thesis several times, the Discrete Transfer Method uses the same algorithms that the Monte Carlo Method use to follow a ray back to its place of origin. This means that the same shading algorithms used in the Monte Carlo Method can also be used in the Discrete Transfer Method. As in the case of Monte Carlo, it has been shown that the Discrete Transfer Method is capable of working with short-wave as well as with long-wave radiation. Furthermore, both methods are capable of dealing with specular reflection.

Since both methods have the same capabilities, it would be interesting to compare them in terms of speed and accuracy.

COMPLETE SIMULATIONS

It should be remembered that radiant heat transfer may not be the dominant heat transfer mechanism in building enclosures. Therefore the DTM needs to be tested as a part of a complete code that incorporates conduction and convection. Of special interest would be the simulation of passive buildings where the environmental conditions, such as solar irradiation and wind velocity, are known and it is desired to calculate the comfort conditions inside the building. In order to do that, the mean radiant temperature variations inside the enclosure would be of interest as well as the airflow inside the enclosure.

REFERENCES

Abraham, J., Magi, V. 1997. " Application of the discrete ordinates method to compute radiant heat loss in a diesel engine " *J. of Numerical Heat Transfer*, Part A. Vol. 31. pp 597 – 610

Behnia, M., Reizes, T.A., De Vahl Davis, G. 1990 . " Combined radiation and natural convection in a rectangular cavity with a transparent wall and containing a non-participating fluid " *Int. J. for Numerical Methods in Fluids*, Vol. 10. pp 305-325

Bohmer, K. Hemker, P., Stetter, H. J. 1984. " The defect correction aproach " *Computing Supplement* 5. pp 1-32

Bressloff, N.W., Moss, J.B. and Rubini P.A., 1995. " Applications of a new weighting set for the discrete transfer radiation model " *Proceedings, 3rd European Conference on Industrial Furnaces and Boilers*. pp 208-215

Burns, P.J., Pryor, D.V., 1989. " Vector and parallel monte carlo radiative heat transfer simulation " *Numerical Heat Transfer*, Part B. Vol 16. pp 97-124

Byun, K.H., Smith T.F. , 1997. " View factors for rectangular enclosures using the direct discrete ordinate method " *J. of Thermophysics*, Vol 11. No 4

Carey C., Scalon T. J., and Fraser S. M. 1993. " SUCCA- an alternative scheme to reduce the effects of multidimensional false diffusion " *Appl. Math. Modelling*. Vol. 17. pp 263-270

Carlson, B. G., and Lathrop, K. D., " Transport theory - the method of discrete ordinates " in: *Computing Methods in Reactor Physics*, H.Greenspan, C.N.Kelber and D.Okrent, eds., Gordon and Breach, New York

Chai, J. C., Lee H. S., Patankar, S. V. 1993a . " Ray effect and false scattering in the discrete ordinates method " *J. of Numerical Heat Transfer*. Part B. Vol 24. pp 373 – 389

Chai,J.C., Lee H.S., Patankar, S. V. 1993b . " Treatment of irregular geometries using a cartesian-coordinates-based discrete-ordinates method " *Radiative Heat Transfer: Theory and Applications*, HTD-Vol 244. pp 49- 54

Chai,J.C., Lee H.S., Patankar, S. V. 1994. " Evaluation of spatial differencing practices for the discrete-ordinates method " *J. of Thermophysics*. Vol 8. No 1. pp 140 - 144

Chandrasekhar, S.,1960. " *Radiative Transfer* " Dover, New York

Chapman, K.S., Zhang, P. 1995. " Radiant heat exchange calculations in radiantly heated and cooled enclosures " *ASHRAE Transactions* .Vol 101. No 1. pp 1236 -1246

Chapman,K.S., Zhang, P., 1996, " Energy transfer simulation for radiantly heated and cooled enclosures " *ASHRAE Transactions*.Vol 102. No 1 .pp 76 –85

Chapman, K.S., DeGreef, J.M. 1997. " Design factor development to obtain thermal comfort with combined radiant and convective in-space heating and cooling systems " *ASHRAE Report*: RP-907

Chapman, K.S., DeGreef, J.M. 1998. " Simplified thermal comfort evaluation of mrt gradients and power consumption predicted with the BCAP methodology " *ASHRAE Transactions* Vol. 101. No 1

Cheong K.B., Song T.H. 1997 " An alternative discrete ordinates method with interpolation and source differencing for two-dimensional radiative transfer problems " *J. of Numerical Heat Transfer*, Part B. Vol 32 . pp 107 – 125

Chui, E.H., Raithby, G.D. 1992. " Implicit solution scheme to improve convergence rate in radiative transfer problems " *J. of Numerical Heat Transfer*. Part B. Vol 22. pp 251-272

Coelho, P.J., Carvalho M.G. 1997. " A conservative formulation of the discrete transfer method " *Transactions of the ASME*. Vol 119. pp 118 –128

Cumber, P.S. 1995. " Improvements to the discrete transfer method of calculating radiative heat transfer " *Int. J. Heat Mass Transfer*. Vol 38. No 12. pp 2251-2258

Cumber, P.S.; Beeri, Z. 1998. " A parallelization strategy for the discrete transfer radiation model " *J. of Numerical Heat Transfer*, Part B. Vol 34 . pp 287 – 302

Curtis, F.G. 1978. "*Applied Numerical Analysis* " Addison-Wesley

Ehlert, J.R.; Smith, T. F. 1992. " View factors for perpendicular and parallel rectangular plates " *J. of Thermophysics*. Vol 7. No 1. pp 173 –175

Ehlert, J.R., Smith, T. F., 1994. " Surface radiation for rectangular enclosures using the discrete-ordinates method " *J. of Thermophysics*. Vol 8 . No 3 . pp 628-631

Fanger, P.O.,1972. " Thermal comfort. analysis and applications in environmental engineering " Mc-Graw-Hill.

Fiveland, W.A. ,1984. " Discrete-ordinates solutions of the radiative transport equation for rectangular enclosures " *J.Heat Transfer* Vol 106. pp 699-706

Fiveland, W.A. ,1987, " Discrete-ordinates methods for radiative heat transfer in isotropically and anisotropically scattering media " *J.Heat Transfer* Vol 109. pp 809-812

Fiveland, W.A. 1988. " Three dimensional radiative heat-transfer solutions by the discrete-ordinates method " *J. Thermophysics Heat Transfer* Vol 2. No 4. pp 309-316

Fiveland, W.A. and A.S. Jamaluddin. 1989. " Three dimensional spectral radiative heat transfer solutions by the discrete-ordinates method " *ASME. Heat Transfer Conference Proceedings, Heat Transfer Phenomena in Radiation, Combustion, and Fires*, HTD Vol. 106, pp. 43-48

Fiveland, W.A. ,1991, " The selection of discrete ordinate quadrature sets for anisotropic scattering " *J.Heat Transfer* Vol 106. pp 89-96

Fiveland, W.A. , Jessee, J.P. 1995, " Comparison of discrete ordinates formulations for radiative heat transfer in multidimensional geometries " *J.Thermophysics and Heat Transfer*, Vol 9. No 1. pp 47-54

Fiveland, W.A., Jessee, J.P. 1996, "Acceleration schemes for the discrete ordinates method " *J.Thermophysics and Heat Transfer*, Vol 10. No 3. pp 445-451

Fiveland, W.A., Jessee, J.P., 1997. " Bounded, high-resolution differencing schemes applied to the discrete ordinates method " *J. Thermophysics and Heat Transfer*, Vol 11. No 4. pp 540-548

Howell., L.H., Beckner.,Vincent E. 1997. " Discrete ordinates algorithm for domains with embedded boundaries " *J. of Thermophysics.* Vol 11. No 4. pp 549-555

Howell, J.R. 1982. " *A Catalog of Radiation Configuration Factors*" McGraw-Hill

Howell, R.H., Suryanarayana, S. 1990. " Sizing of radiant heating systems: part i. – ceiling panels " *ASHRAE Transactions,* Vol 96, Part 1.pp 652 –665

Howell, R.H., Suryanarayana, S. 1990. " Sizing of radiant heating systems: part ii. –heated floors and infrared units. " *ASHRAE Transactions,* Vol 96, Part 1. pp 666-675

Hyde, D.J., Truelove J.S. 1997. " The discrete ordinates approximation for multidimensional radiant heat transfer in furnaces " *Report: HTFS RS 189.* Thermodynamics Division. A.E.R.E., HARWELL

Incropera, F. and DeWitt, D. 1985. "_Fundamentals of heat and mass transfer ", Wiley, 4th ed. pp 731-737

Jamaluddin, A.S., Smith P.J. 1992. " Discrete-ordinates solution of radiative transfer equation in nonaxisymmetric cylindrical enclosures " *J. of Thermophysics and Heat Transfer.* Vol 6, No 2 . pp 242 – 245

Kim, Tae-Kuk., Lee, H.S. 1989. " Radiative transfer in two-dimensional anisotropic scattering media with collimated incidence" *J. of Quantum Spectroscopy* Radiant. Transfer. Vol 42, No 3. pp 225-238

Kim, T.Y., Baek, S.W. 1991. " Analysis of combined conductive and radiative heat transfer in a two-dimensional rectangular enclosure using the discrete ordinates method " *International Journal of Heat and Mass Transfer,* Vol 34, No 9.pp 2265-2273

Lathrop, K. and Carlson, B., 1965. " Discrete-ordinates angular quadrature of the neutron transport equations " Los Alamos, NM, *Rept LASL-3186*

Lathrop, K.D., 1968 . " Ray effects in discrete ordinates equations " *Nuclear Science and Engineering,* Vol 32. pp 475-498

Lathrop, K.D. 1969. " Spatial differencing of the transport equation: positivity vs. accuracy " *J. of Computational Physics.* Vol 4 . pp 475 – 498

Lathrop, K.D., 1971. " Remedies for ray effects " , *Nuclear Science and Engineering,* Vol 45.pp 255-268

Lathrop, K.D., Carlson, B.G. " Properties of the new numerical approximations to the transport equation " *J. of Quantum Spectroscopy.* Radiant Transfer. Vol 11.pp 921 – 948

Lee, Clarence E. 1962. " The discrete sn approximation to transport theory " Los Alamos, NM, *Rept LA-2595*

Lewis, E.E., Miller, W.F. 1984. " Computational methods of neutron transport " Wiley, New York

Liou, B.T., Wu, C.Y. 1997. " Ray effects in the discrete-ordinates solution for surface radiation exchange" *International Journal of Heat and Mass Transfer.* Vol 32.pp 271-275

Liu F., Becker A., Pollard A. 1996 " Spatial differencing schemes of the discrete ordinates method " *J. of Numerical Heat Transfer,* Part B. Vol 30 .pp 23 – 43

Liu, J., Shang, H.M., Chen, Y.S. 1997. " Analysis of the discrete ordinates method with even parity formulation " *J. of Thermophysics and Heat Transfer*. Vol 11. No 2.pp 253-260

Meng, F.L.; McKenty, F., Elkaim, D, and R. Camarero 1992. " Predicting radiative heat transfer in two-dimensional rectangular and axisymmetric enclosures using the discrete transfer method " *In Conduction, Radiation and Phase Change, 2nd Int. Conf. In Advanced Computational Methods in Heat Transfer*, pp 161 – 180, Computational Mechanics Inc., Billerica, MA.

Naraghi, M.H.N, Chung, B.T.F. 1984. " A stochastic approach for radiative exchange in enclosures with nonparticipating medium " *J. of Heat Transfer.*, Vol. 106. pp 690 –698

Ozeki,Y.,S.Higuchi,T.Salto,S.Ohgaki, Y.Sonda. 1993. " Simulation on temperature and flow field in the atrium " *ASHRAE transactions. Room air convection and ventilation effectiveness.*pp 479-489

Patankar, S.V. 1980 . " *Numerical heat transfer and fluid flow* " , Hemisphere Publishing Corporation. Washington D.C.

Patel, M.K., Cross, M., Markatos C. 1988. " An assessment of flow oriented schemes for reducing false diffusion " *Int. J. for Numerical Methods in Engineering.* Vol. 26.pp 2279 – 2304

Ramankutty, M.A., Crosbie, A. L., 1998 " Modified discrete-ordinates solution of the radiative transfer in three-dimensional rectangular enclosures " *J. Quantum Spectroscopy and Radiant Transfer*, Vol 60, No 1.pp 103 – 134

Sanchez, A., Smith, T.F. ,1992, " Surface radiation exchange for two-dimensional rectangular enclosures using the discrete ordinates method " *J. Heat Transfer* Vol 114. pp 465-472

Schild P. 1997. " Accurate prediction of indoor climate in glazed enclosures " *Doktor Ingenior(Ph.D) dissertation*. Faculty of Mechanical Engineering. Norwegian University of Science and Technology

Selcuk, N., Kayakol N.1997, " Evaluation of discrete ordinates method for radiative transfer in rectangular furnaces " *Int. J. Heat Mass Transfer*. Vol 40. No 2. pp 213-222

Shah, N. G., 1971. " Computation of radiant heat transfer " *Ph. D Thesis, Imperial College of Technology*, London University

Shapiro, A.B. 1985. " Computer implementation, accuracy, and timing of radiation view factor algorithms " *J. of Heat Transfer*, Vol 107, No 3 , pp. 730- 732

Siegel R. 1973. " Net radiation method for enclosure systems involving partially transparent walls " *NASA TN D-7384 Report.*

Siegel, R. and Howell, J., 1992 , " *Thermal radiation heat transfer* ", Hemisphere Publishing Corporation. Washington, DC.

Smith, T.F., Beckermann, C., Weber, S.W.,1991 " Combined conduction, natural convection, and radiation heat transfer in an electronic chassis " *ASME Transactions*. Vol. 113. pp 382 – 391

Sowell, E.F., and P.F. O'Brien. 1972. " Efficient computation of radiant-interchange configuration factors within an enclosure " *J. of Heat Transfer*, Vol 94, No 3 , pp 326-328

Stefanizzi, P., Wilson, A., Pinney, A. 1990 " Internal long-wave radiation exchange in buildings: comparison of calculation methods: I Review of algorithms " *Building Services Engineering Research and Technology*. Vol 11. No 3. pp 81 -85

Stefanizzi, P., Wilson, A., Pinney, A. 1990 " Internal long-wave radiation exchange in buildings: comparison of calculation methods: II Testing of algorithms. " *Building Services Engineering Research and Technology*. Vol 11. No 3. pp 86 -96

Thurgood, C.P. 1992 . " A critical evaluation of the discrete ordinates method using HEART and t_n quadrature " Ph.D Thesis. Queen's University at Kingston.

Thurgood, C.P., Pollard, A., Becker, H.A. 1995. " The Tn quadrature set for the discrete ordinates method " *ASME Transactions*. Vol 117 . pp 1068 -1070

Truelove, J.S. 1987 "Discrete-ordinates solutions of the radiative transport equation". *J. Heat Transfer* Vol 109. pp 1048-1051

Walton, G. 1980. " A new algorithm for radiant interchange in room loads calculations " " *ASHRAE Transactions* Vol 86. Part 2. No 2599

Wendroff, B. 1969 " A difference scheme for radiative transfer" ". *J. of Computational Physics*. Vol 4 .pp 211- 229

Xiang-Yang Zhou, Chu-Guang Zheng, Yu-Yi Ma. 1996. " Comparison of several discrete arithmetic schemes for simulating a constrained jet and a lab-scale tangential fired furnace". *Computer in applied mechanics*. Vol. 130. pp 279-288

Yuguo, Li. 1992. " Simulation of flow and heat transfer in ventilated rooms." Ph.D. Thesis. Department of Mechanics/Applied Computational Fluid Dynamics. Royal Institute of Technology. S-100 44. Stockholm, Sweden.